# Estimation of Mean Transit Time and Transit Time Distribution in Meso-scale Catchments using Lumped Hydrological Model with Isotopic Tracers

January 2014

Wenchao MA

# Estimation of Mean Transit Time and Transit Time Distribution in Meso-scale Catchments using Lumped Hydrological Model with Isotopic Tracers

A Dissertation Submitted to

the Graduate School of Life and Environmental Sciences,

the University of Tsukuba

in Partial Fulfillment of the Requirements

for the Degree of Doctor of Philosophy in Science

(Doctoral Program in Geoenvironmental Sciences)

**Wenchao MA**

# Abstract

The catchment transit time, which is defined as the elapsed time from when a water molecule enters a catchment until it exits, is a lumped descriptor that reflects storage, flow pathways and sources of water in the catchment. The steady-state assumption for the catchment transit time is a controversial issue in catchment hydrology. The principal objectives of the present study are threefold: (1) to establish methodology for properly estimating time-variant mean transit time (MTT) and transit time distribution (TTD), (2) to clarify temporal variability of MTT and TTD in meso-scale catchments for re-examining the steady-state assumption, and (3) to identify inter-catchment variability of long-term average MTT (LAMTT) and its controlling factors.

In this study, an approach to estimate the time-variant MTT and TTD using a five-layer tank model with isotopic tracers was proposed and tested for the five sub-catchments (SCs; SC1 to SC5) within Fuji River catchment, central Japan. Model parameters were optimized during the calibration phase based on hydrometric and isotopic observations and then validated in a separate validation phase. The LAMTT (mainly from 2003 to 2012) was estimated to be from 8.0 years for SC1 to 16.5 years for SC3. These values are almost comparable with previously reported ones using the independent methods for the same region. Daily MTT was highly variable with relative standard deviation ranges from 14.6% to 40.7%. Instantaneous TTD also varied markedly; the peak transit time is longer in drier periods than in wetter periods and form of the TTDs could not be approximated by any functions previously proposed. Although optimized model-parameters have some uncertainties, potential errors in estimating the MTT are relatively small (e.g., < ±3.0 years). Therefore, the tracer-aided tank model is concluded to be useful for estimating temporal variations in MTT and TTD with high reliability. The predominant factor controlling temporal variability of MTT is precipitation amount. Precipitation

alters TTD, with increases in younger components, and shortens the MTT. Thus, the steady-state assumption is inappropriate. Inter-catchment comparison of LAMTT revealed that it is correlated with mean slope, coverage of Mesozoic sand stone/shale, coverage of forest (or conversely the other land use types), evaporation, interception and storage (especially, of the 4-th tank) for each catchment. All of these are related to the amount of groundwater storage, which is smaller in mountainous areas and greater in plain areas. The amplitude of MTT and TTD changed in such significant way have not yet introduced in previous research. As well as such a topographic control of LAMTT for meso-scale catchments is a new finding, since the most previous studies have focused on mountainous small catchments.

KEYWORDS  transit time; tank model; isotope tracer; catchment hydrology; Fuji river

# Contents

# List of Tables

# List of Figures

# List of Symbols

| Symbol | Definition | Unit |
|--------|-----------|------|
| $A_i$ | surface area of the division | km$^2$ |
| $A(i)$ | mean age of water in i tank | yr |
| $A_Q$ | rate of aging | - |
| $D(i,j)$ | concentration of the date tracer in the ith tank at the j-th time | yr |
| $D_Q(j)$ | concentration of the date tracer in total runoff water | yr |
| $e_a$ | actual vapour pressure | kPa |
| $e_s$ | saturation vapour pressure | kPa |
| $ET$ | evapotranspiration | mm day$^{-1}$ |
| $ET_o$ | reference evapotranspiration | mm day$^{-1}$ |
| $E_s$ | soil evaporation | mm day$^{-1}$ |
| $e_s$ | saturation vapour pressure | kPa |
| $F_E$ | $E_s/ET$ (= 0.1 in the present study) | - |
| $f_E(i)$ | weighting factors at the i-th tank for soil evaporation | - |
| $f_T(i)$ | weighting factors at the i-th tank for root water uptake | - |
| $G$ | soil heat flux density | MJ m$^{-2}$day$^{-1}$ |
| $h_a$ | vapor pressure | mm |

| | | |
|---|---|---|
| $h(i)$ | water level in the tank | mm |
| $h_H(i)$ | level of lateral outlets | mm |
| $h_V(i)$ | level of top of vertical pipes connecting bottom outlets | mm |
| $I$ | interception | mm day$^{-1}$ |
| $k$ | coefficient of tank model | - |
| $k_V(i)$ | conductance parameters that regulate $q_H(i)$ | - |
| $k_V(i)$ | conductance parameters that regulate $q_V(i)$ | - |
| $n$ | number of rainfall stations | - |
| $P$ | precipitation | mm day$^{-1}$ |
| $P_i$ | precipitation at rainfall station $i$ | mm day$^{-1}$ |
| $Q$ | total runoff | m$^3$day |
| $q_H(i)$ | horizontal (exactly speaking, toward a stream network) water flux | m$^{-1}$day |
| $q_V(i)$ | vertical water flux | m$^{-1}$day |
| $R_n$ | net radiation at the crop surface | MJm$^{-2}$day$^{-1}$ |
| $P_i$ | precipitation at rainfall station i | mm day$^{-1}$ |
| $T$ | daily air temperature at 2 m height | °C |
| $T_r$ | transpiration | mmday$^{-1}$ |
| $u_2$ | wind speed at 2 m height | m s$^{-1}$ |
| $X(t)$ | storage of tank model | m |

| $Y_i^{mean}$ | mean of simulated value | $m^3 day^{-1}$ |
|---|---|---|
| $Y_i^{obs}$ | observed value | $m^3 day^{-1}$ |
| $Y_i^{sim}$ | simulated value | $m^3 day^{-1}$ |
| $y(t)$ | output of tank model | m |
| $\delta$ | isotope composition of sample water relative to a standard | ‰ |
| $\delta a$ | isotopic composition of atmospheric water vapor | ‰ |
| $\delta D$ | stable isotope composition of hydrogen in water | ‰ |
| $\delta^{18}O$ | stable isotope composition of oxygen in water | ‰ |
| $\delta_Q$ | isotopic composition of total runoff | ‰ |
| $\Delta\varepsilon$ | kinetic fractionation | - |
| $\gamma$ | psychrometric constant | kPa °C |
| $\rho$ | total resistance to water vapor transfer from the evaporating surface to the air | - |
| $\rho_M$ | resistance to molecular diffusion of water vapor | - |

# Chapter 1
# Introduction

## 1.1 Background

Transit (or travel) time is defined as the elapsed time when water molecule exits a system (or reservoir; e.g., catchment, aquifer, lake, etc.) since it entered the system (e.g., Bolin and Rodhe, 1973). In catchment scale, it means the time water spends travelling through a catchment to the stream network (McDonnell, et al. 2010). The catchment transit time (CTT) is a lumped descriptor that reflects storage, flow pathways and sources of water in a catchment (McGuire and McDonnell, 2006). It allows us to examine how catchments retain and release water contaminated, for instance, by chemical/nuclear accidents. Especially for meso-scale catchments, which are usually tightly connected with spatial variation of geology, landuse, soil and topography (Niehoof et al., 2002). Therefore, quantifying CTT, which may depend on soil (Soulsby et al., 2006; Hrachowitz et al., 2010), topography/landscape (McGuire et al., 2005; Tetzlaff et al., 2009; Hrachowitz et al., 2010), catchment size (Soulsby et al., 2006; Hrachowitz et al., 2010), climate and the other geographical/geological settings (McDonnell et al., 2010). To figure out the relationship between CTT and the potential impact factors is fundamental for better management of catchments.

The transit time can be defined for each molecule. In general, water flowing or sampled at a given time and location would be an integrative mixture of molecules having different transit time. Therefore, we should consider both mean transit time (MTT) and transit time distribution (TTD) for all constituent molecules. In a steady state the MTT equals to the turnover time (= $M/F$; $M$ is the total mass of mobile water and $F$ is the total flux) and thus indicates capacity of water storage as the whole catchment, if total flux (i.e., runoff) was known. On the other hand, TTD provides information about

diversity of flow pathways within a catchment and their temporal response characteristics to water inputs (i.e., available precipitation). Relatively short CTT components would be strongly linked to how quickly event-driven contamination pulse arises, while longer CTT components may helpful in addressing how long time contamination persists.

In earlier works using environmental tracers (e.g., Maloszewski and Zuber, 1982; Maloszewski et al., 1983; Richter et al., 1993; DeWalle et al., 1997; Ozyurt and Bayari, 2003), some idealized, hypothetical TTD functions with steady-state assumption have been employed to estimate MTT. The same or similar, time-invariant TTD functions were applied into unsteady-state (i.e., variable flow) cases for reproducing tracer concentration variation (Zuber, 1986) and for estimating temporally averaged MTT (Ozyurt and Bayari, 2005). Amin and Campana (1996) proposed hypothetical, time-variant TTD functions, while they were not tested by observed data. In a field experiment where step change in tracer concentration was given across a small catchment, Rodhe et al. (1996) estimated a non-idealized TTD. Lindström and Rodhe (1986) utilized a lumped hydrological model to simulate temporal variation of observed tracer concentration in stream water and then TTD was obtained by applying a virtual tracer pulse to the model with steady-state boundary conditions. Recently, McGuire et al. (2007) predicted time-variant TTD under field conditions using a simple hillslope model calibrated by hydrometric and tracer observations. Botter et al. (2010) also obtained time-variant TTD using a hillslope-scale stochastic soil moisture model with variable boundary conditions. These approaches clarified that TTD was highly variable in time corresponding to precipitation input, and temporally averaged TTDs had near-exponential form with a short time-lag, while they have been limitedly applied into small catchments. Sayama and McDonnell (2009) developed a time-space accounting scheme (T-SAS) with a distributed hydrologic model for tracking not only temporal but also spatial sources of runoff components. These progresses in recent studies clarified that MTT were not always constant and temporally averaged TTDs had near-exponential form with a short time-lag.

However, models used in these studies were highly complex with many uncertain model-parameters, so that reliability of estimated MTT and TTD remains unclear. In addition, many of them have been limitedly applied into small catchments.

## 1.2 Objectives

The principal objectives of the present study are threefold: (1) to establish methodology for properly estimating time-variant MTT and TTD, (2) to clarify temporal variability of MTT and TTD in meso-scale catchments for re-examining the steady-state assumption, and (3) to identify inter-catchment variability of long-term average MTT (LAMTT) and its controlling factors. The reason why we highlight meso-scale (approximately $10^1$ - $10^3$ km$^2$; Uhlenbrook et al., 2004) catchments is because those are more strongly linked to human sphere than small remote catchments are. Achieving our goals would provide useful information for better understanding catchment hydrology and biogeochemical cycle and for managing chemical/nuclear disaster risks.

## 1.3 Outline of this study

A literature review of previously related researches is given in Chapter 2. In Chapter 3, study area and method are described. The methodology for MTT and TTD calculations are described in this part. The results and discussions are presented in Chapter 4 and Chapter 5 respectively. Finally, conclusions were given in Chapter 6.

# Chapter 2
# Review of the literature

## 2.1 Definition of transit time

There are several terms conceptually similar to the transit time, such as the age, turnover time, residence time, and others (McGuire and McDonnell, 2006; Li, 2010 and others). Bolin and Rodhe (1973) defined the age of the water parcel as the time that a water parcel has spent since it entered the reservoir, where the water age considered as a water-parcel-specific quantity and is time dependent and spatially varying within a system. Li (2010) expressed the turnover time (also named flushing time) as the time required to replace a certain mass or volume of water. For a well-mixed, steady-state system, a more quantitative description was presented by Geyer et al. (2000) as "the ratio of the mass of a scalar in a reservoir to the rate of renewal of the scalar." Accordingly, Fischer et al. (1979) expressed the flushing time in a reservoir system. As mentioned in Chapter 1, the transit time is defined as the elapsed time from when the water molecule exit a system (Bolin and Rodhe, 1973), in contrast to the definition of the age that water molecules have spent inside a flow system. The residence time is a more general term representing the time scale of water cycle and has been used as the mean age, mean transit time or turnover time (Bolin and Rodhe, 1973; McGuire and McDonnell, 2006; Li, 2010). McGuire and McDonnell (2006) stated that the distinction between residence time and transit time is often overlooked in the literature (including in their own previous works); however, a distinction can clearly be made.

Again, it should be noted that transit time differs for each individual molecule. Thus, we can define the MTT as the average of transit time for all molecules and TTD over all molecules in a mass of water collected at a given time and location (i.e., outlet of the catchment).

## 2.2 Methods to estimate transit time

To simulate water movement or flow path in natural circumstances is a crucial work for hydrological processes. However, it is very difficult to characterize the hydrologic response of a catchment with simple descriptors. Many efforts have been taken for simulating the water movement in more detailed (Dunne, 1970). This could be considered as the expression of transit time as MTT and TTD. MTTs are usually estimated by modeling input-output relationships of conservative tracers such as stable isotopes or chloride according to various assumed TTDs (e.g. Hrachowitz et al., 2009a; Kirchner et al., 2010). To estimate the TTD of a given catchment, conservative tracers in rainfall and stream flow are generally measured, and these input-output signals are related using theoretical transfer functions. Classic examples of such transfer functions are the piston flow model, the exponential model, the dispersion model, and the gamma distribution model (Małoszewski and Zuber, 1982; McGuire and McDonnell, 2006, shown as Figure 2.1). The exponential model (EM) is a basic and widely used one-parameter model (e.g., Maloszewski et al., 1983; Stewart and McDonnell, 1991; McGuire et al., 2002), conceptualizing the catchment as well mixed linear reservoir. As shown by Kirchner et al. (2000) using spectral analysis, the Gamma distribution model (GM) with a shape parameter a = 0.5 is the mathematically ideal representation of stream signals exhibiting 1/f noise. The long tail of the gamma distribution enables this model to reproduce the long internal memory of many catchments. The two parallel linear reservoir (TPLR) models, as applied by Weiler et al. (2003) and on the basis of three parameters, allows separating the system into a fast and a slow component according to the partition parameter $\Phi$ (Hrachowitz et al., 2009). Functions of typical models are given in Table 2.1.

Concerning the water flow pattern relevant to transit time or the age of water, Dunn (2010) using a semi-distributed conceptual hydrological model showed that the primary control on the stream water

MTT is storage within the unsaturated zone and compared the results of different flow path gradient and length. McGuire et al. (2007) presented spatially-explicit model constrained by soil hydrologic properties, runoff, and applied tracer data and used it to identify the dominant processes necessary to explain both water and solute flux from a steep hill slope to explore transit times (Figure 2.2). Botter et al. (2010) proposed a mathematical framework for the general definition and computation of TTDs defined by the closure of a catchment control volume, where the input flux is an arbitrary rainfall pattern and the output fluxes are green and blue water flows (Figure 2.3). Sayama and McDonnell (2009) used a physically based hydrologic model together with field data to explore how catchment properties, particularly soil depth, controls the age and source of stream flow, and presented a new time-space accounting scheme (T-SAS) to simulate the pre-event and event water fractions, MTT, and spatial source of stream flow at the watershed scale (Figure 2.4). Theories for calculating the mean age and MTT have been proposed by Duffy (2010) to construct a dynamical system for the mean age and concentration under steady or transient flow conditions, and demonstrated that intermittency of wetting and drying periods affect the age of solutes.

Van der Velde et al. (2010) argued on the basis of numerical simulations that the TTD is not only rapidly changing in time but also highly irregular in shape, reflecting rainfall and drought events during the transit of water particles through the catchment. A model assuming the time-invariant transit time distributions or steady conditions cannot reproduce MTT accurately, so it is important for transit time calculation to investigate time variant flow pathways and their effect on transit time calculation (Lindstrom and Rodhe, 1992).

## 2.3 Estimation of MTT and TTD on meso-scale catchment

The hydrological responses are dominated by processes, which are difference at various spatial sacales (Blöschl and Sivapalan, 1995; Uhlenbrook et al. 2004). The same applies to estimate of transit time issues.

In different scale catchment, mechanisms of water response are usually different. For a micro-scale catchment, response to rainfall is usually dominated by the runoff generation process at hillslopes or near stream areas. (e.g. Anderson and Burt, 1990; McDonnell, 1990; Montgomery et al., 1997; Uhlenbrook et al. 2004). For meso-scale catchments, processes from smaller scales formed into a complex way produce into an integrated response, (e.g. Scherrer and Naef, 2003; Uhlenbrook, 2004). At the same time, Bronstert et al, 1995 demonstrated a prevailing opinion that floods of medium and high probability in meso-scale catchments are most strongly influenced by land cover. However, for the macro-scale catchments, spatial and temporal distribution of rainfall or snow melt or the routing of runoff are dominated. As Niehoff et al. (2002) mentioned spatial data of landuse, soil and topography should be paid attention for storm-runoff generation processes in a meso-scale catchment. Meanwhile, basing on the meso-scale catchment are commonly connected with resident condition of human being, so meso-scale catchments are often of great interest for water resources development and for development interventions aimed at uplifting rural livelihoods (Love et al, 2011). So, to study the pattern and potential law of the MTT and TTD behave in a meso-scale catchment is significant and imperative.

How to choose parameterization of land-surface and land cover and how to integrate the data representing from smaller scale into a meso-scale catchment using lumped model is a challenge in this study.

7

Table 2.1 Descriptions of ideal function of transit time distribution.

| Model | TTD $g(\tau)$ | MTT | Parameter Description |
|---|---|---|---|
| Exponential | $\tau_m^{-1} \exp\left(-\dfrac{\tau}{\tau_m}\right)$ | $\tau_m$ | -- |
| Two parallel linear reservoirs | $\dfrac{\varphi}{\tau_f} \tau_m \exp\left(-\dfrac{\tau}{\tau_f}\right) + \dfrac{1-\varphi}{\tau_s} \tau_m \exp\left(-\dfrac{\tau}{\tau_s}\right)$ | $\varphi \tau_f + (1-\varphi) \tau_s$ | $\tau_f$ is MTT of fast reservoir; $\tau_s$ is MTT of slow reservoir; $\varphi$=volume of fast reservoir/total volume |
| Gamma | $\dfrac{\tau^{\alpha-1}}{\beta^\alpha \Gamma(\alpha)} \exp\left(-\dfrac{\tau}{\beta}\right)$ | $\alpha\beta$ | $\alpha$ is shape parameter; $\beta$=scale parameter |
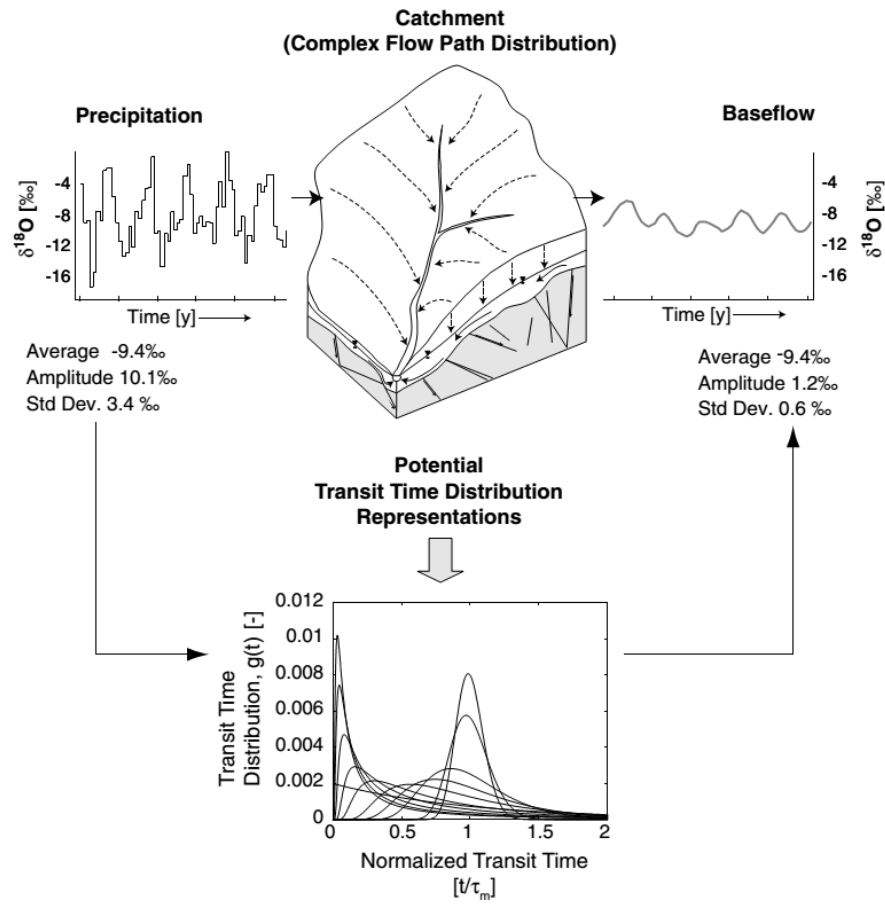
Figure 2.1 Conceptual diagram of the lumped parameter transit time modeling approach (McGuire and McDonnell, 2006). Catchments receive temporal tracer (e.g., $\delta^{18}O$) inputs that are transported along diverse flow paths in the unsaturated and saturated zones as tracers migrate through the subsurface toward the stream network.
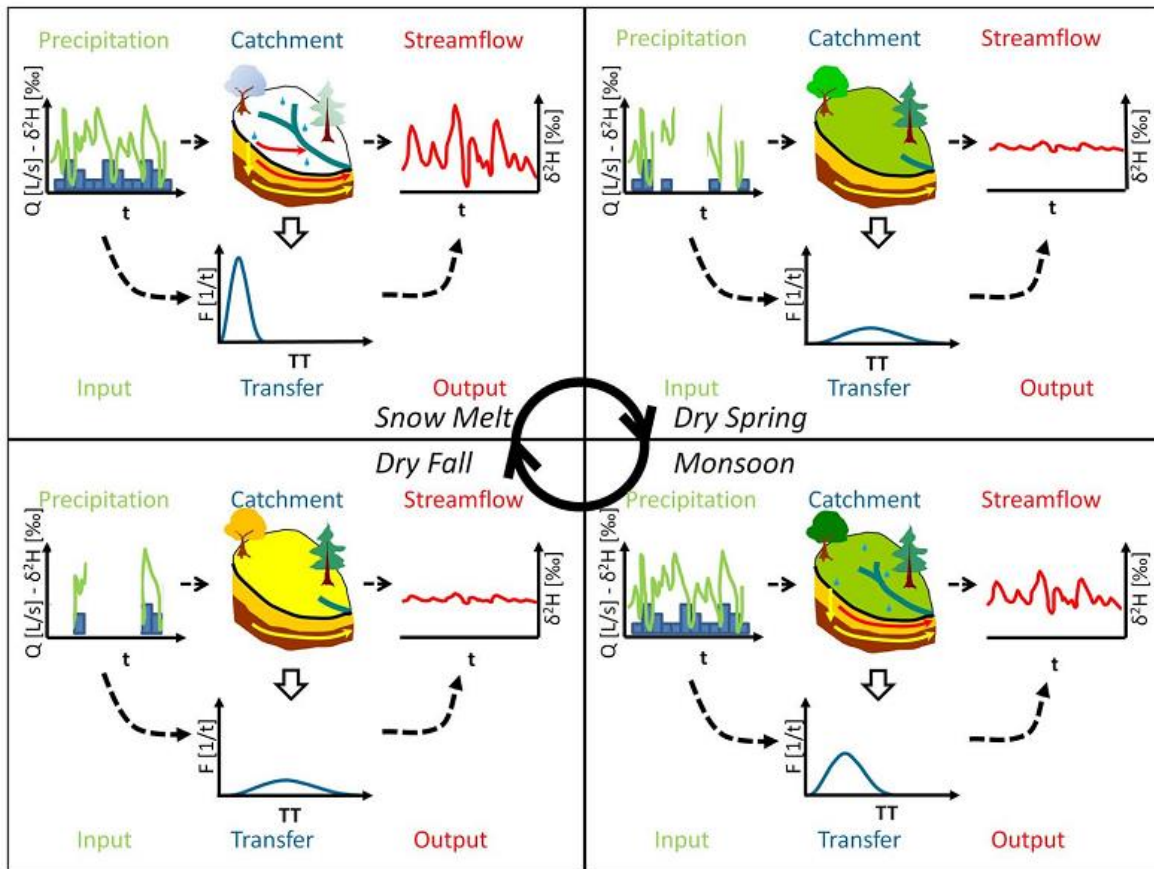
Figure 2.2 Changes in water storage and associated flow paths in a southwestern United States semiarid catchment (Marshall Gulch) undergoing seasonal shifts in water and energy availability (Heidbuchel et al., 2012). During snowmelt in spring, water input is high, and energy input is low, resulting in increased storage, the activation of predominantly fast flow paths (interflow and overland flow), and rapid transfer of water.
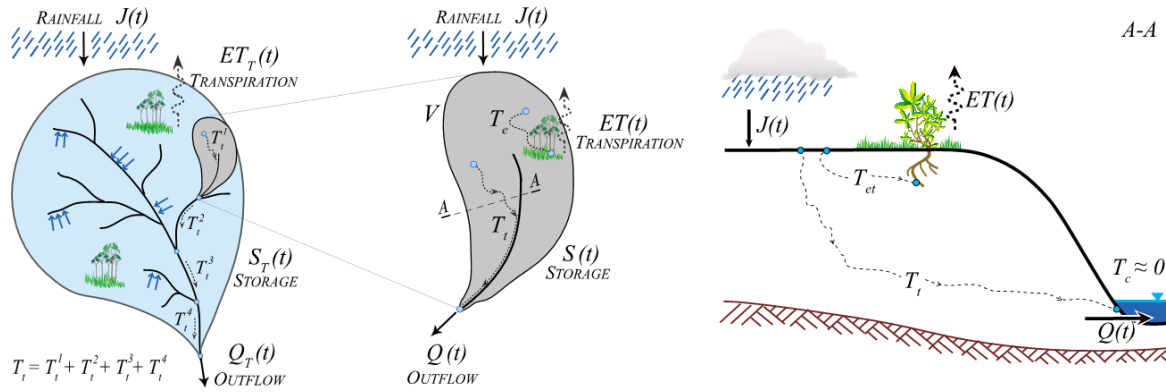
Figure 2.3 Schematic representation of the control volume V within which transport processes are analyzed (Botter et al., 2010). (Left) An entire catchment where individual travel times are additive and composed geomorphically by serial and parallel arrangement through path probabilities. (Middle) The actual transport volume V considered in this study, chiefly composed of unchanneled areas. Note that the patchwork of such transport volumes covers the catchment. (Right) A cross section of V emphasizing the key components of exit time, the evapotranspiration time ($T_e$) and the travel time ($T_t$).
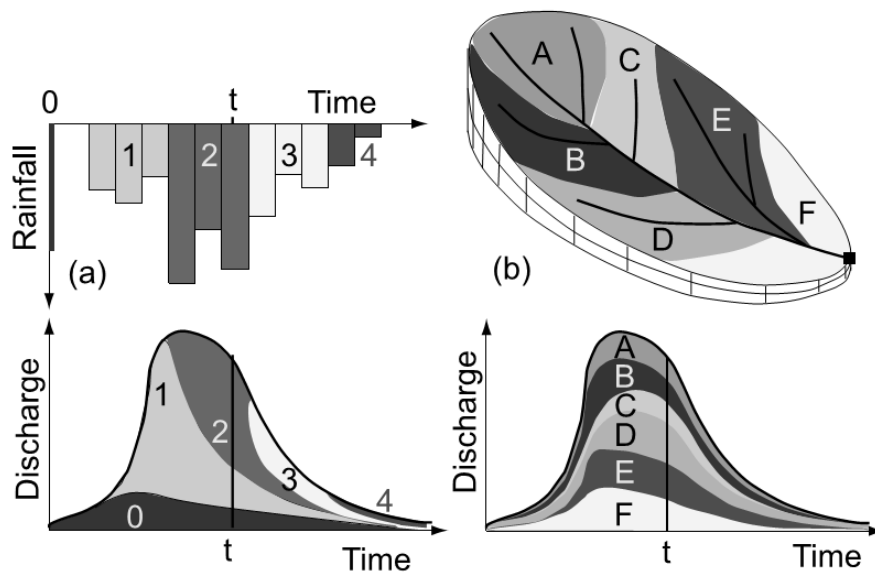
Figure 2.4 Schematic diagram of separating the temporal and spatial hydrograph components (Sayama and McDonnell, 2009); (a) individual rainfall hyetograph segments are propagated through the storm hydrograph, and (b) The geographic source apportionment of flow.

# Chapter 3
# Methodology

## 3.1 Study area

The study catchments (SCs) are located within the Fuji river catchment (35.5˚-36.0˚N, 138.2˚-138.9˚E), which is in the central of Japan (Figure 3.1). The area of the catchment is 2172.7 km$^2$ as a whole and elevation ranges from approximately 234.7 m to 2962.8 m. Northern, eastern and southern parts of the catchment are characterized by mountainous topography, while central and eastern parts are alluvial fans and lowlands. Mountains are formed mostly by granite and partly by andesitic/basaltic rocks. The alluvial fans are covered by gravels with a thickness of 20-30 m, underlain by a clay layer with almost the same thickness. According to the meteorological observation records at Kofu station of Japan Meteorological Agency, climatic mean (1981-2010) of annual precipitation is 1135.2 mm with mean temperature of 14.7 ºC, mean relative humidity of 65%, and mean wind speed of 2.2 m/s. Dominant land use/land cover type is forest at mountainous areas, orchard and vegetable fields at alluvial fans, and residential areas and paddy fields at alluvial lowlands.

The five SCs were defined considering with the location of a gauging station maintained by Ministry of Land, Infrastructure, Transport and Tourism (MLIT), Japan.

## 3.2 Data set

### 3.2.1 Precipitation

Precipitation has been considered as the main component of the driving force within the entire hydrologic cycle (Brutsaert, 2005), and therefore the driving force in hydrologic modeling. The spatial distribution of precipitation could change significantly especially for basin- or catchment-scale. However, it is necessary to consider the average precipitation as input over the entire area in hydrologic analyses at the basin- or catchment-scale. In the past, precipitation data mainly observed from raingauge, however, many method have been regarded as effective for restrict the precipitation into catchment scale, such as, Thiessen polygon method (Thiessen, 1911, Brutsaert, 2005), the Inverse distance method, the Isohyetal method (Reed and Kincer, 1917) and others. The study catchment was defined considering with the location of a gauging station maintained by Ministry of Land, Infrastructure, Transport and Tourism (MLIT), Japan.

### *Radar data*

It is important to use the quantitative precipitation to model run-off and flow processes. However, the accurate result in kind of difficult situation not only for the urban area but also for the forest area. By considering the geographical characters of research area, which consisted by more than 70% forest area and other landuse. The more accurate input of precipitation is key point for the simulations. So, the radar data was reasonably considered as priority choice. Within this study, the radar data series is from 1st January 2006 to 30th September 2012. However, the period before 2006 also is noticeable for the MTT and TTD calculating. So, we applied the hydro-meteorological stations' precipitation data that modified by considering the elevation affection for regressing to the sub catchment. The locations of the hydro-meteorological stations could be found from the Figure 3.2 and Figure 3.3. For the period

since 2006, we used radar-AMeDAS (Automatic Meteorological Data Acquisition System) precipitation data produced by Japan Meteorological Agency (JMA). The data represent map of 1-hr-accumulated precipitation estimated from combined observations using radars and rain gauges (e.g., Makihara 1996 for details). Its spatial resolution is approximately 1 km × 1 km (see Figure 3.4).

*Thinessen polygon method (TPM)*

 Thinessen polygon method also named as Voronoi diagrams, which means those associated with points located at random in the plane by a homogeneous planar Poisson point process (Boots, 1986). Concordant with the high reliable data precipitation as input, the water balance calibration as well as validation period was set within the period from 1$^{st}$ January 2006 to 30$^{th}$ September 2012, at the same time, the water discharge data of the monitoring site was considered as the upper boundary of the validation period.

$$\langle P \rangle = \frac{1}{A} \sum_{i=1}^{n} A_i P_i \tag{1}$$

$$A = \sum_{i=1}^{n} A_i \tag{2}$$

where, $A_i$ is the surface area of the division, $n$ is the number of rainfall stations, $P_i$ is the precipitation at rainfall station $i$. Areal precipitation for whole catchment as an input was estimated by Thiessen Polygon Method (Brutsaert, 2005) using daily precipitation observed by rain gauge at 29 weather stations of JMA AMeDAS data and modified by considering the ratio between the Radar data and TPM data (see Figure 3.5).

3.2.2 River discharge

Observed daily river discharge data that in daily step are produced by MLIT, were used for calibration and validation in the water flow part. For SC2-SC5 (seen as Figure 3.3), the calibration period was 2006-2007 and validation period was 2008-2010. But for SC1, the calibration period was 2006 and validation period was 2007 and 2008. Initial values of *h(i)* were determined by trials and errors.

3.2.3 Meteorological data

Meteorological data (solar radiation, air temperature, relative humidity, and wind speed) observed by Japan Meteorological Agency (JMA) at three weather stations were utilized for computing $ET_o$. We applied values at a nearest station for the whole catchment (Figure 3.3).

The method we applied FAO Penman-Monteith (Allen et al., 1998) for calculating the potential evapotranspiration.

$$ET_o = \frac{0.408\Delta\left(R_n - G\right) + \gamma \dfrac{900}{T+273} u_2\left(e_s - e_a\right)}{\Delta + \gamma\left(1 + 0.34u_2\right)} \tag{3}$$

where, $ET_o$ reference evapotranspiration; $R_n$ net radiation at the crop surface; $G$ means soil heat flux density; $T$ means daily air temperature at 2 m height; $u_2$ means wind speed at 2 m height; $e_s$ is saturation vapour pressure; $e_a$ is actual vapour pressure; $e_s$-$e_a$ means saturation vapour pressure; slope vapour pressure curve; $\gamma$ is psychrometric constant.

3.2.4 Isotope data

In addition to the existing data set, we newly performed monthly isotopic monitoring for river water at the gauging station from April of 2010 to March of 2012. Monthly monitoring for precipitation

16

isotope was also carried out at Kofu city (Figure 3.2). Hydrogen and oxygen stable isotope ratios ($^2$H/$^1$H and $^{18}$O/$^{16}$O) of collected water samples were measured with a liquid water isotope analyzer (L1102-i, Picarro, CA, USA) based on wavelength-scanned cavity ring-down spectroscopy (WS-CRDS), a kind of tunable diode laser adsorption spectroscopy (TDLAS). Measured results are expressed using δ values (i.e., δ$^{18}$O and δD) relative to the Vienna Standard Mean Ocean Water (V-SMOW). Measurement errors for the analyzer used are 0.1‰ for δ$^{18}$O and 1‰ for δD (Yamanaka and Onda, 2011). Using δ$^{18}$O and δD, deuterium excess ($d \equiv$ δD-8δ$^{18}$O) was calculated.

From Figure 3.6, river water isotope composition as well as precipitation isotope composition was plotted from May 2010. The isotope composition value of precipitation varies in larger ranges than river water isotope composition. The local meteoric water line followed as a liner regression with a slope as 7.59, and incept as 8.07 (Figure 3.7), where the number of precipitation sample were 166, and with 0.960 as $R^2$ for regression results. By considering regression four seasons' precipitation composition separately, it is easy to conclude that the seasonal change of the local water isotope are different, especially by comparing the slopes and interceptions (Figure 3.8).

## 3.3 Model description

### 3.3.1 Overview of tank model

Hydrological models are efficient and powerful tools in rainfall/runoff process simulation. These models have been developed into several types depending on the hydrological data characteristics. In the hydrological model applications, the four-layered tank model proposed by Sugawara (1995) (see Figure 3.9) is considered a useful model in rainfall/runoff simulations and verifications because of its simplified model frame, reasonable function in runoff response and ability to provide good simulation

results. As being a semi-physical hydrological model, Tank model is simpler to determine parameters for meso-scale catchment than distributed model, which own many characters increasing more uncertainty and difficulty for setting parameters at the same time. Although the merits and demerits of lumped model and distributed model have not yet totally assured, it is worthy and ascendant to apply lumped model in this study. Fitting the model parameters is the major work in applying this hydrological model. The trial-and-error procedure has been commonly used for calibration. However, the manual calibration process is tedious owing to the 16 model parameters involved in the four-layered tank model. The simulation results easily produce much uncertainty because of the subjective factors involved. Therefore, a number of studies have been performed to determine a more efficient calibration procedure.

3.3.2 Water balance

In the present study, a hydrologic model is employed for predicting MTT and TTD. Among large numbers of model types, we selected so-called Tank Model (Sugawara and Maruyama, 1956; Sugawara, 1961), one of famous rainfall-runoff models (Brutsaert, 2005). While the Tank Model is a lumped conceptual model and relatively easy to handle, it can consider different flow paths and water pools having different temporal characteristics by arranging a set of several tanks. Therefore, it has been used not only for predicting runoff but also for simulating temporal change in water quality (e.g., Kato, 2005). Ikawa et al. (2011) successfully reproduced temporal variation of observed isotopic composition of stem flow using a two-layer tank (i.e., canopy tank and stem tank) model. And the basic principle for water balance could be considered as:

$$\frac{d}{dt}X(t) = x(t) - y(t), \qquad y(t) = k \cdot X(t) \qquad (4)$$

18

where $X(t)$ means the storage $x(t)$ is the input of the model, and $y(t)$ is the output of the model, k means the coefficient of the model to balance or adjust the output and storage of the model. Specifically, in this research, the storage involved the hydrologic accounting as:

$$X(t) = P - E - Tr - I - Outflow \tag{5}$$

Although the most common type of the tank model has four tanks in series (Sugawara, 1995), in the present study a five-layer tank model (Figure 3.9) was developed to conceptually represent the overland flow, rapid throughflow, delayed throughflow, groundwater flow and bedrock flow. Vertical water flux, $q_V(i)$, and horizontal (exactly speaking, toward a stream network) water flux, $q_H(i)$, for the $i$-th tank are computed by the following equations, respectively:

$$q_H(i) = \max\left[k_H(i)(h(i) - h_H(i)), 0\right], \tag{6}$$

where $h(i)$ is the water level in the tank, $h_V(i)$ is the level of top of vertical pipes connecting bottom outlets, $h_H(i)$ is the level of lateral outlets, and $k_V(i)$ and $k_H(i)$ are the conductance parameters that regulate $q_V(i)$ and $q_H(i)$, respectively. Total runoff, $Q$, is given as:

$$q_V(i) = \max\left[k_V(i)(h(i) - h_V(i)), 0\right] \tag{7}$$

$$Q = \sum_{i=1}^{5} q_H(i). \tag{8}$$

Equations (1) and (2) seem to obey Darcy's low; the conductance parameters are analogous to hydraulic coefficients, and the difference between $h(i)$ and $h_V(i)$ or $h_H(i)$ correspond to hydraulic gradient. However, for the vertical fluxes in this model, water level (i.e., analogous to potential) in a lower tank do not affect flow from an upper tank and the flow direction is always downward. This simplification allows us to avoid an iteration procedure in computing fluxes and potentials, so that

computation time can be reduced markedly. Similarly, for the horizontal fluxes (or runoff components), water level in a stream channel is not considered, and the scale of the distance between the stream channel and a point, of which hydraulic status is represented by water level in the tank, is unknown. Such a vague expression introduces uncertainties mainly in determining $k_H(i)$, while it may implicitly represent the variable source area concept. Magnitude of $\Delta h_{H\text{-}V}$ ($\equiv h_H(i) - h_V(i)$; $> 0$, in normal cases) controls relative importance of horizontal and vertical flows in each layer, so that values of $k_V(i)$, $k_H(i)$ and $\Delta h_{H\text{-}V}$ are determined through calibration comparing observed and predicted hydrograph. Values of $h_V(i)$ or $h_H(i)$ themselves do not affect water flow but regulate isotope transport described in section of 'Isotope transport part' (Figure 3.9).

Water budget equations for the 1st and the other four tanks are given as follows, respectively,

$$\frac{dh(i)}{dt} = P - I - f_T(i)T_r - f_E(i)E_s - q_V(i) - q_H(i) \quad for \quad i = 1 \tag{9}$$

$$\frac{dh(i)}{dt} = q_V(i-1) - f_T(i)T_r - f_E(i)E_s - q_V(i) - q_H(i) \quad for \quad i = 2 \text{ to } 5 \tag{10}$$

where $t$ is the time, $P$ is the precipitation, $I$ is the interception loss, $T_r$ is the transpiration, $E_s$ is the soil evaporation, and $f_T(i)$ and $f_E(i)$ are the weighting factors at the $i$-th tank for root water uptake and soil evaporation, respectively. We adopted daily time step for computing the above equations. The water storage of each layer could be considered as the depth of each tank layer, so the total storage means the total depth of each tank layer for each catchment.

We assume $I = f_I P$ with $f_I = 0.85$ on daily basis, considering with previous reports for humid temperate forests (Sugita and Tanaka, 2009). Evapotranspiration, $ET$ ($= T_r + E_s + I$), is estimated as

$$ET = K_c ET_o \tag{11}$$

where $K_c$ is the single crop coefficient and $ET_o$ is the reference evapotranspiration obtained from FAO Penman-Monteith equation (Allen et al., 1998). We applied the value of $K_c$ for conifer trees (= 1). According to Kubota and Tsuboyama (2004), proportion of soil evaporation to total evapotranspiration at forests generally ranges from 3% to 20% with an average of 10%. Thus, we give $E_s$ and $T_r$ as follows,

$$E_s = \max\left[F_E ET, 0\right], \tag{12}$$

$$T_r = \max\left[ET - I - E_s, 0\right]. \tag{13}$$

where $F_E$ (= 0.1 in the present study) is the $E_s/ET$. At forests in the central Japan, root water uptake zone are usually situated shallower than 50 cm depth from the ground surface, while some species does uptake water from the soil deeper than 1 m (Yamanaka et al., 2009). So, we assumed $f_T(1, 2, 3, 4, 5) = (0, 0.7, 0.3, 0, 0)$. In addition, we assumed that soil evaporation does not occur deeper tanks, that is, $f_E(3, 4, 5) = (0, 0, 0)$. Values for $f_E(i)$ at shallower tanks depend on water existence in the tank, as follows,

$$f_E(1) = \begin{cases} 1 & for \quad h(1)^{t+1} > 0 \\ 0 & for \quad h(1)^{t+1} \leq 0 \end{cases} \tag{14}$$

$$f_E(2) = \begin{cases} 1 & for \quad h(2)^{t+1} > 0 \\ 0 & for \quad h(2)^{t+1} \leq 0 \end{cases} \tag{15}$$

where superscript "$t+1$" means the value for the next time step.

Although $f_T(i)$, $f_E(i)$, $f_I(i)$, $K_c(i)$, and $F_E(i)$ should depend on land use type and/or vegetation condition, we set the values for typical forests in the study area, since the forest is the most dominant land cover in the most of study catchments (Table 4.4).

### 3.3.3 Isotope balance

Isotope budget equations in the 1$^{st}$ and the other tanks are expressed as the following:

$$\frac{dh(i)\delta_w(i)}{dt} = (P-I)\delta_P - \left[f_T(i)T_r + q_V(i) + q_H(i)\right]\delta_w(i) - f_E(i)E_s\delta_E \qquad \text{for i = 1} \qquad (16)$$

$$\frac{dh(i)\delta_w(i)}{dt} = q_V(i-1)\delta_P - \left[f_T(i)T_r + q_V(i) + q_H(i)\right]\delta_w(i) - f_E(i)E_s\delta_E \qquad \text{for i = 2 to 5} \qquad (17)$$

where $\delta$ is the isotopic composition (i.e., $\delta^{18}O$ or $\delta D$), and subscripts $P$, $E$ and $w$ denote precipitation, soil evaporation and water in each tank. Instantaneous, complete mixing within each tank is assumed in this model. Time step is daily same as in water flow part.

The $\delta_E$ can be given by the following Craig-Gordon model (Craig and Gordon, 1965; Gat, 1996):

$$\delta_E = \frac{\delta_w(i)/\alpha - h_a\delta_a - (1-1/\alpha)\times10^3 - \Delta\varepsilon}{1-h_a+\Delta\varepsilon/10^3} \qquad \text{for i = 1 or 2} \qquad (18)$$

where $\alpha$ is the equilibrium isotopic fractionation factor as a function of temperature (see Majoube, 1971 for experimental functions), $h_a$ is the relative humidity of air, and $\delta_a$ is the isotopic composition of atmospheric water vapor. The kinetic fractionation, $\Delta\varepsilon$, is defined as

$$\Delta\varepsilon = (1-h_a)\frac{\rho_M}{\rho}\left[(D/D_i)^n - 1\right]\times10^3 \qquad (19)$$

where $\rho_M$ is the resistance to molecular diffusion of water vapor, $\rho$ is the total resistance to water vapor transfer from the evaporating surface to the air, $D$ is the water vapor diffusivity in the air, $D_i$ is the water vapor diffusivity for heavy isotope, and $n$ is a semi-empirical parameter (= 1/2 for fully turbulent condition). According to experimental results of Cappa et al. (2003), $D/D_i$ equals to 1.0319 for oxygen and 1.0164 for hydrogen. A representative value of $\rho_M/\rho$ is 0.32 (Yamanaka, 2009). Exactly

speaking $h_a$ is vapor pressure normalized by saturation vapor pressure at evaporating-surface temperature rather than air temperature, while we used relative humidity in common sense for convenient.

Finally, isotopic composition of total runoff, $\delta_Q$, can be obtained as:

$$\delta_Q = \frac{\sum_{i=1}^{5} q_H(i)\delta_w(i)}{Q} . \tag{20}$$

Values of $h_V(i)$ are determined by comparing predicted and observed $\delta_Q$. In the common type of tank model for predicting runoff only, $h_V(i)=0$ is assumed. In other words, $h_V(i)$ cannot be determined without tracers.

3.3.4 Estimation scheme for time-variant mean transit time (MTT)

To predict time-variant MTT using a calibrated/validated tank model, we introduce a virtual (or imaginary) "age" tracer in to the model (Such an approach has been already attempted by Goode (1996) for groundwater and Khatiwala et al. (2001) for Ocean). Concentration of this conservative and nonreactive tracer, $A(i)$, is computed by

$$\frac{dh(i)A(i)}{dt} = q_V(i-1)A(i-1) - \left[ f_T(i)T_r + q_V(i) + q_H(i) \right] A(i) - f_E(i)E_s A(i) + 1 \quad \text{for i} = 2 \text{ to } 5. \tag{21}$$

If we define the age as the elapsed time after the water entering to the catchment across the ground surface, then $A(1) = 0$ throughout the simulation period. Solving $A(i)$ under this boundary conditions, the value of $A(i)$ indicates the mean age of water in each tank, and MTT, $A_Q$, can be predicted as

$$A_Q = \frac{\sum_{i=1}^{5} q_H(i)A(i)}{Q} . \tag{22}$$

If we take a time step of 1 day, unit of $A(i)$ and $A_Q$, is day; the last term, which is unity, indicates the rate of ageing.

3.3.5 Estimation scheme for time-variant transit time distribution (TTD)

A scheme for predicting time-variant TTD is different from that for MTT. In this scheme, a virtual (or imaginary) "date" tracer is introduced to the model as pulse (or artificial) input at a time window rather than as continuous (or natural) input. Now we consider concentration of the date tracer, $D(i, j)$, in the $i$-th tank at the $j$-th time window. Although length of the time window is arbitrary, we took 30 days in the present study. The $D(i, j)$ at the $1^{st}$ tank can be assigned as follows,

$$D(1, j) = 1 \qquad \text{for } 30(j\text{-}1) < t < 30j, \qquad (23)$$

And then temporal evolution of $D(i,j)$ at each tank was computed by the following equation:

$$\frac{dh(i)D(i)}{dt} = q_V(i-1)D(i-1) - \left[f_T(i)T_r + q_V(i) + q_H(i)\right]D(i) - f_E(i)E_sD(i) \qquad \textit{for } i = 2 \text{ to } 5. \quad (24)$$

Also, we can compute concentration of the date tracer in total runoff water:

$$D_Q(j) = \frac{\sum_{i=1}^{5} q_H(i)D(i, j)}{Q}. \qquad (25)$$

The value of $D_Q(j)$ at a given time represents proportion of water that entered below the ground at $j$-th time window to the total runoff water at the time. For example (see Figure 3.10), when $t = 180$ (d), $D_Q(1)$ means proportion of water having transit times from 150 to 180 (d) and $D_Q(6)$ indicates that for transit times from 0 to 30 (d). On the other hand, when $t = 360$ (d), $D_Q(1)$ and $D_Q(6)$ reflect proportion of water with transit times from 330 to 360 (d), and from 180 to 210 (d), respectively. Consequently, $D_Q(j)$ corresponds to the TTD function and it is time-variant.

One problem is that the maximum transit time to be evaluated is limited by the simulation period. For instance, if we conduct 1-yr simulation, contribution from water having transit time longer than 1 year cannot be accounted for, even though total contribution of old waters with unknown transit time can be estimated. Therefore, contribution-weighted-mean of the transit time based on $D_Q(j)$ are not always equivalent to the MTT predicted by the another scheme given in section 3.3.4.

To obtain time-variant TTD, McGuire et al. (2007) employed similar approach. However, they evaluated it as temporal variation of a tracer concentration that is applied instantaneously at a given time in a model; it corresponds to a single $D_Q(j)$ time-series in our scheme. In this context, an approach of Botter et al. (2010) is the same. On the other hand, we evaluate TTD by combination of multiple $D_Q(j)$ time-series. Although this procedure is somewhat complicated, it should represent TTD more correctly for stream water sampled at a given time. The difference between these two approaches is examined in section 5.1. The main scheme could be referred as Figure 3.11, and the upper boundary setting for models as well as parameter period was shown as Figure 3.12.

Table 3.1 Annual average river discharge (m3/s) at outlet of each sub-catchments (SCs).

|    | 2002 | 2003 | 2004 | 2005 | 2006 | 2007 | 2008 | 2009 | 2010 |
|----|------|------|------|------|------|------|------|------|------|
| Y1 | --   | --   | 9.70 | 4.88 | 6.17 | 4.93 | 3.34 | --   | --   |
| Y2 | 9.44 | 13.79 | 14.51 | 8.19 | 10.27 | 8.81 | 9.23 | 7.10 | 14.15 |
| Y3 | --   | 29.87 | 31.19 | 20.67 | 26.14 | 19.50 | 17.27 | 21.71 | 26.10 |
| Y4 | --   | 18.03 | 21.26 | 14.26 | 13.11 | 13.28 | 12.49 | 13.28 | 16.33 |
| Y5 | 57.24 | 75.27 | 79.65 | 44.22 | 49.85 | 53.29 | 68.97 | 51.30 | 67.90 |
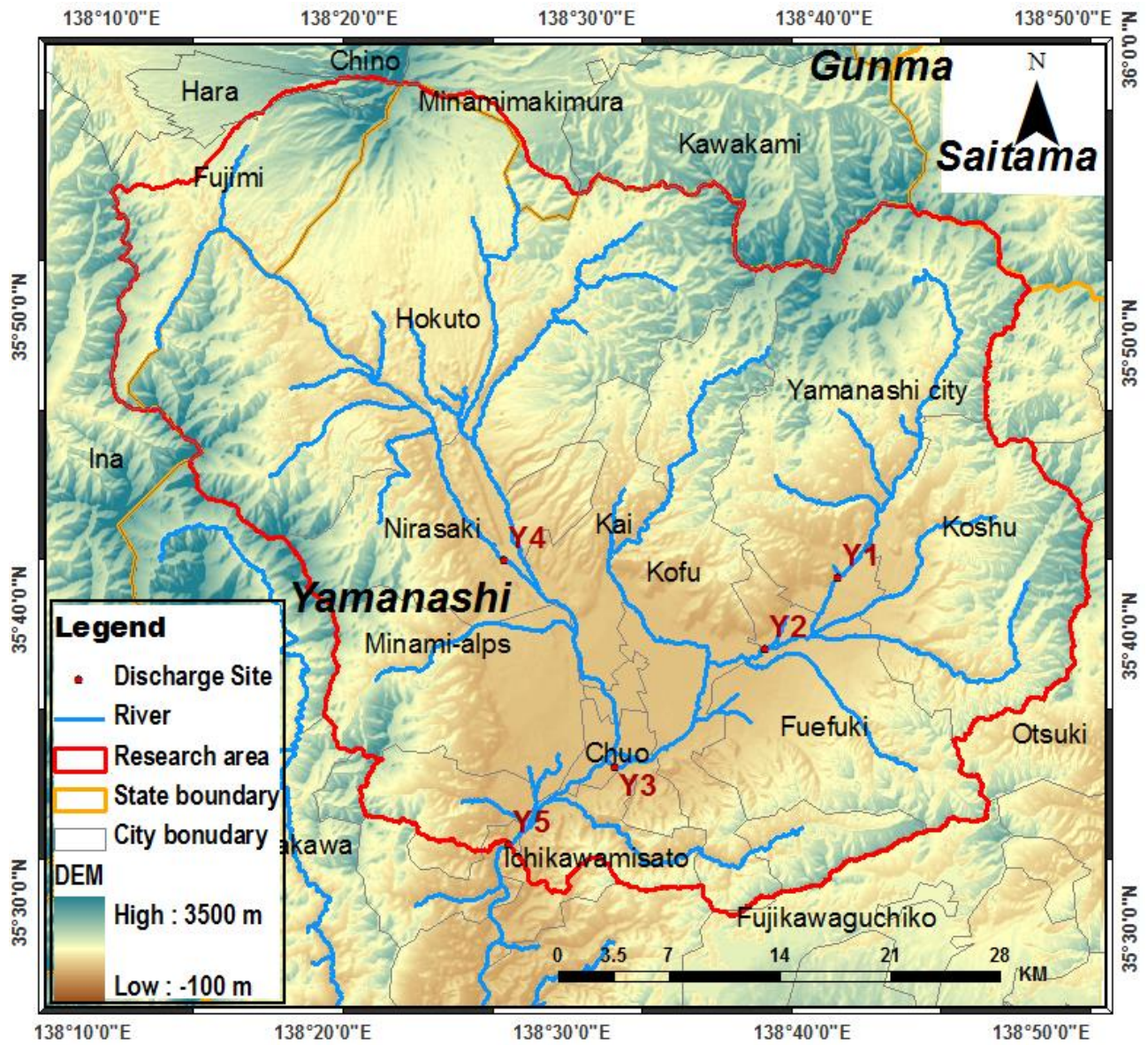
Figure 3.1 Map of study area.
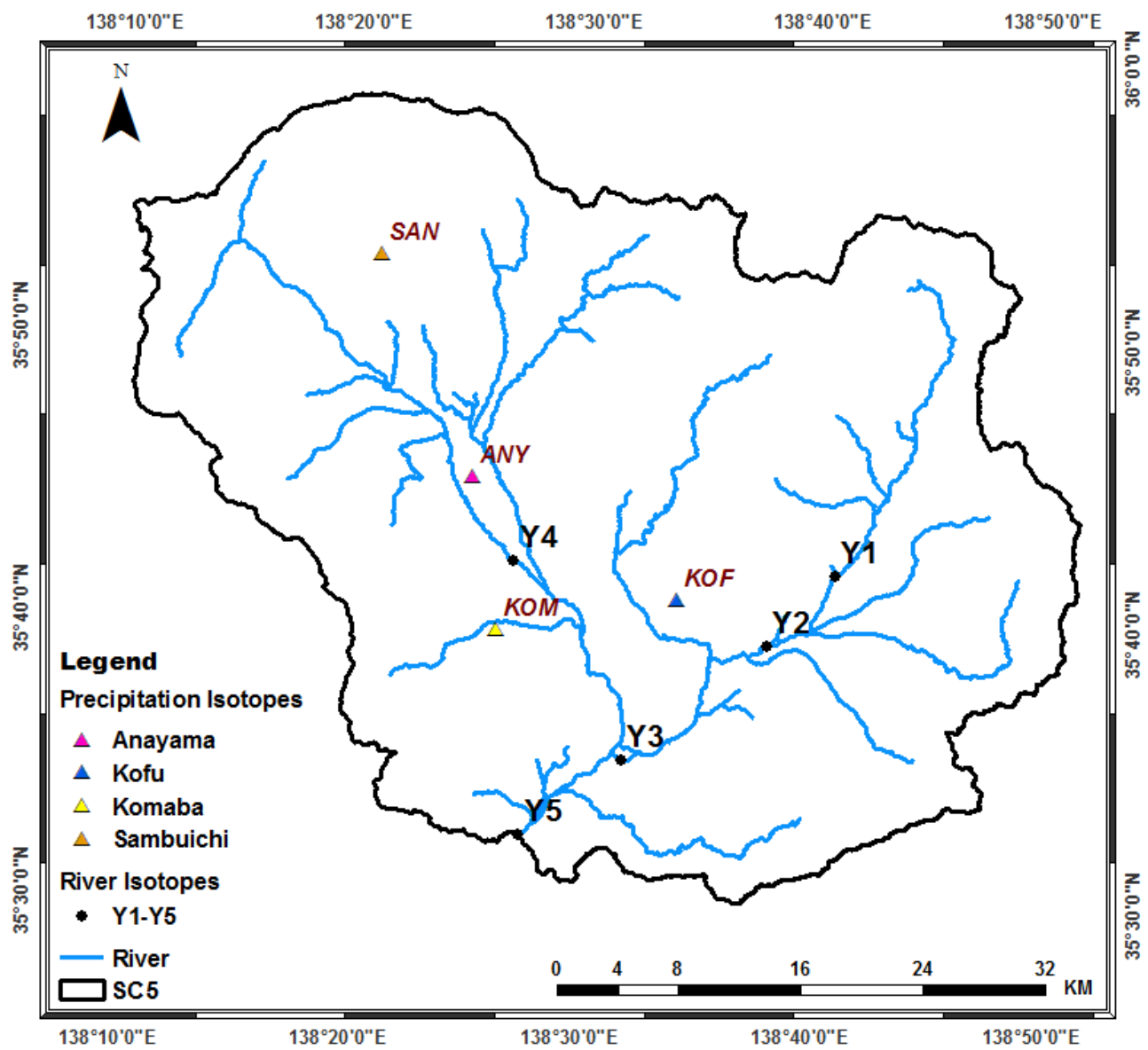
Figure 3.2 Locations of isotopic monitoring sites.
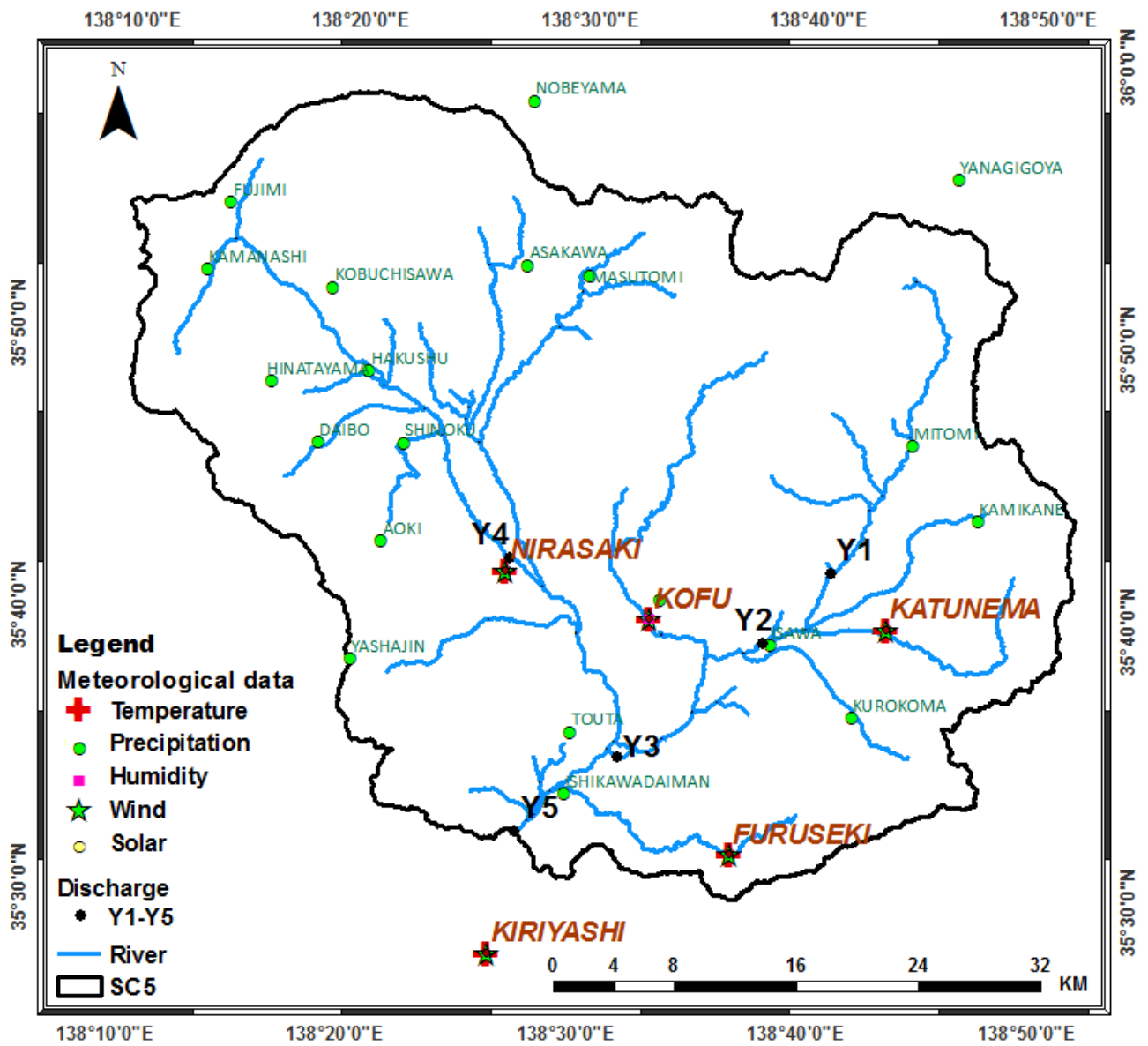
Figure 3.3 Locations of meteorological observation stations.
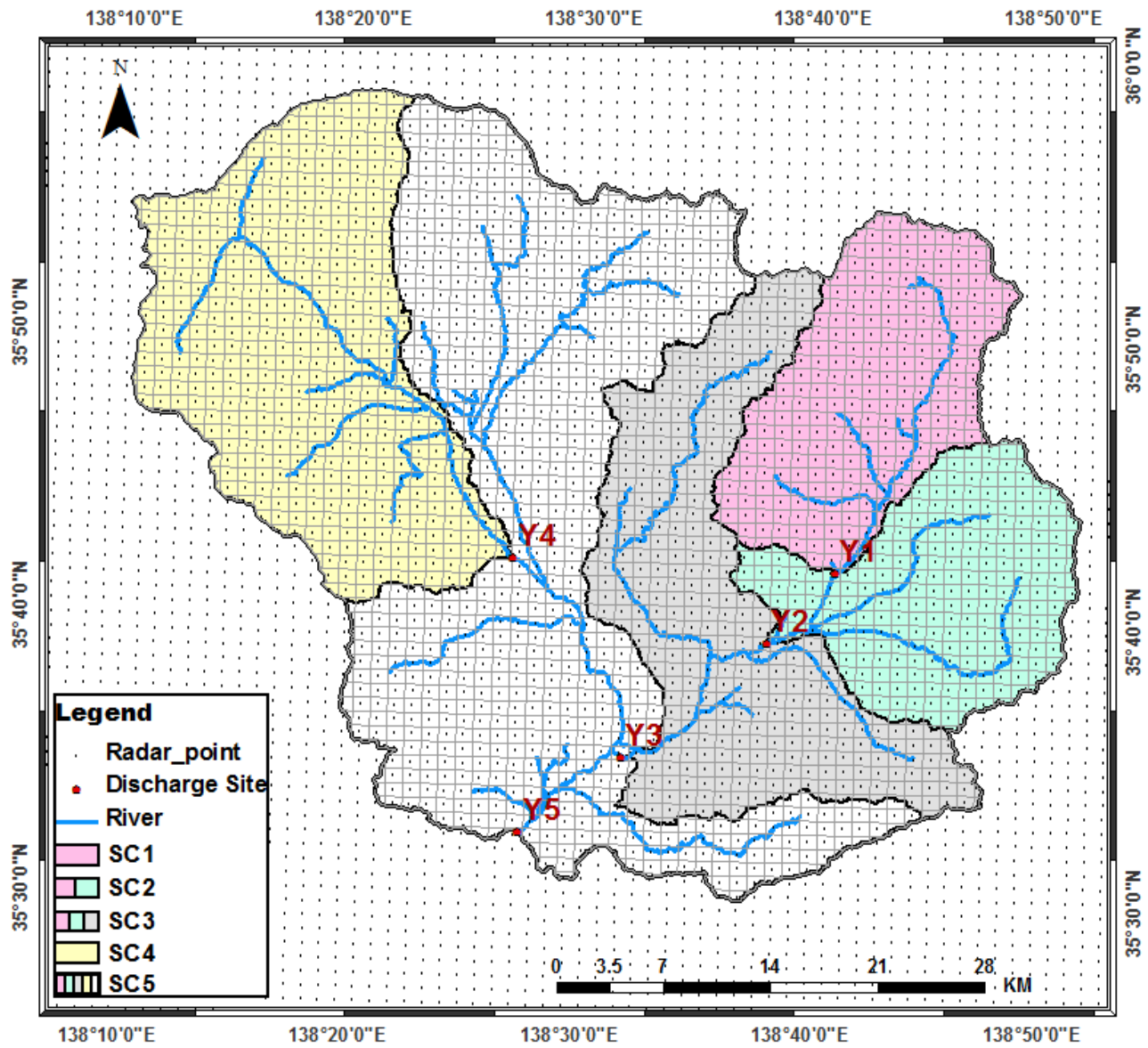
Figure 3.4 Gridding of Radar data.
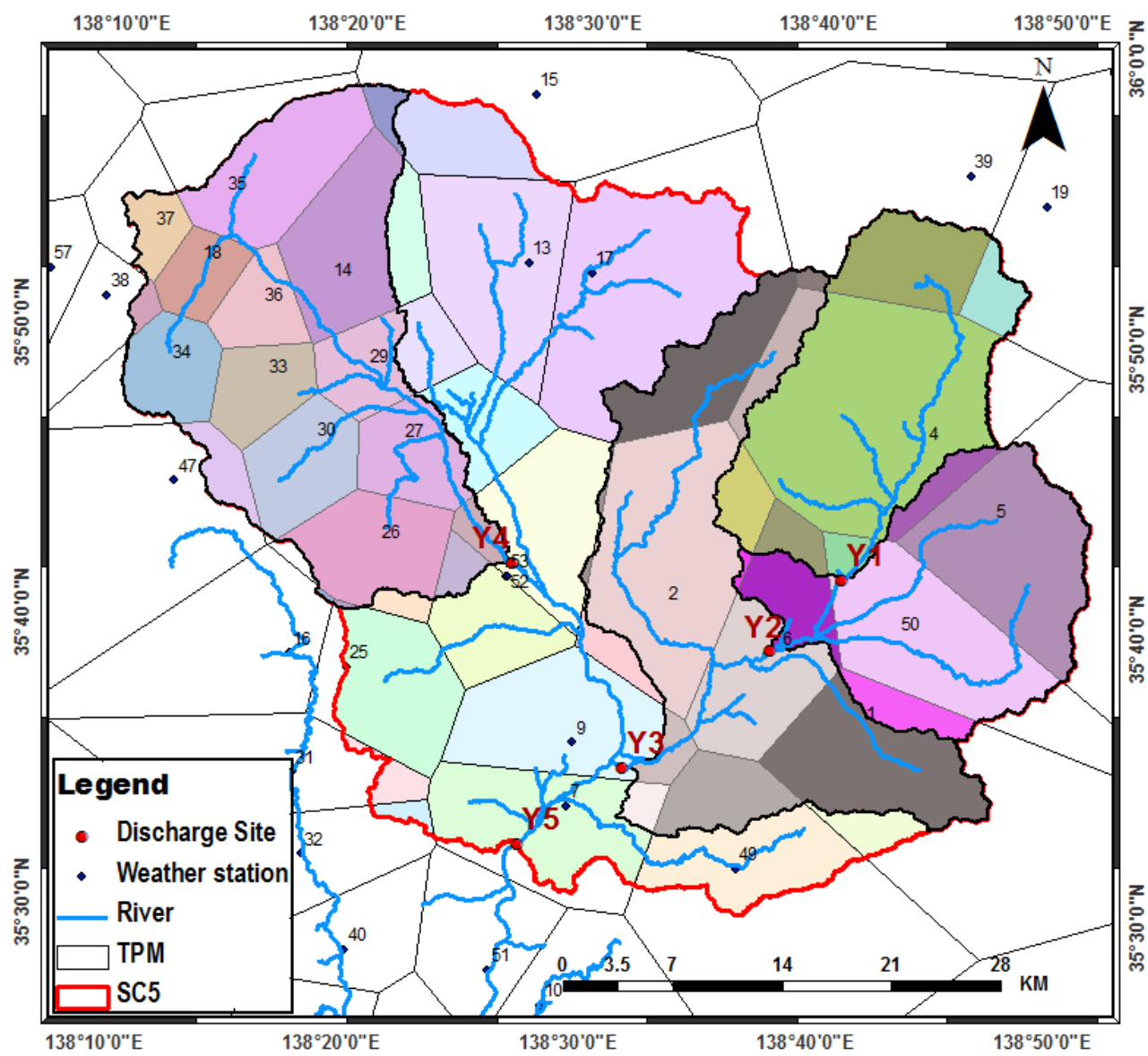
Figure 3.5 Thinessen polygons for estimating areal precipitation.
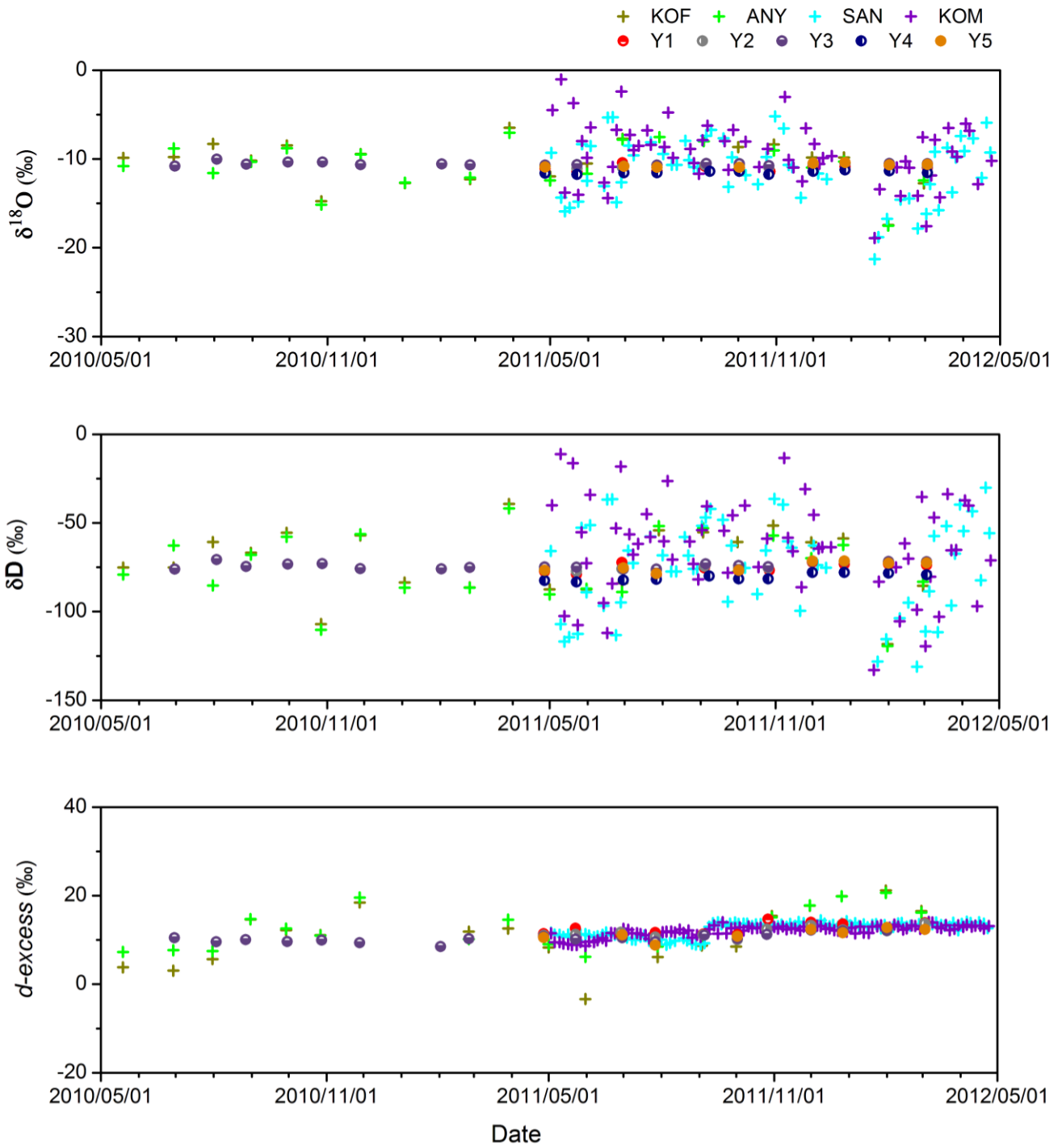
Figure 3.6 Time series of isotopic composition of precipitation (crosses) and river water (circles); (a) δD, (b) δ¹⁸O, and (c) d-excess.
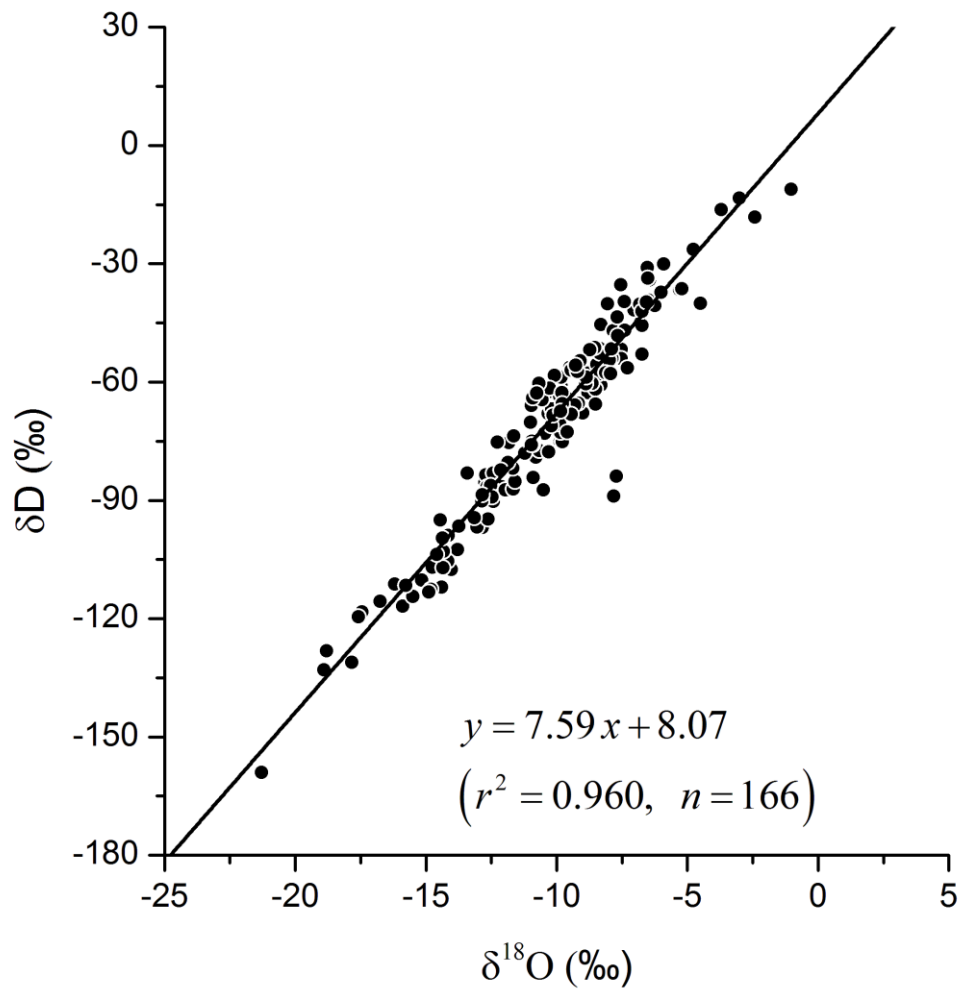
Figure 3.7 Relationship between $\delta^{18}O$ and $\delta D$ of precipitation.
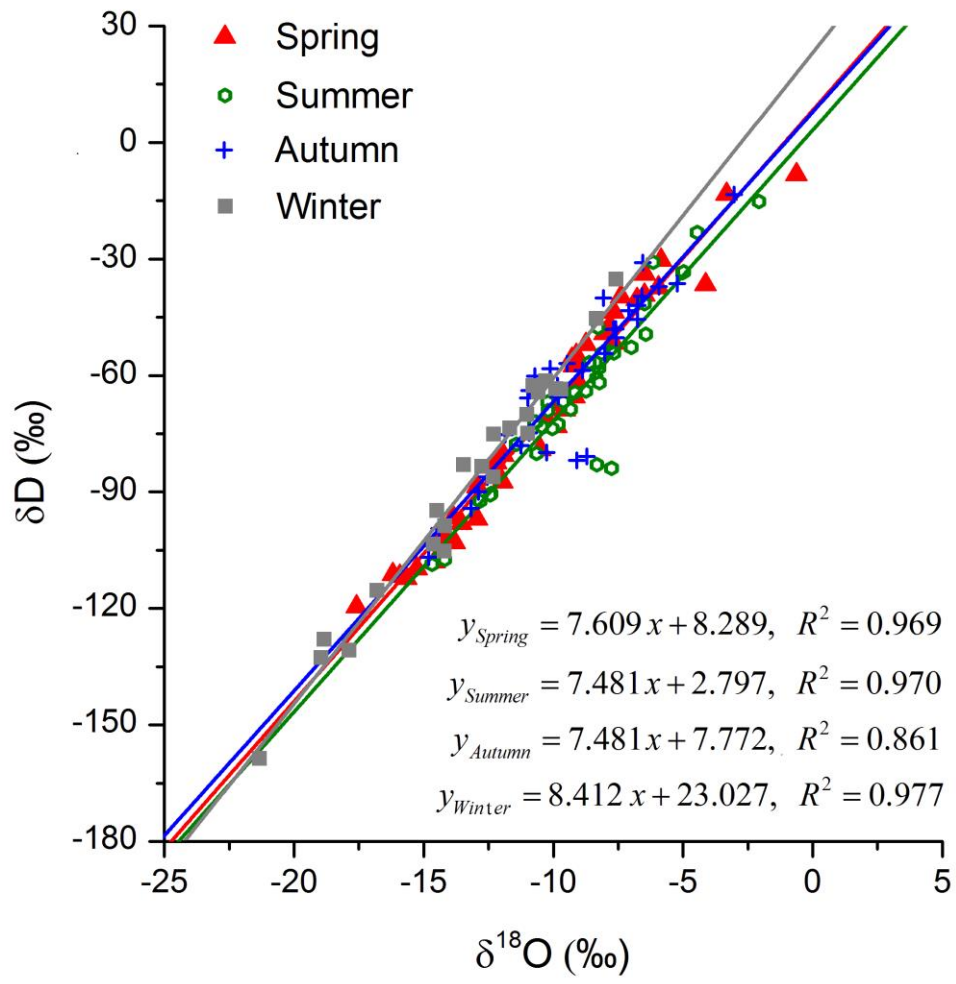
Figure 3.8 Relationship between δ<sup>18</sup>O and δD of precipitation in each season.

The equations shown in the figure:

$$y_{Spring} = 7.609\,x + 8.289, \quad R^2 = 0.969$$

$$y_{Summer} = 7.481\,x + 2.797, \quad R^2 = 0.970$$

$$y_{Autumn} = 7.481\,x + 7.772, \quad R^2 = 0.861$$

$$y_{Winter} = 8.412\,x + 23.027, \quad R^2 = 0.977$$
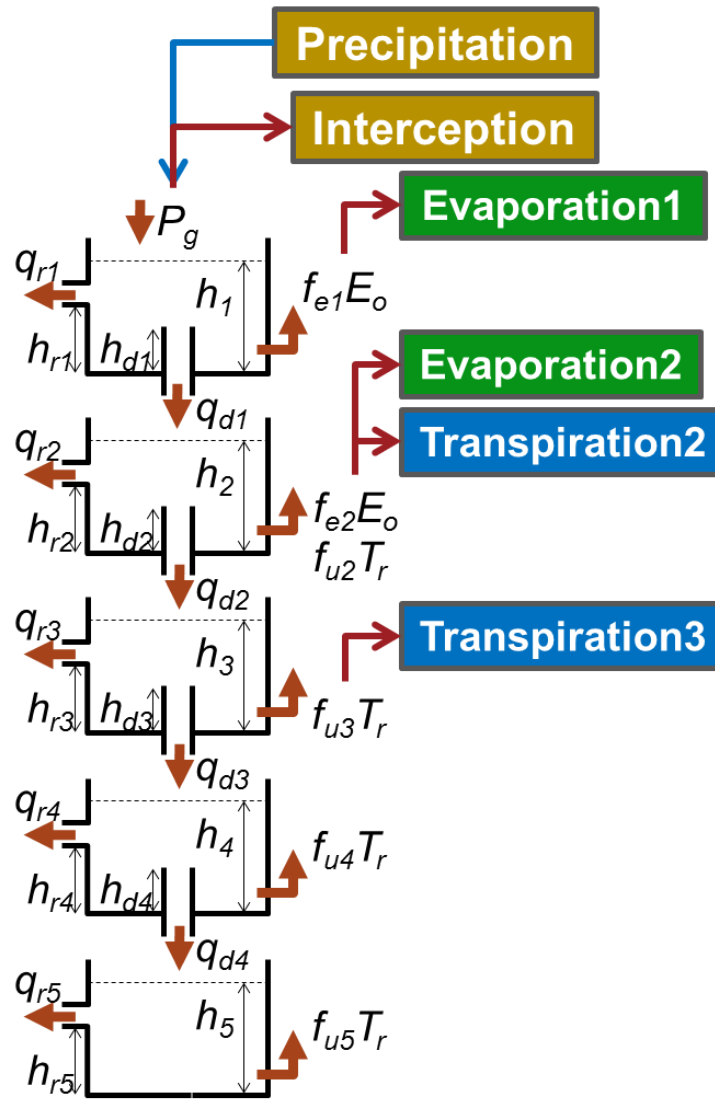
Figure 3.9 Structure of the tank model with five-layers.
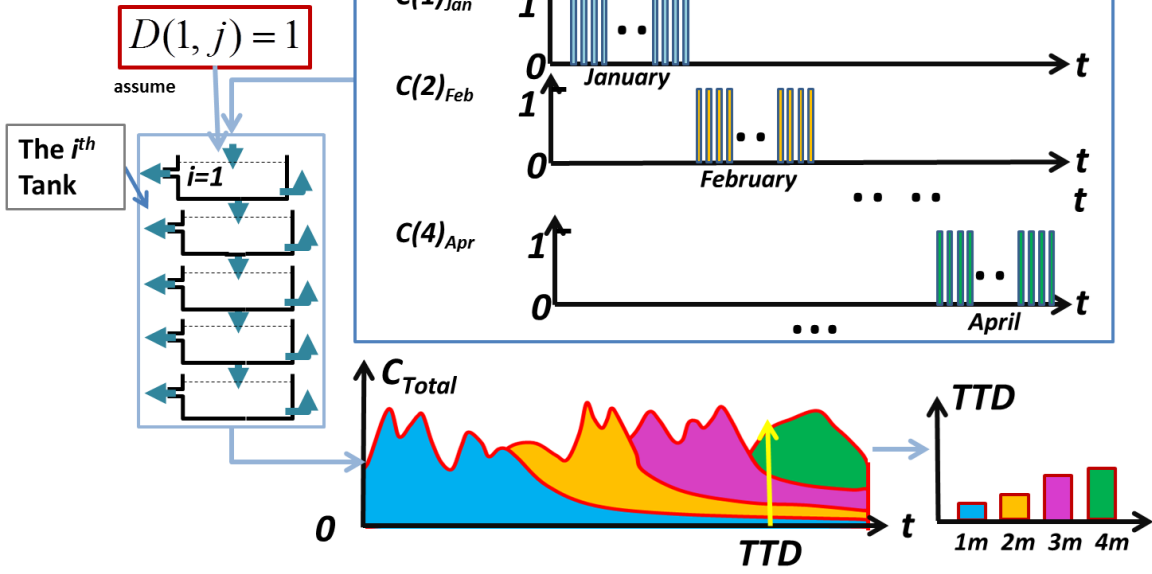
Figure 3.10 Schematic illustration of TTD calculation.
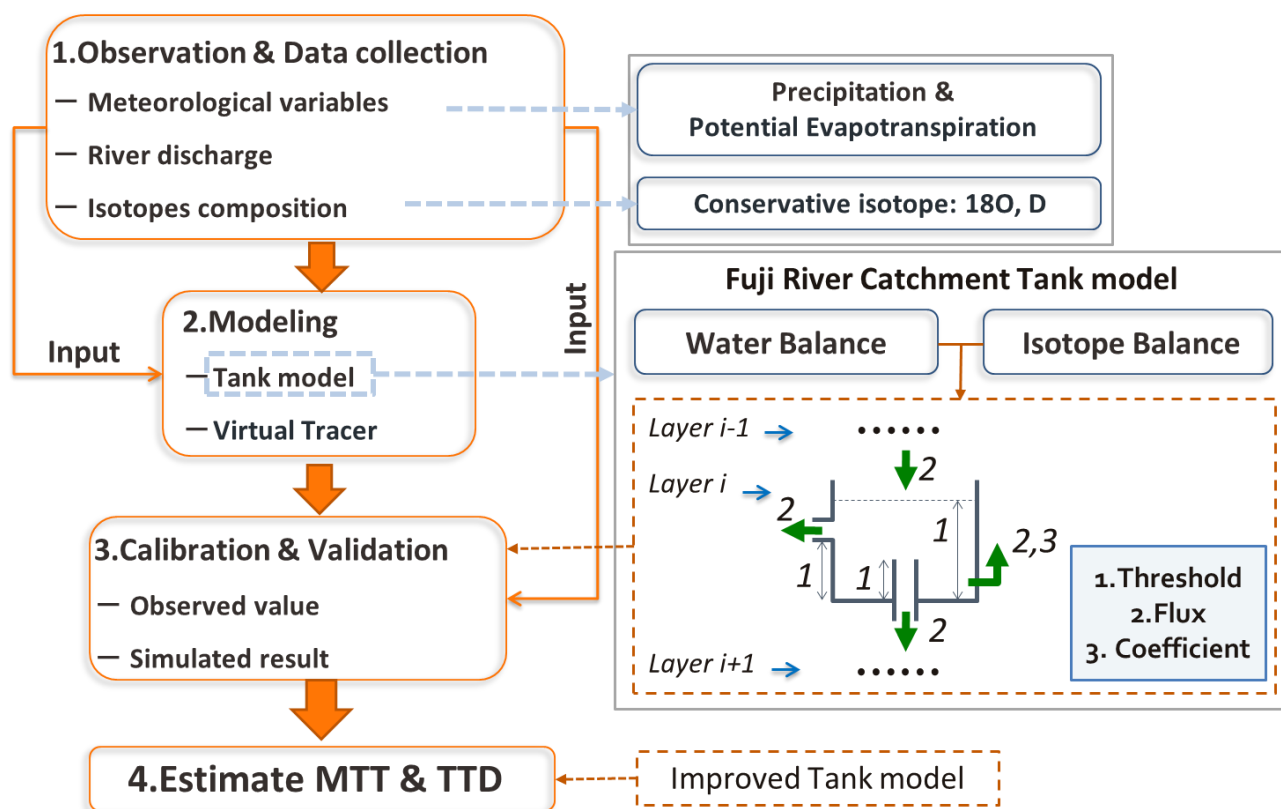
Figure 3.11 Flowchart of estimating MTT and TTD.
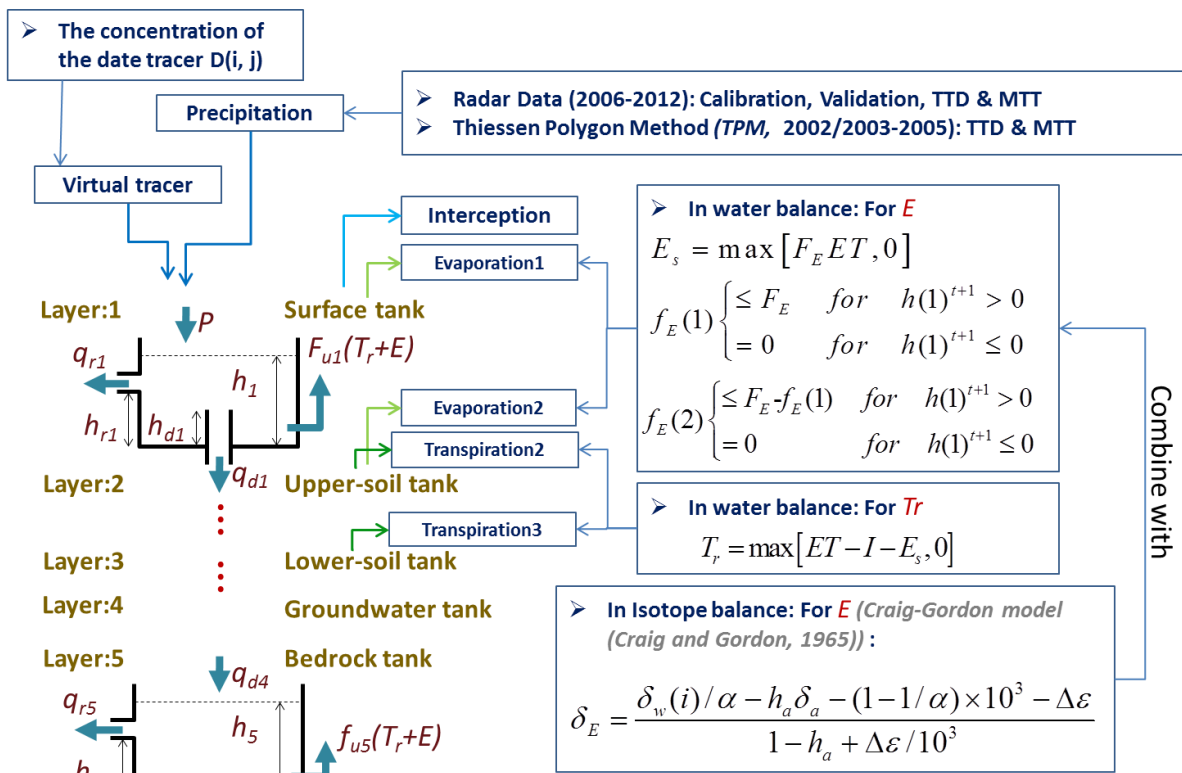
Figure 3.12 Upper boundary conditions of the model

The content of the figure includes:

➢ The concentration of the date tracer D(i, j)

Precipitation

➢ Radar Data (2006-2012): Calibration, Validation, TTD & MTT
➢ Thiessen Polygon Method *(TPM, 2002/2003-2005): TTD & MTT*

Virtual tracer

Interception

Evaporation1

Layer:1

$P$

Surface tank

$q_{r1}$ $h_1$ $F_{u1}(T_r+E)$

Evaporation2

Transpiration2

$h_{r1}$ $h_{d1}$

Layer:2 $q_{d1}$ Upper-soil tank

Transpiration3

Layer:3 Lower-soil tank

Layer:4 Groundwater tank

Layer:5 Bedrock tank

$q_{d4}$

$q_{r5}$ $h_5$ $f_{u5}(T_r+E)$

$h_{r5}$

➢ In water balance: For *E*

$$E_s = \max\left[F_E ET, 0\right]$$

$$f_E(1)\begin{cases} \leq F_E & for & h(1)^{t+1} > 0 \\ = 0 & for & h(1)^{t+1} \leq 0 \end{cases}$$

$$f_E(2)\begin{cases} \leq F_E\text{-}f_E(1) & for & h(1)^{t+1} > 0 \\ = 0 & for & h(1)^{t+1} \leq 0 \end{cases}$$

➢ In water balance: For *Tr*

$$T_r = \max\left[ET - I - E_s, 0\right]$$

➢ In Isotope balance: For *E (Craig-Gordon model (Craig and Gordon, 1965))* :

$$\delta_E = \frac{\delta_w(i)/\alpha - h_a\delta_a - (1-1/\alpha)\times 10^3 - \Delta\varepsilon}{1 - h_a + \Delta\varepsilon/10^3}$$

Combine with

# Chapter 4
# Results

## 4.1 Water balance

Hydrograph in water balance simulation for calculation and validation from 2006 to 2010 (from 2006 to 2008 for SC1 by considering the data condition) were shown in Figure 4.1. Table 4.1 shows the calibration and validation results evaluated by Nash-Sutcliffe Efficiency (NSE), which is a normalized statistic that determines the relative magnitude of the residual variance ("noise") compared to the measured data variance ("information") (Nash and Sutcliffe, 1970). The NSE is represented by the following equation.

$$NSE = 1 - \left[ \sum_{i=1}^{n} \left( Y_i^{obs} - Y_i^{sim} \right)^2 / \sum_{i=1}^{n} \left( Y_i^{obs} - Y_i^{mean} \right)^2 \right] \qquad (1)$$

where Y is the runoff, and super scripts obs, sim and mean denote observed, simulated and observed mean values, respectively. When NSE equal to 1, the result is the best. On the contrast, when NSE is smaller than 1 and approaching to 0, simulation is getting worse. If the NSE is around or more than 0.4, one can judge the performance is acceptable. The calibration and validation were carried out with the goal of the best agreement between simulated and observed runoff at the outlet of each SCs. After the determination of parameters in the calibration period, one can examine the result in the validation period (Table 4.1). The optimized simulation shown in Figure 4.1 exhibited a good agreement with observed runoff. For getting better-optimized combination of model parameters,

20,635 times of simulations were carried out. Optimized parameters settings finally obtained are summarized in Table 4.2.

For SC1 the model was calibrated within the period of 1$^{st}$ Jan. 2006 and 31$^{st}$ Dec. 2006, and the period for validation is between 1$^{st}$ Jan. 2007 to 31$^{st}$ Dec. 2009. For SC2-SC5 the calibration period is between 1$^{st}$ Jan. 2006 and 31$^{st}$ Dec. 2007, and the validation period is between 1$^{st}$ Jan. 2008 to 31$^{st}$ Dec. 2010, as shown in Table 4.1. The simulated results fit the observed data acceptably (Figure 4.1), where most of the NSE is higher than 0.3; in case of SC5, NSE is higher than 0.6 in calibration period and around 0.5 in validation. For all of the SCs water balance simulation, deflected discharge from observed data shown in SC2 in 2009 and others, as shown in Figure 4.1. The observed discharge from SC2 is relatively lower than those from other SCs, especially in 2009.

The long-term mean values of hydrological variables for each SC are summarized in Table 4.3. Especially for the value of evaporation (*E*) and transpiration (*Tr*) could be considered as small amount comparing to the precipitation amount. Long-term average runoff both for observed and simulated values could be checked from Table 4.3. At the same time, storage of each layer of each SC has been calculated as the thickness of each tank. Total storage shown in Table 4.4 was considered as the sum of the storage over all layers.

## 4.2 Isotope balance

Transit time is expected to depend upon not only water flow but also water storage within the catchment (or tank in the model). Water balance simulation or simulated discharge is sensitive to the change in water storage and less sensitive to the water storage itself. On the other hand, isotope balance simulation is more sensitive to water storage. Therefore, better performance of isotope balance simulation can be linked to better estimation of transit time.

The river water $\delta^{18}$O and $\delta$D were relatively stable than the precipitation isotopes data, as shown in Figures 4.2 to 4.6. The calibration and validation period for isotopes simulation were slightly different among SCs as summarized in Table 4.5. The table shows RMSE of simulated $\delta^{18}$O and $\delta$D. The RMSE values for $\delta^{18}$O are smaller than those for $\delta$D. By considering the total performance of $\delta^{18}$O and $\delta$D, combined RMSE (=(RMSE_$\delta$D/8+RMSE_$\delta^{18}$O)/2) was used for choosing the optimal results. The combined RMSE of SC3 and SC5 are smaller than other SC. On the contrast, the combined RMSE of SC4 is 1.08. For SC3, simulated results well corresponds to observed data, not only for $\delta^{18}$O and $\delta$D, but also for d-excess (Figure 4.4). However, in most SCs and variables, non-negligible differences between the simulated and observed values still exist, probably because of spatial heterogeneity of the isotope compositions of precipitation.

## 4.3 Spatial and temporal variation of MTT

Figures 4.7 to 4.11 represent the MTT variations with precipitation at SC1 to SC5. Daily results were shown for about ten years, as well as monthly results. As precipitation happen, MTT were changed significantly. The MTT ranges from several years to decades. In case of SC1 and SC4, the MTT are all lower than the other SCs, and the ranges of MTT at SC1 were mainly from 2.6 yr to 13.0 yr, which with 8.0 yr as average value. At SC4, MTT were mainly between 6.8 yr to 12.5 yr. At SC2, the ranges of MTT variation are from 5.4 yr to 31.4 yr. At SC5, the minimum value is 5.1 yr and the maximum value is 31.5 yr. The MTTs at SC2 and SC5 tend to be greater than other SCs, especially during dry periods. The amplitudes of MTT variations were different for each SC; the coefficient of variation (CV) at SC2 and SC5 are greater than the other SCs (Table 4.6). At SC4 with the smallest variation, CV was about 14.55%. The ranges at SC3 are between 6.7 yr to 25.5 yr, with intermediate values of MTT as compared to the other SCs.

For monthly results, more obviously trend of MTT variation associated with precipitation can be seen from lower panels of Figures 4.7 to 4.11. For example, as precipitation amount is greater, MTT is smaller, and high MTT exists during relatively dry periods, vice versa. MTT values tend to be higher during dry periods and smaller during wet periods. The amplitudes of the change are different for each SC; the amplitude at SC4 is the smallest. The comparison of monthly MTT and precipitation showed more obvious relationships than daily values, probably because random noise in the MTT-precipitation relationship is cancelled out by averaging procedures.

LAMTT in winter, which could be considered as typical value in the dry period, tends to be higher than in the other seasons (Table 4.6). On the contrast, LAMTT in summer (i.e., rainy season) showed smallest value.

## 4.4 Spatial and temporal variation of TTD

Two examples of estimated TTD are shown in Figure 4.12. The first case (4 Sep. 2011) reflects situations just after a large storm event. The peak of transit time is located on the left-hand edge; the youngest component (i.e., transit time < 30 days) is the most dominant contributor, accounting for more than 20% of total river water. The shape of the TTD is similar to an exponential form, while there are 1-yr periodic variations, probably due to seasonal variations in precipitation. Conversely, the second case (17 Feb. 2011) reflects low flow conditions during a long drought period. The peak in transit time shifts toward a greater (i.e., older) time domain and the peak height is small (< 0.5%). The shape of the TTD for this case is similar to neither exponential nor any other known functions. Consequently, it is clear that the TTD is highly variable over time, reflecting that the history of precipitation variation and the assumption of idealized TTD functions, which have often been applied in previous studies, are not appropriate.

In the present study, TTD computation was performed for six years (2006−2011), so that components older than six years (= 2,190 days) cannot be explicitly evaluated. Because the MTT extends to more than 20 years, Figure 4.12 does not show the entire range of TTD. In other words, integration of the TTD shown in Figure 4.12 cannot give the actual MTT. Therefore, the use of a TTD estimation scheme is not recommended for the purpose of MTT estimation.

Figure 4.13 shows the comparison of TTD between five SCs. Not only the cases for the SC3, but also for the cases of the other SCs, the difference of TTD due to wetness conditions mentioned above can be found. At SC1 and SC3, younger components of water account for relatively higher percentage than in the other SC for both wet and dry cases.

Table 4.1 Evaluation for simulations of water balance.

| | SC1 | | SC2 | | SC3 | | SC4 | | SC5 | |
|---|---|---|---|---|---|---|---|---|---|---|
| | Period | NSE | Period | NSE | Period | NSE | Period | NSE | Period | NSE |
| Calibration | *2006* | 0.2711 | *2006-2007* | 0.4342 | *2006-2007* | 0.3746 | *2006-2007* | 0.5019 | *2006-2007* | 0.6025 |
| | *2007* | 0.343 | *2008* | 0.326 | *2008* | 0.404 | *2008* | 0.064 | *2008* | 0.570 |
| Validation | *2008* | 0.010 | *2009* | 0.058 | *2009* | 0.217 | *2009* | 0.403 | *2009* | 0.342 |
| | | | *2010* | 0.289 | *2010* | 0.297 | *2010* | 0.311 | *2010* | 0.487 |

Table 4.2 Parameters setting for each layer.

| | SC1 | SC2 | SC3 | SC4 | SC5 |
|---|---|---|---|---|---|
| *Kr1* | 7.5E-06 | 7.3E-06 | 6.2E-05 | 4.0E-06 | 5.3E-06 |
| *Kr2* | 1.6E-06 | 4.2E-06 | 6.7E-07 | 3.7E-07 | 1.9E-06 |
| *Kr3* | 1.0E-07 | 4.5E-07 | 8.6E-08 | 7.5E-08 | 2.5E-07 |
| *Kr4* | 2.6E-08 | 4.8E-08 | 6.4E-08 | 8.0E-09 | 3.0E-08 |
| *Kr5* | 2.0E-09 | 5.4E-08 | 8.7E-08 | 6.8E-08 | 1.1E-09 |
| *Kd1* | 1.3E-05 | 1.1E-05 | 5.8E-05 | 1.5E-05 | 8.0E-06 |
| *Kd2* | 2.5E-06 | 7.5E-05 | 8.2E-07 | 1.5E-06 | 7.7E-06 |
| *Kd3* | 3.9E-07 | 8.1E-08 | 2.1E-06 | 8.5E-07 | 1.2E-07 |
| *Kd4* | 4.7E-08 | 3.0E-07 | 5.7E-09 | 4.6E-08 | 1.3E-08 |
| *Hr1* | 2.5 | 14.3 | 3.0 | 6.1 | 5.3 |
| *Hr2* | 22.0 | 11.3 | 5.0 | 15.9 | 19.5 |
| *Hr3* | 73.0 | 30.0 | 140.0 | 85.8 | 13.3 |
| *Hr4* | 338.6 | 29.5 | 230.0 | 190.0 | 183.3 |
| *Hr5* | 617.3 | 20.9 | 50.0 | 188.7 | 425.8 |
| *Hd1* | 10.4 | 21.4 | 8.0 | 10.0 | 12.4 |
| *Hd2* | 30.0 | 59.8 | 15.0 | 18.1 | 42.5 |
| *Hd3* | 85.0 | 80.0 | 210.0 | 101.1 | 42.9 |
| *Hd4* | 369.0 | 90.0 | 300.0 | 290.0 | 203.3 |
| *Hd5* | 671.7 | 420.2 | 350.0 | 308.7 | 454.3 |

Table 4.3 Area and long-term* mean hydrological variables characterizing each SC

| Variables** | SC1 | SC2 | SC3 | SC4 | SC5 |
|---|---|---|---|---|---|
| Area ($km^2$) | 268.03 | 518.54 | 905.70 | 480.27 | 2172.72 |
| Total depth of water over all tanks in the model (m) | 62.88 | 99.60 | 131.09 | 103.53 | 223.85 |
| $P$ (mm/d) | 3.658 | 3.223 | 3.328 | 4.073 | 3.803 |
| $ET$ (mm/d) | 3.117 | 2.852 | 3.123 | 3.928 | 3.129 |
| $E$ (mm/d) | 0.075 | 0.106 | 0.090 | 0.067 | 0.092 |
| $Tr$ (mm/d) | 0.925 | 1.316 | 0.936 | 1.031 | 0.918 |
| $I$ (mm/d) | 0.600 | 0.429 | 0.393 | 0.615 | 0.445 |
| $Q_{obs}$ (mm/d)* | 5.806 | 10.610 | 24.279 | 15.316 | 60.862 |
| $Q_{sim}$ (mm/d) | 7.454 | 16.733 | 30.637 | 17.259 | 78.392 |
| $P - Q_{sim}$ (mm/d) | 1.255 | 0.435 | 0.405 | 0.969 | 0.686 |
| $ET/(P - Q_{sim})$ (%) | 40.275 | 15.251 | 12.974 | 24.657 | 21.909 |

* 2004-2012 for SC1, 2002-2012 for SC2, 2003-2012 for SC3, 2003-2012 for SC4, and 2002-2012 for SC5.

** $P$ is the precipitation, $ET$ is the evapotranspiration, $E$ is the soil evaporation, $Tr$ is the transpiration, $I$ is the interception, $Q_{obs}$ is the observed runoff, $Q_{sim}$ is the simulated runoff

Table 4.4 Storage of water in each layer and total storage.

|  | SC1 | SC2 | SC3 | SC4 | SC5 |
|---|---|---|---|---|---|
| Layer1 (m) | 0.55 | 3.15 | 0.77 | 0.61 | 11.05 |
| Layer2 (m) | 14.57 | 13.68 | 18.03 | 24.51 | 19.12 |
| Layer3 (m) | 3.37 | 21.54 | 13.90 | 21.30 | 12.44 |
| Layer4 (m) | 8.10 | 15.02 | 25.89 | 12.34 | 21.21 |
| Layer5 (m) | 36.29 | 46.21 | 72.50 | 44.77 | 160.03 |
| Total (m) | 62.88 | 99.60 | 131.09 | 103.53 | 223.85 |

Table 4.5 Evaluation for simulations of isotope balance.

| | | Period | RMSE $(\delta^{18}O)$ | RMSE $(\delta D)$ | RMSE $((\delta D/8 + \delta^{18}O)/2)$ |
|---|---|---|---|---|---|
| SC1 | Calibration | 2011.04-2011.07 | 0.54 | 4.6 | 0.56 |
| | Validation | 2011.08-2012.03 | 0.57 | 1.8 | 0.40 |
| SC2 | Calibration | 2011.04-2011.10 | 1.00 | 7.1 | 0.80 |
| | Validation | 2011.10-2012.03 | 0.30 | 3.2 | 0.35 |
| SC3 | Calibration | 2010.05-2011.07 | 0.23 | 1.6 | 0.24 |
| | Validation | 2011.08-2012.03 | 0.24 | 2.4 | 0.22 |
| SC4 | Calibration | 2011.05-2011.10 | 1.17 | 8.8 | 1.08 |
| | Validation | 2011.11-2012.03 | 0.17 | 1.1 | 0.16 |
| SC5 | Calibration | 2011.04-2011.10 | 0.21 | 1.9 | 0.23 |
| | Validation | 2011.10-2012.03 | 0.27 | 3.6 | 0.36 |

Table 4.6 Long-term statistics of estimated mean transit time.

| | SC1 | SC2 | SC3 | SC4 | SC5 |
|---|---|---|---|---|---|
| Average (yr) | 7.96 | 14.20 | 16.54 | 9.89 | 14.62 |
| Minimum (yr) | 2.56 | 5.39 | 6.70 | 6.84 | 5.05 |
| Maximum (yr) | 12.96 | 31.38 | 25.49 | 12.51 | 31.47 |
| SD* (yr) | 2.17 | 5.78 | 3.91 | 1.44 | 6.01 |
| CV** (%) | 27.26 | 40.69 | 23.62 | 14.55 | 41.11 |
| $LAMTT_{Spring}$ (yr) | 7.99 | 12.81 | 16.67 | 9.81 | 14.49 |
| $LAMTT_{Summer}$ (yr) | 6.80 | 10.60 | 13.76 | 8.59 | 10.60 |
| $LAMTT_{Autumn}$ (yr) | 7.22 | 12.47 | 14.76 | 9.78 | 12.12 |
| $LAMTT_{Winter}$ (yr) | 9.67 | 20.82 | 21.00 | 11.41 | 21.03 |

*SD: Standard deviation;

**CV: Coefficient of variation
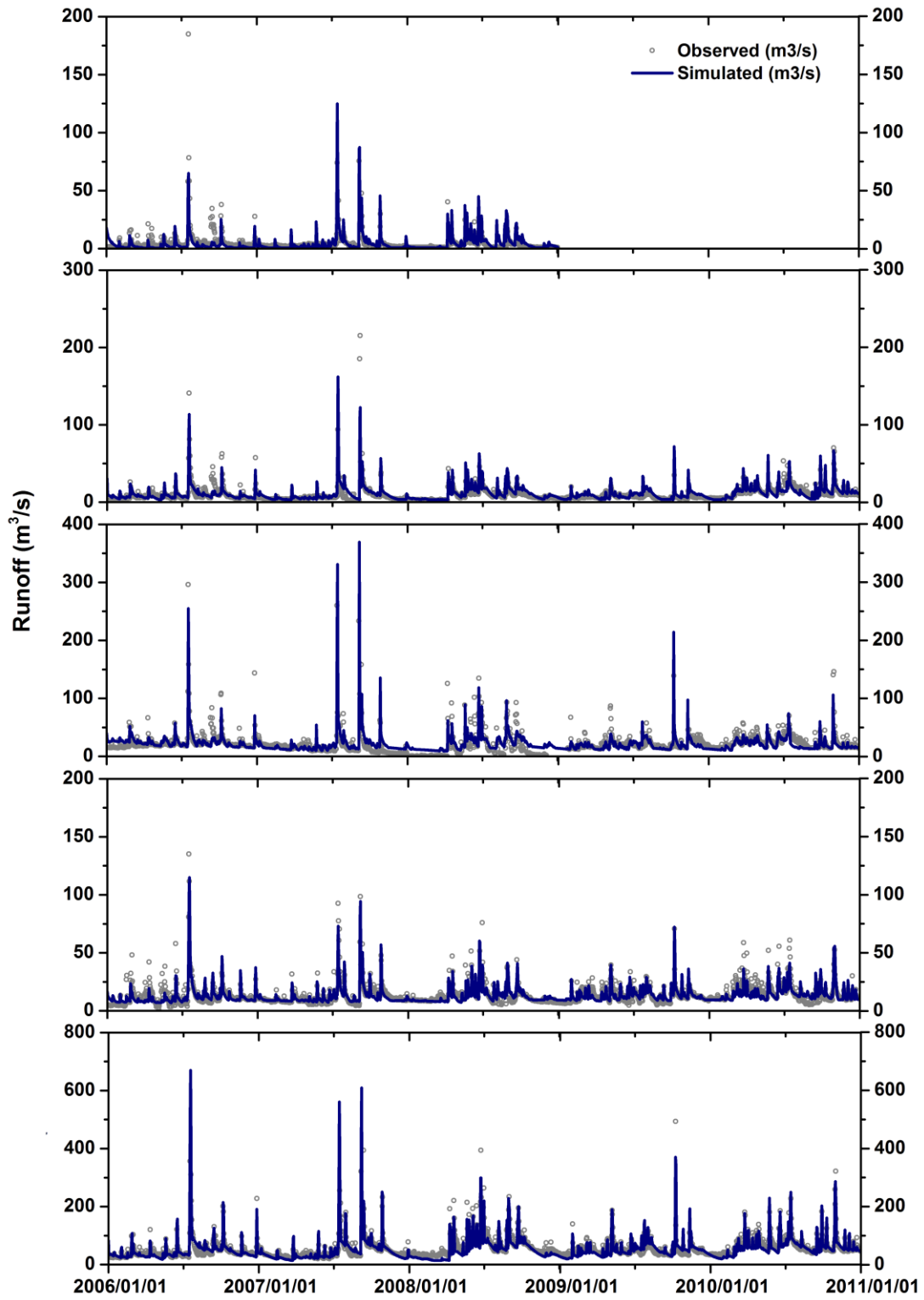
Figure 4.1 Comparison between observed and simulated hydrographs for both calibration and validation phases.

50

Figure 4.2 Comparison between observed and simulated isotope compositions for both calibration and

validation phases in SC1.

Figure 4.3 Comparison between observed and simulated isotope compositions for both calibration and

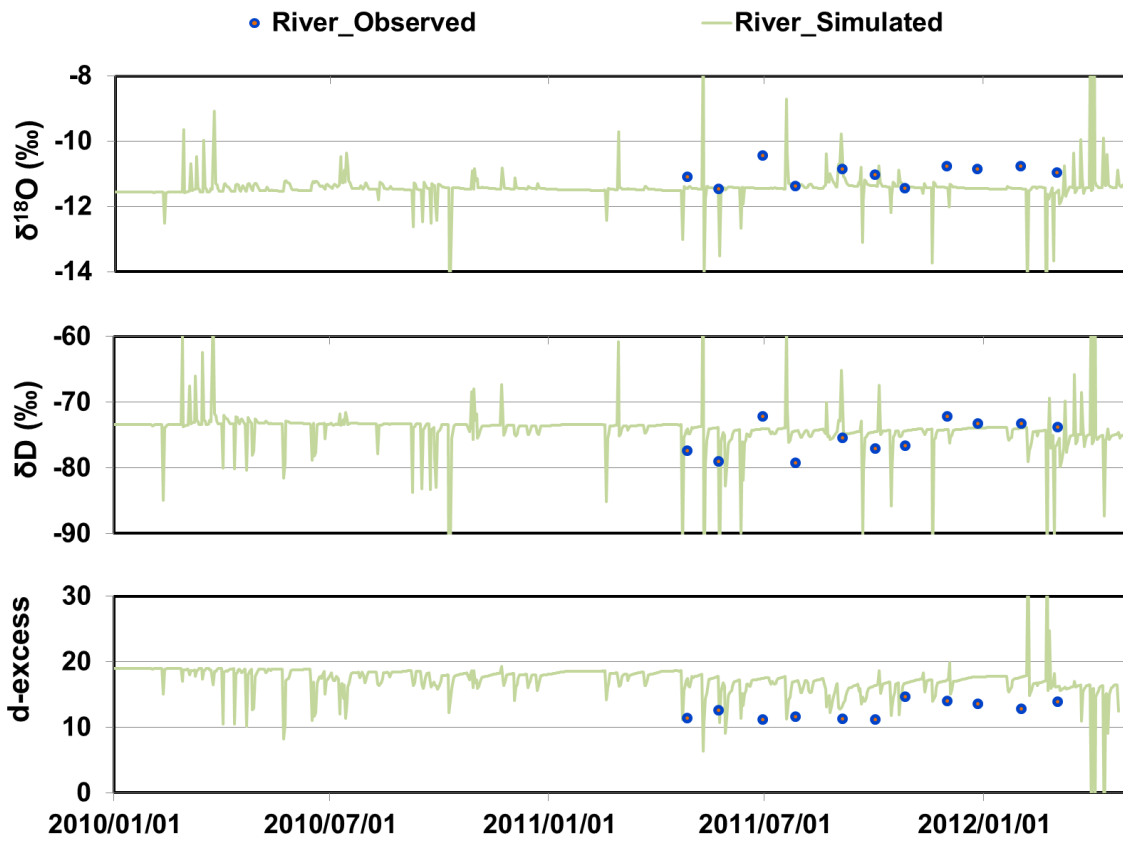validation phases in SC2.
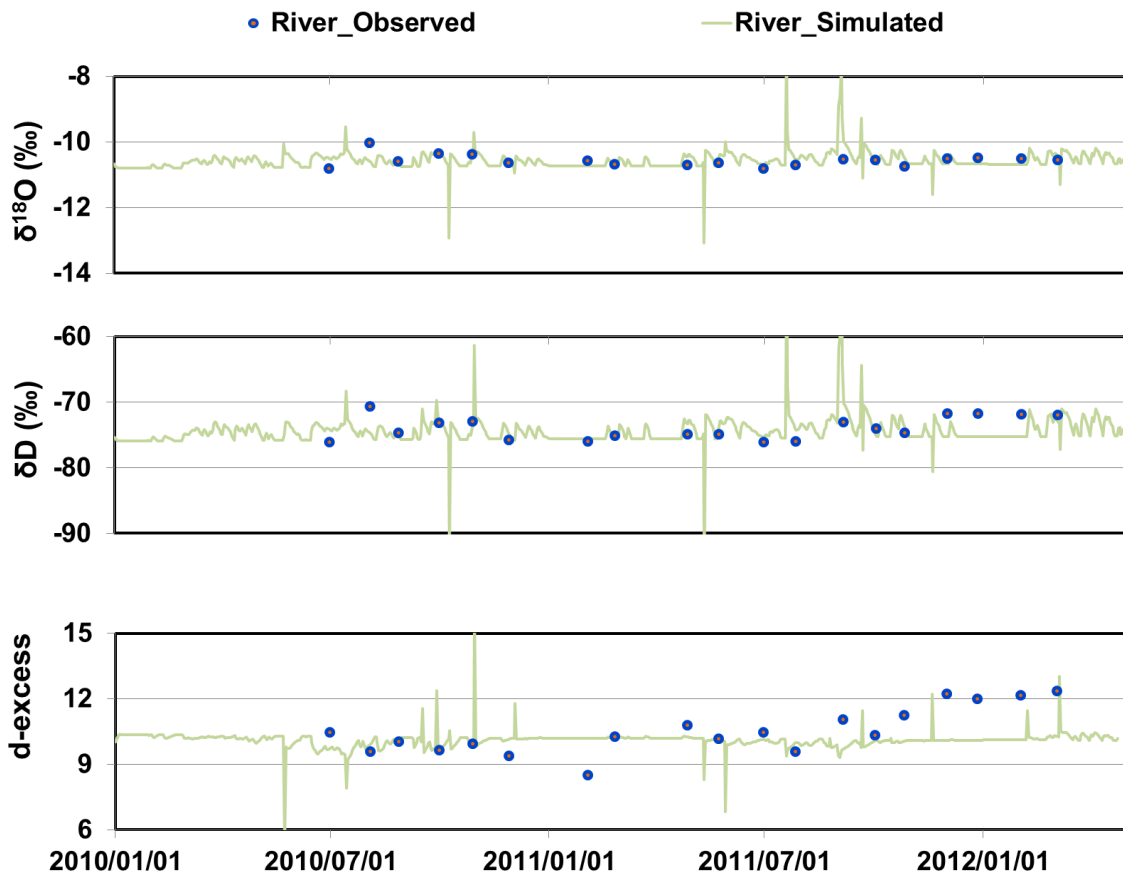
Figure 4.4 Comparison between observed and simulated isotope compositions for both calibration and

validation phases in SC3.
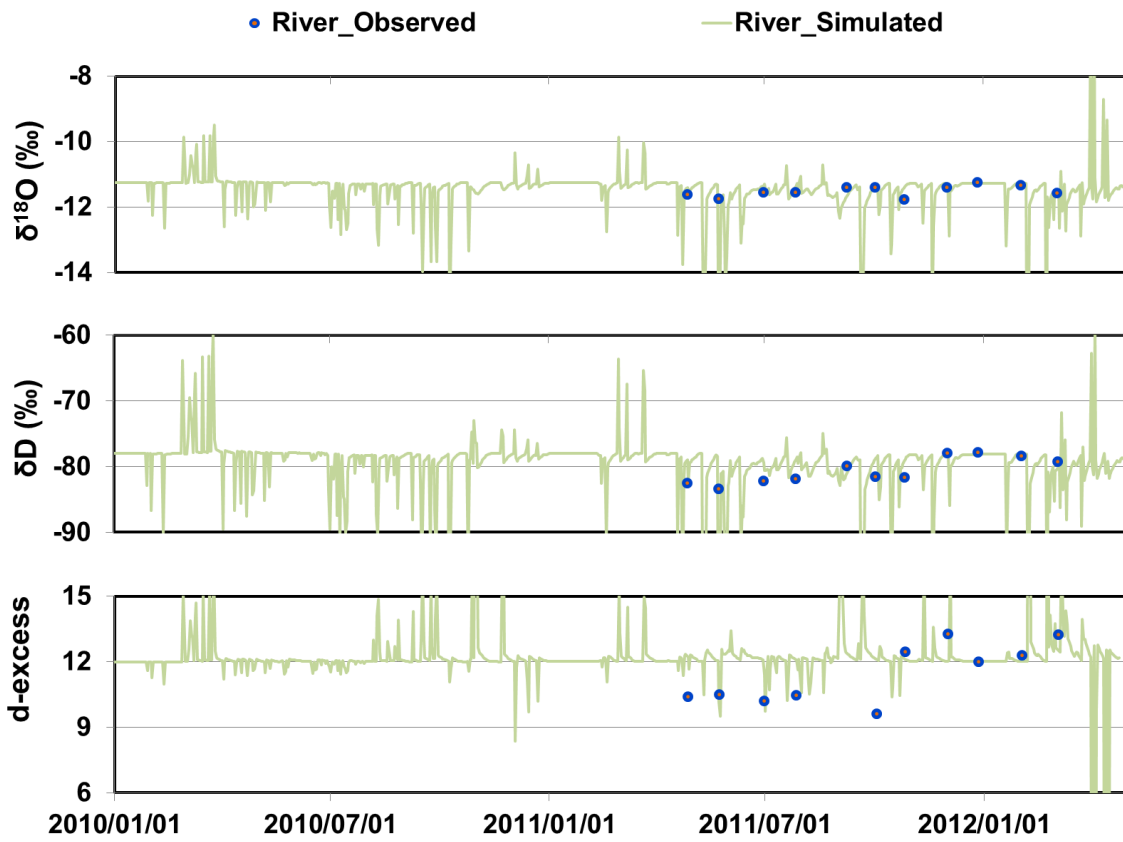
Figure 4.5 Comparison between observed and simulated isotope compositions for both calibration and

validation phases in SC4.
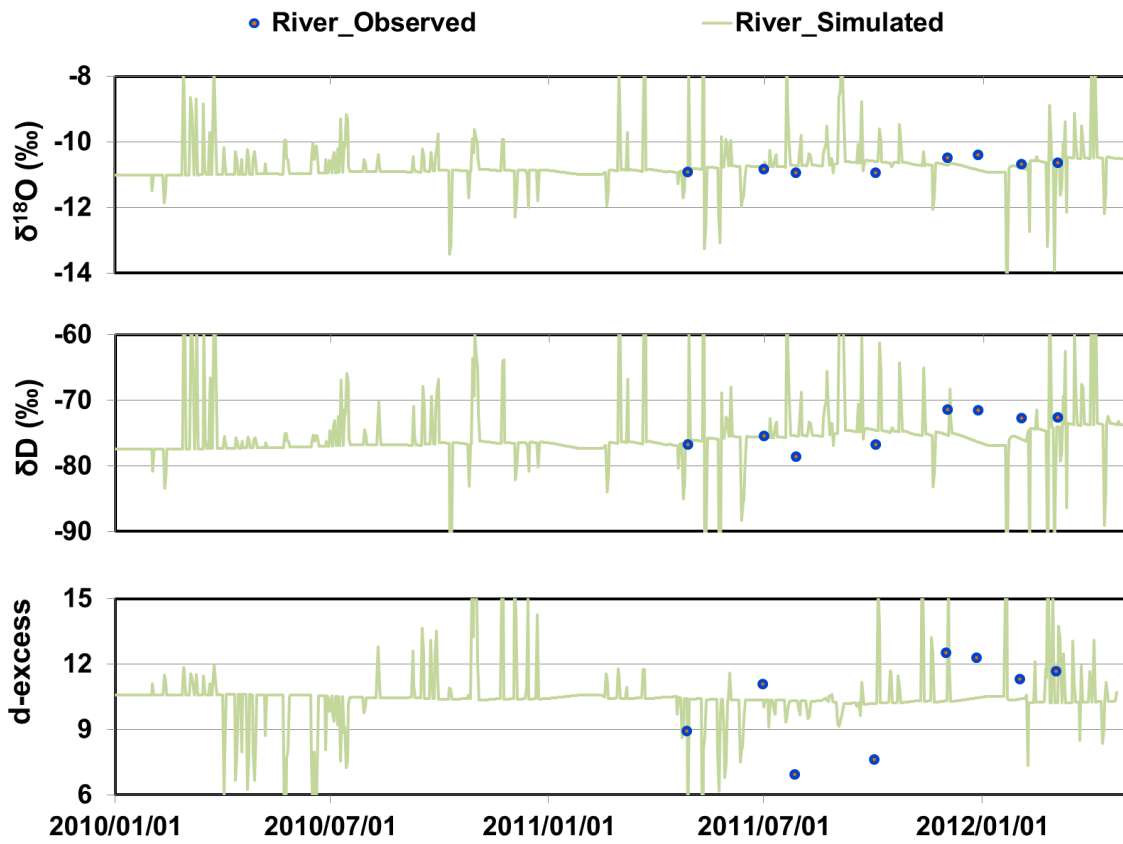
Figure 4.6 Comparison between observed and simulated isotope compositions for both calibration and

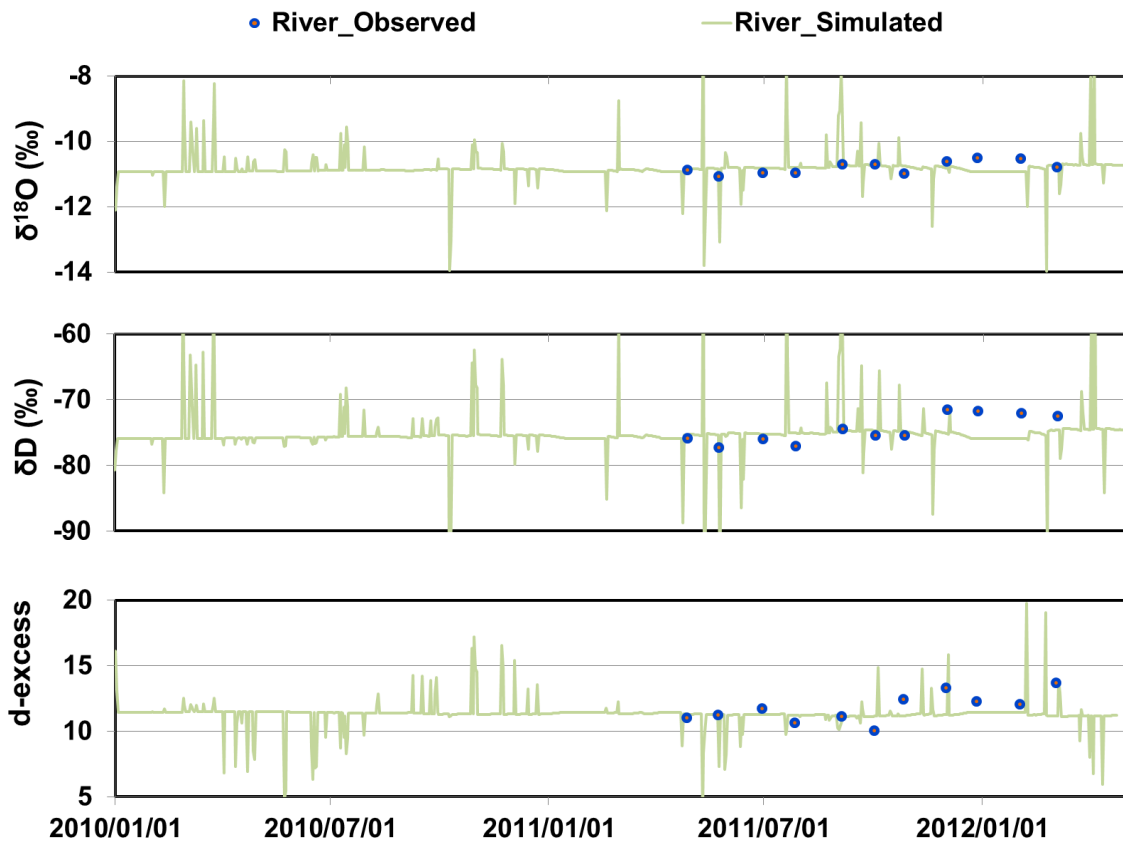validation phases in SC5.
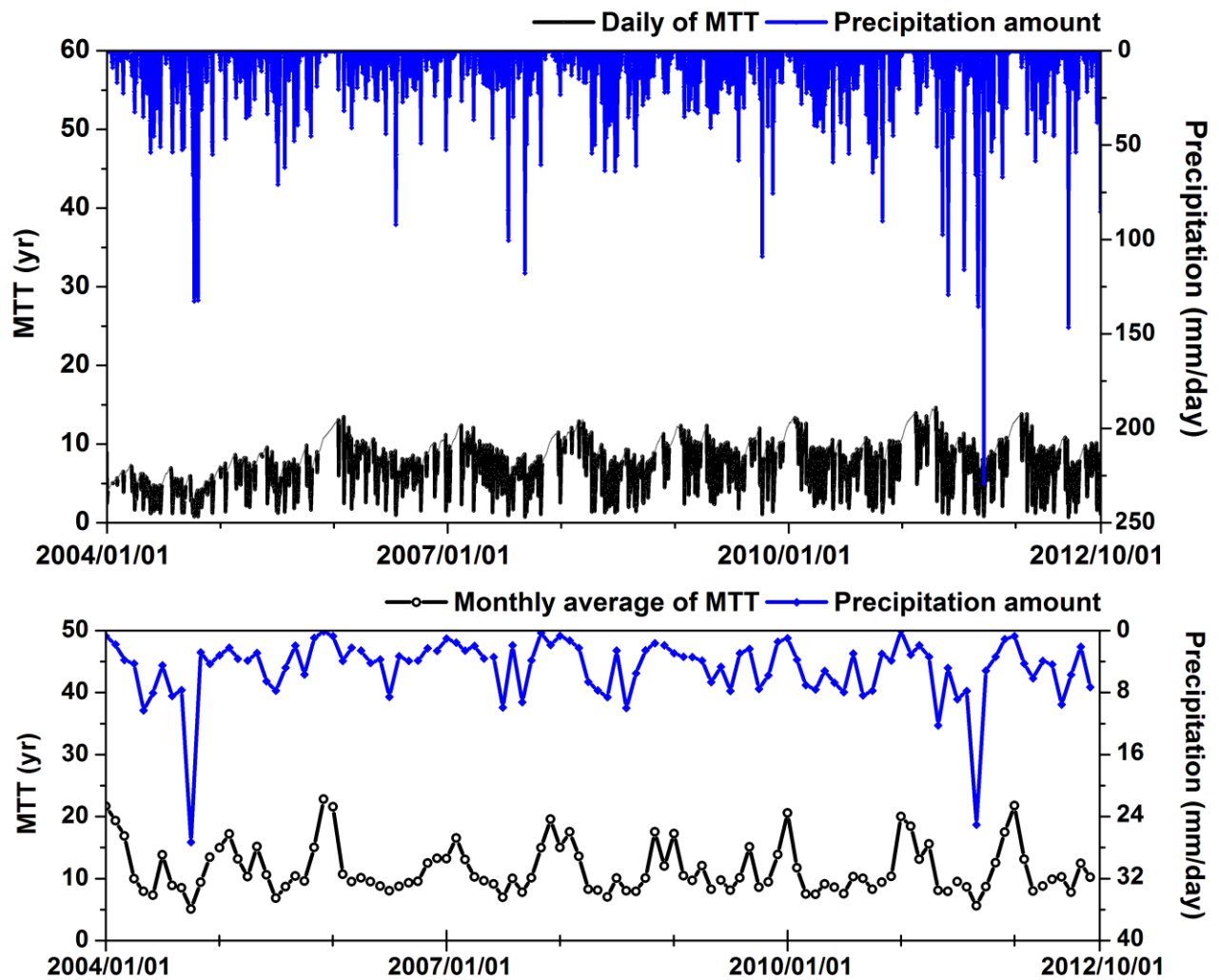
Figure 4.7 Temporal variations of MTT and precipitation in SC1; (upper) daily values and (lower) monthly
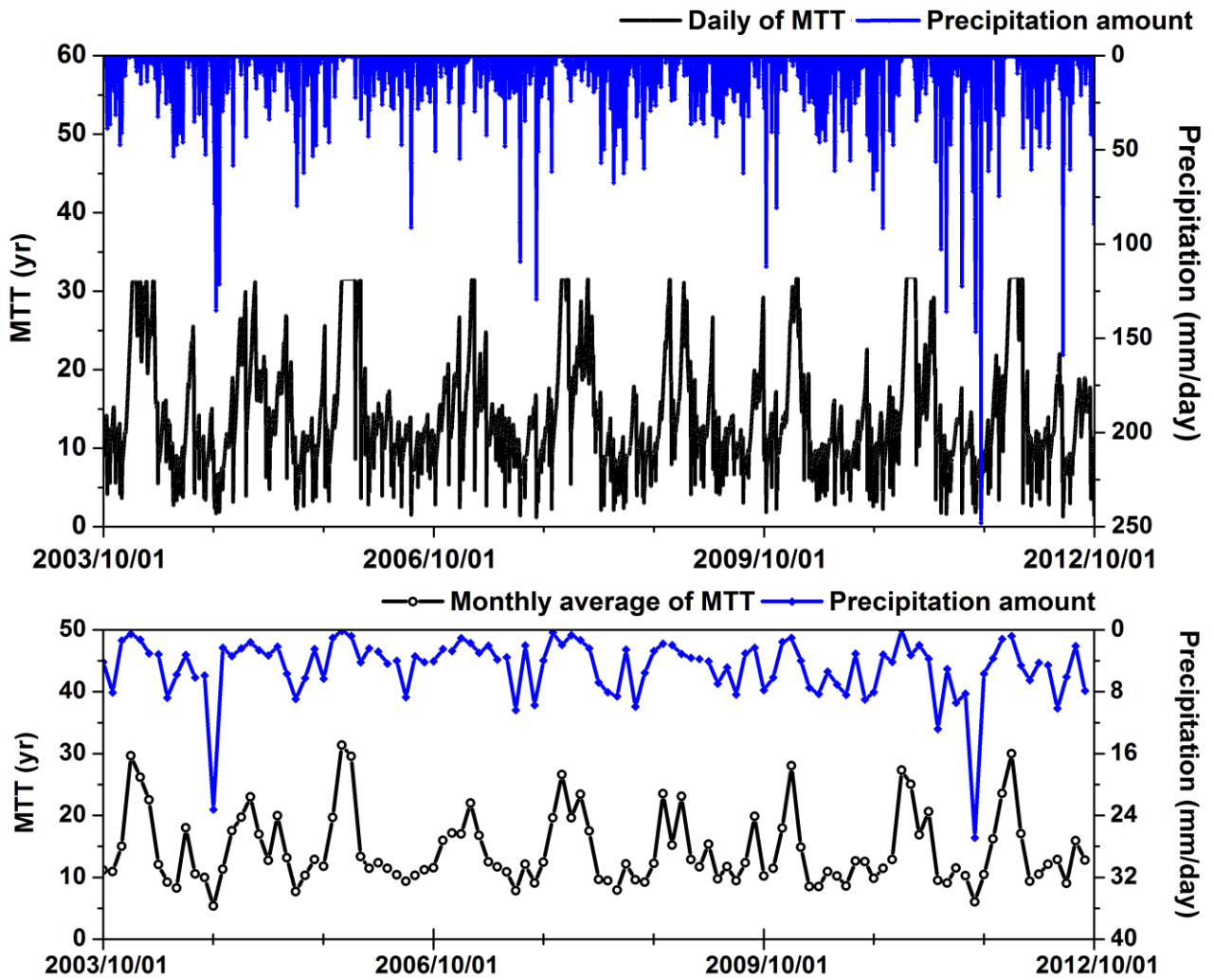
values.

Figure 4.8 Temporal variations of MTT and precipitation in SC2; (upper) daily values and (lower) monthly
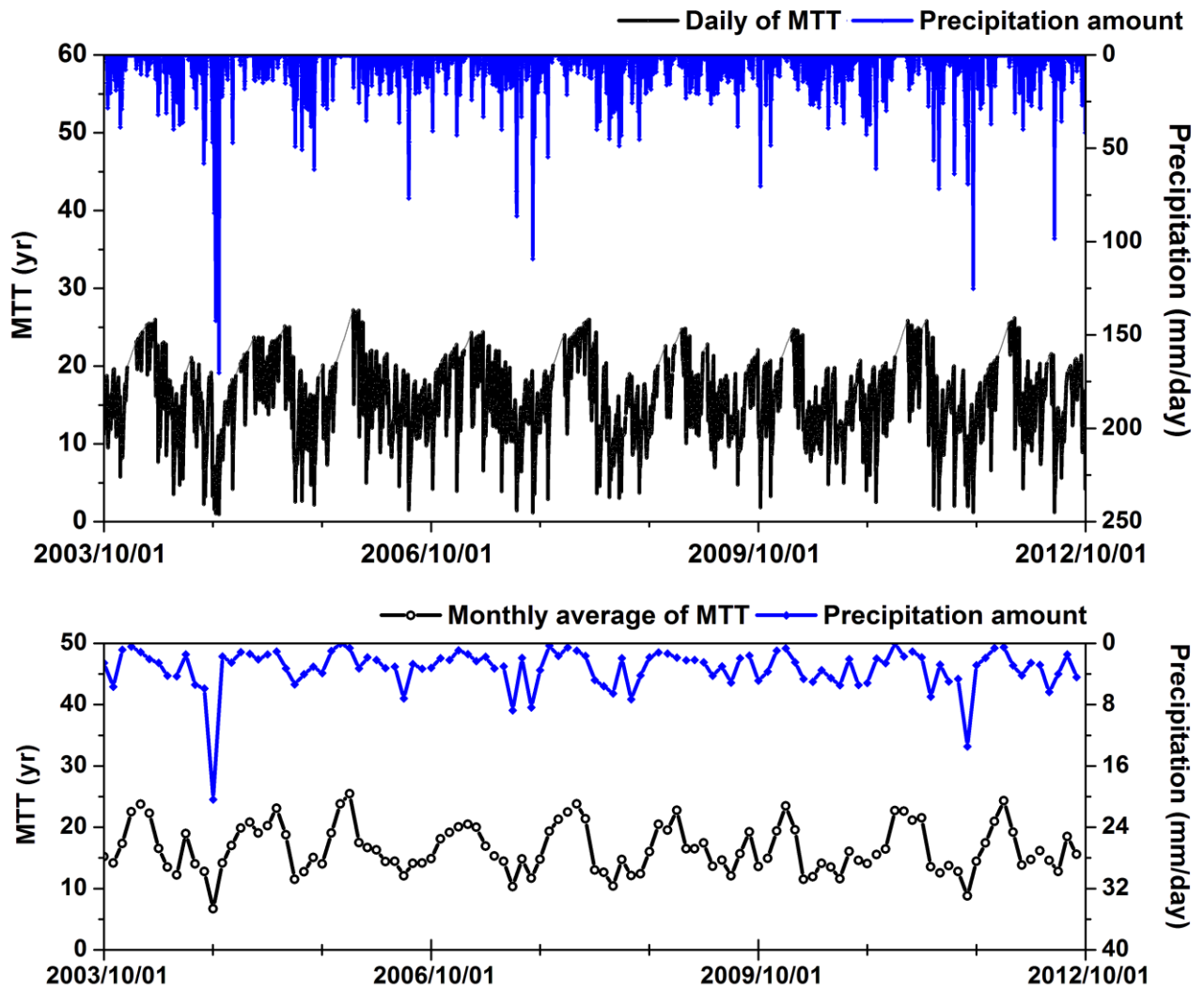
values.

Figure 4.9 Temporal variations of MTT and precipitation in SC3; (upper) daily values and (lower) monthly
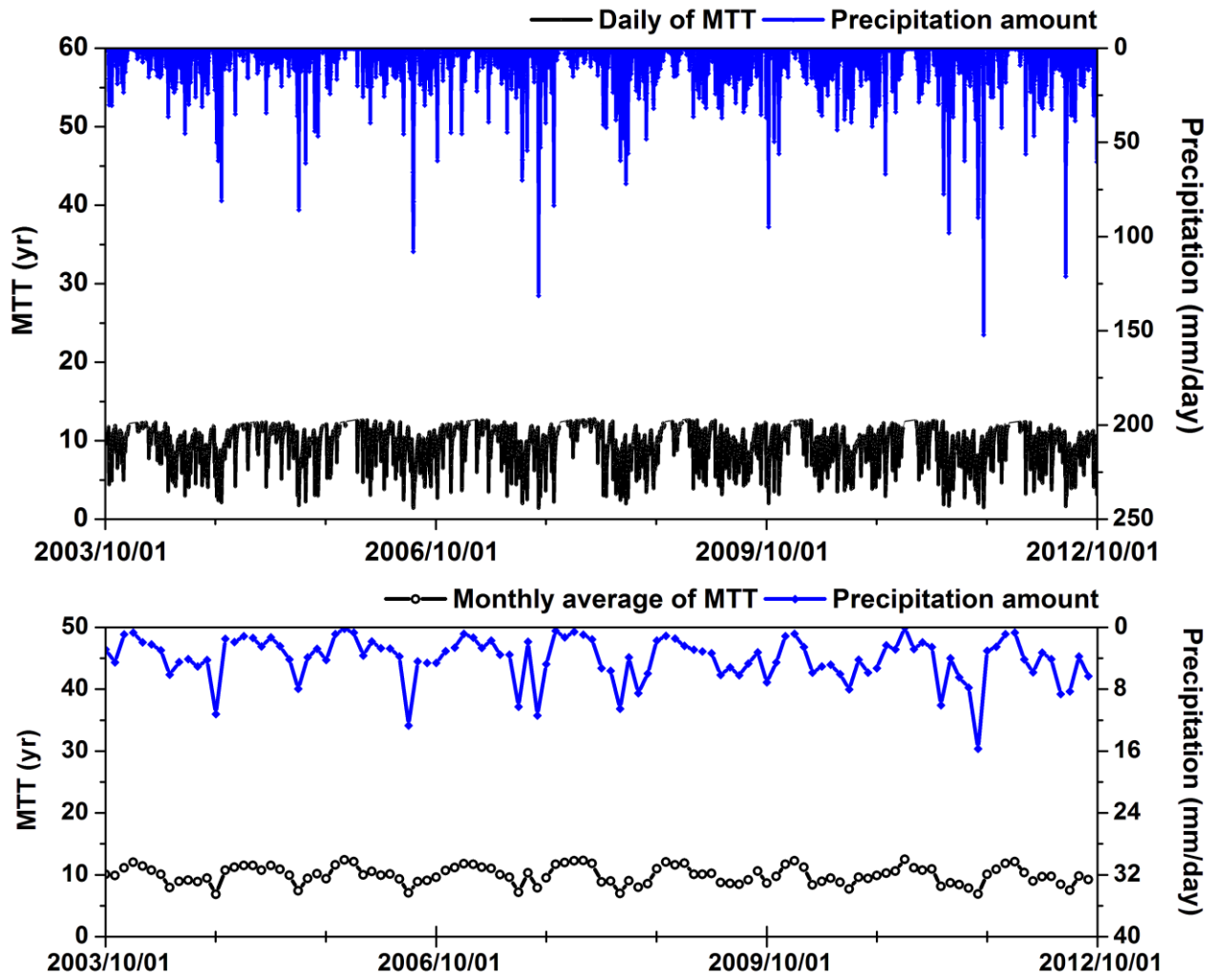
values.

Figure 4.10 Temporal variations of MTT and precipitation in SC4; (upper) daily values and (lower) monthly
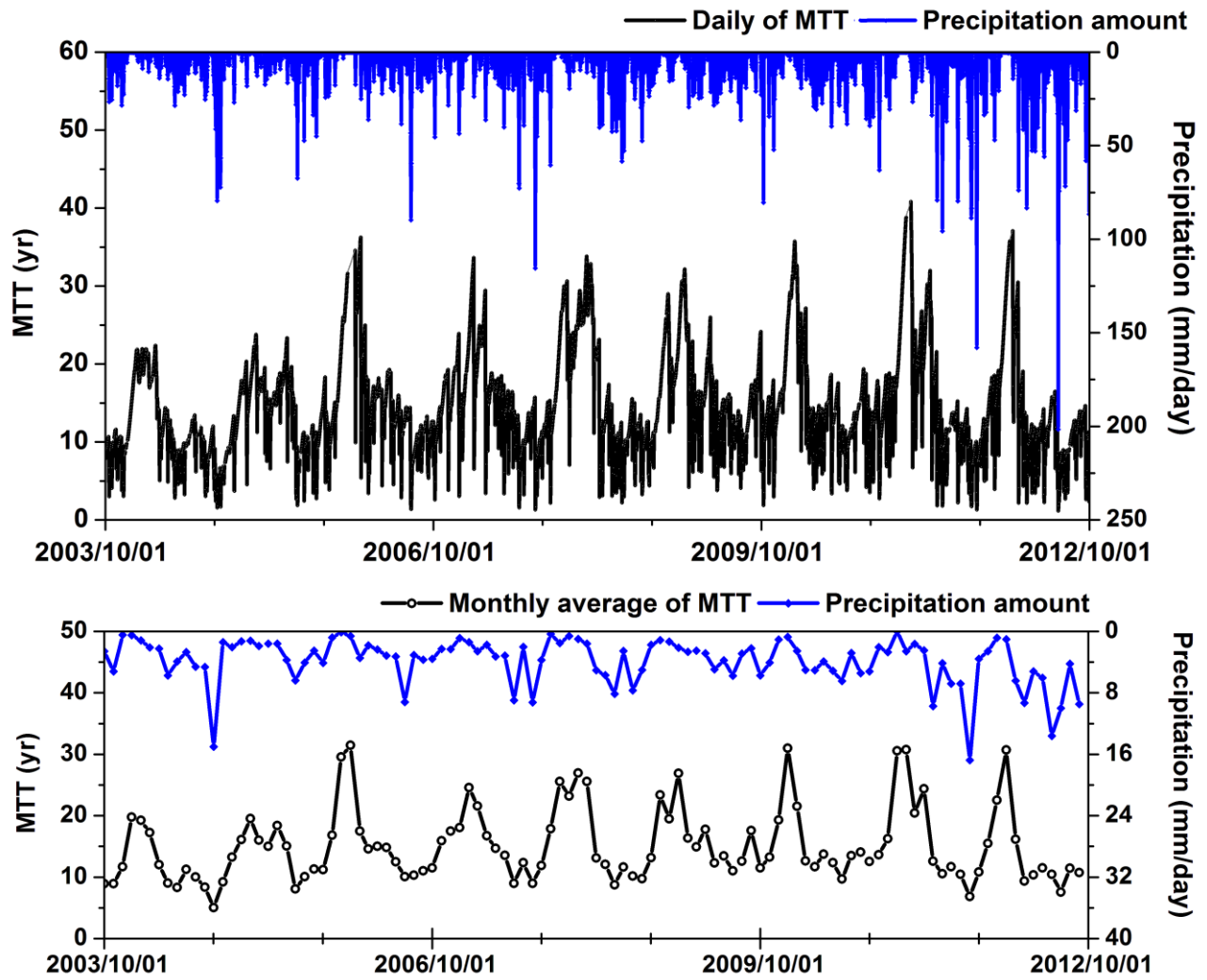
values.

Figure 4.11 Temporal variations of MTT and precipitation in SC5; (upper) daily values and (lower) monthly values.
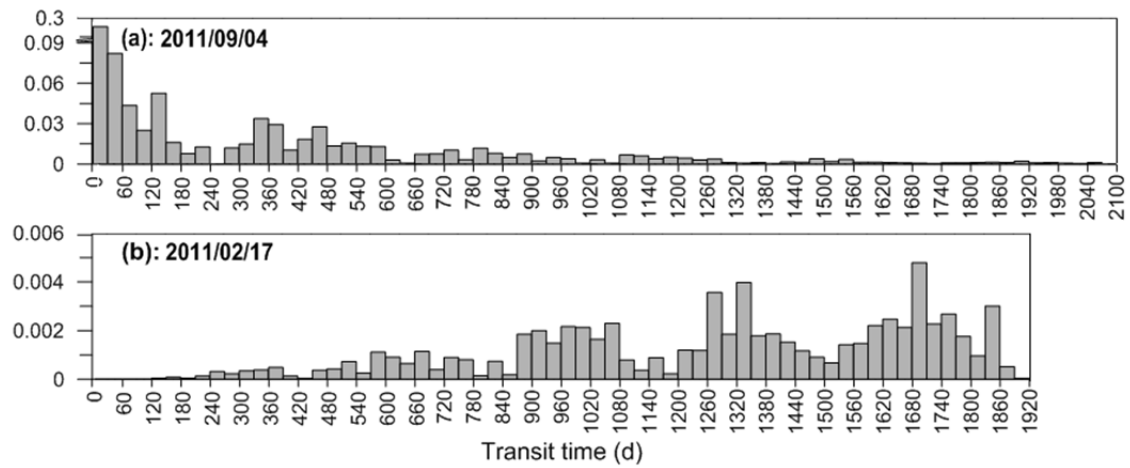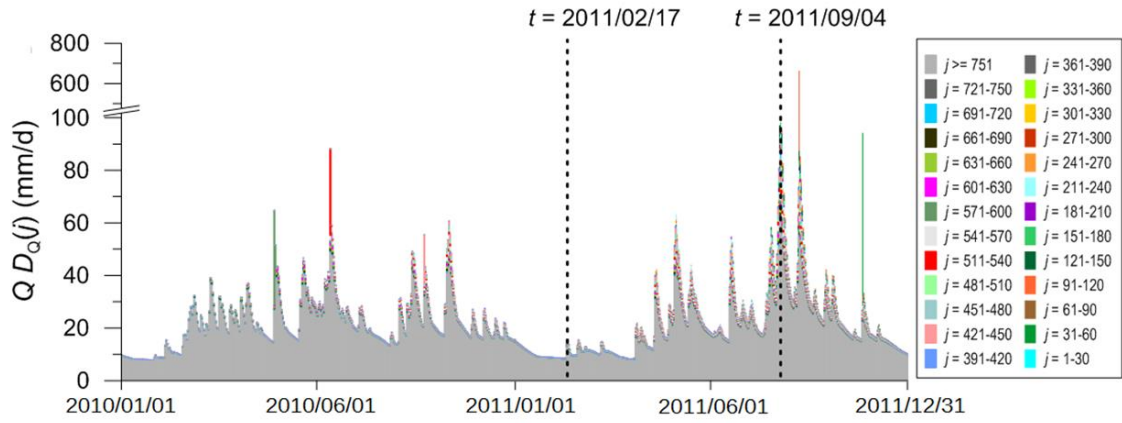
Figure 4.12 Examples of (top) hydrograph separated by different time source and selected TTD of (a) wet and (b) dry cases).

(a) *t* = 2011/09/04

Case 2 of wet:
Precipitation$_{30}$=411.41mm

SC1
SC2
SC3
SC4
SC5

Transit time (day)

(b) *t* = 2011/02/17

Case 1 of dry:
Precipitation$_{30}$=18.55mm

SC1
SC2
SC3
SC4
SC5
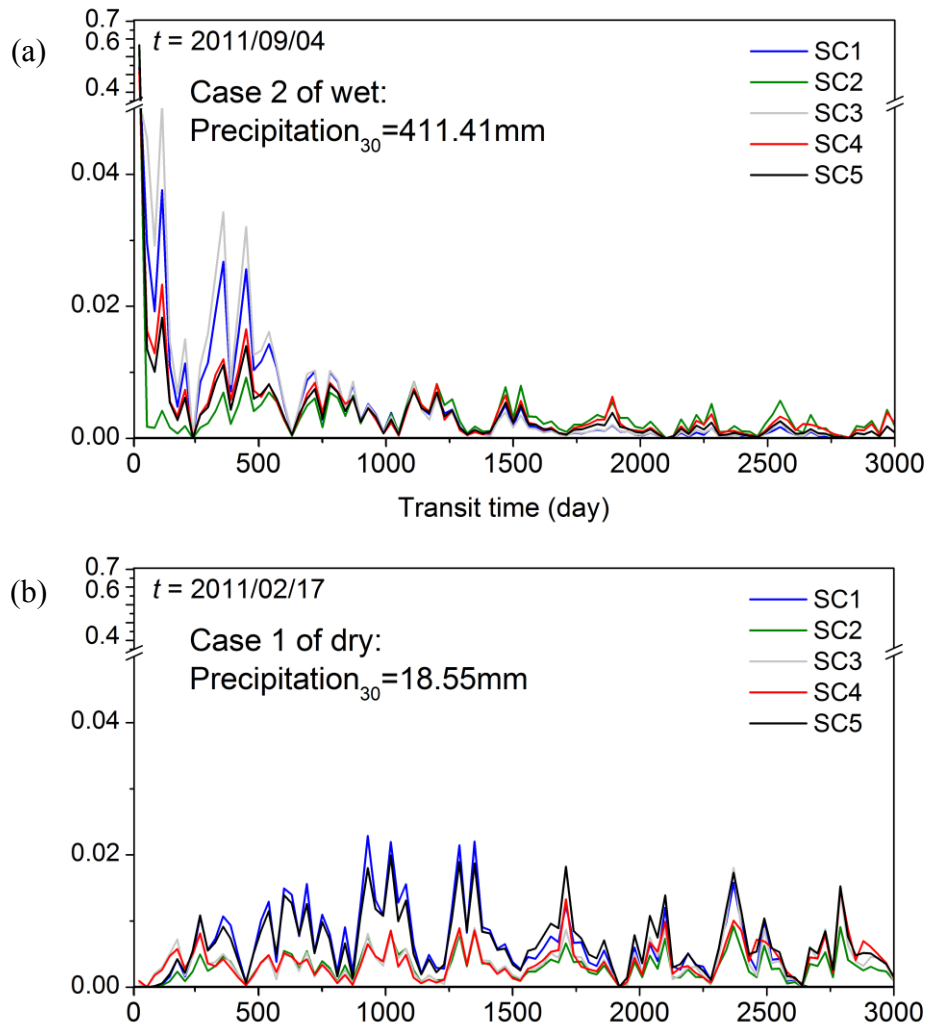
Figure 4.13 Inter-catchment comparison of selected TTDs; (a) wet and (b) dry cases.

# Chapter 5
# Discussion

## 5.1 Sensitivity of simulation

Sensitivity analyses enable to distinguish which uncertainty-sources impact the output predominantly. It is a common and useful way to find an optimal solution and to evaluate uncertainty from plenty of results that provided by Monte Carlo simulation (Moel et al., 1971). This method performs sampling from a possible range of the input parameter values followed by model evaluations for the sampled values. An essential component of every Monte Carlo simulation is the generation of random samples. These generating methods produce samples drawn from a specified distribution (typically a uniform distribution). The random numbers from this distribution are then used to transform model parameters according to some predetermined transformation equation. The optimal result was chosen from more than 20,000 times of Monte Carlo simulation (Figure 5.1), within which optimal range of each parameter have been magnified in the smaller boxes. For inspecting the sensitivity of the MTT, results of 100 Monte Carlo simulations were chosen for clarifying relationship of LAMTT with NSE for water flow simulation or RMSE for isotope transport simulation (Figure 5.2). From Figure 5.1, variation of the MTT deviations from the optimal value were ranged around 3.0 years with 5% changes of model parameters. In other words, the MTT would change around 3 years if the uncertainty within 5% errors of model parameters. Figure 5.3 shows MTT change caused by errors of each parameter.

## 5.2 Temporal variability of MTT and TTD

Concerning if the data length for calculating transit time is long enough or not, it is necessary to discuss the length of the ten-year data have been used in this study. From Figure 4.7 to Figure 4.11, as well as the standard deviation in Table 4.6, the pattern of MTT change of year to year is not so much different. So, ten-year data is long enough for investigating the daily variation of MTT and TTD in this study.

As mentioned in section 4.6, temporal variation of MTT seems to be induced by occurrence of precipitation events. In this section, relationship between temporal variations of MTT and precipitation amount is examined at four different time scales. For daily values, the inverse relationship between MTT and precipitation amount was clearly found (Figure 5.4 (a) to Figure 5.8 (a)). However, $R^2$ values are generally low for most of SCs, except for SC4 ($R^2 > 0.4$). On the other hand, for monthly values, $R^2$ values are relatively high up to 0.87 for SC4 (Figure 5.4 (b) to Figure 5.8 (b)). This may be because random noise in the relationship tends to be canceled out. For both time scales, exponential decay fitting provides better results than line fitting does. This means that change in MTT per unit increase in precipitation is not constant but is getting small with increasing precipitation amount. The reason for this is because deep groundwater, which cannot be refreshed quickly and thus have greater age, contributes to runoff even though precipitation amount is very large.

Inter-catchment comparison of relationships between monthly average MTT and monthly total precipitation at each SC is shown in Figure 5.9. The y-intercept of the regression curve ranges from 10.40 for SC1 to 23.99 for SC2, which could be considered as the MTT when monthly precipitation equals to 0. The inter-catchment difference of the y-intercept is similar to that for LAMTT (Table 4.6). However, as precipitation amount is getting greater, monthly average MTT of all the SCs approaches to a same value. As the result, the change in MTT per unit increase in precipitation is greater at SC2,

SC3 and SC5 than at SC1 and SC4. Possible factors controlling such an inter-catchment difference are discussed in the next section.

Fundamentally the same characteristics mentioned above can be found for the seasonal (i.e., 3-month interval) time scale (Figure 5.10). However, correlation between annual average MTT and annual total precipitation is relatively weak (Figure 5.11), indicating that year-to-year variation of MTT is not very large.

# 5.3 Factors controlling spatial variability of long-term average MTT (LAMTT)

To identify the relative significance of various factors characterizing each catchment in controlling LAMTT, the relationships of LAMTT with the several topographic indices (Table 5.1; Figure 5.14), percentage of slope ranks (Table 5.2), coverage of surface soil types (Table 5.3; Figure 5.12), coverage of land use types (Table 5.4; Figure 5.18), coverage of surface geology types (Table 5.5; Figure 5.16) and water balance component (Table 4.3) were analyzed. Scatter plots of LAMTT versus these factors are shown in Figures 5.13, 5.15, 5.17, 5.19, 5.20, and 5.21.

In this study, not significant relationship between area and LAMTT was found (Figure 5.15); this is no contradictory with previous studies. Although Hrachowitz et al. (2010) have shown that the MTT tends to be greater as catchment size increases, high values of MTT have also been obtained for the small size catchments. Linear relationship between catchment-mean elevation and LAMTT could not be seen (Figure 5.15). McGuire et al. (2005) have also shown no direct relationship between MTT and elevation. The catchment-mean slope showed a weak negative relationship with LAMTT. This is

similar with the results of McGuire et al. (2005). For the other topographical indexes, the maximum length of river and total storage showed no strong relationship.

For geological factors, the following geological composition found in the study area have been taken into consideration: basalt of undefined geological time (Ba), welded tuff of Quaternary (Wt), sandstone-shale-conglomerate of Mesozoic (Ss), and granite of undefined geological time (Gr). Among them, Ss showed positive relationship with LAMTT (Figure 5.17).

Coverage of the forest has positive relationship with LAMTT, while agricultural land and range grass land showed negative relationship (Figure 5.19). The forest is the dominant land-use type over the whole study area and its percentage ranges from 67% to 94% (Table 5.4). The residual percentage is mainly occupied by agricultural land and range grass land, so the relationship between land use type and LAMTT can be summarized by coverage of the forest or the other land use.

Although the absolute value of evaporation and interception are not large very much as compared to the total amount of precipitation (Table 4.2), obvious relationships of them with LAMTT can be seen (Figure 5.20). Figure 5.21 shows the relationship between storage of each layer at each SC and LAMTT; a strong relationship between the storage in 4th layer and LAMTT. In the tank model, 4th layer tank is proxy of groundwater storage. Therefore, it is inferred that groundwater storage plays an important role in controlling LAMTT.

Table 5.6 and Figure 5.22 summarize correlation of LAMTT with selected factors or between the factors, which have high correlation coefficient. From Figure 5.22, it is clearly found that coverage of forest in each SC has negative correlation with evaporation and positive correlation with interception. Forests distribute at high-slope areas, so that forest coverage has positive correlation with areal percentage of slope between 3-90˚. In addition, forest coverage and percentage of slope between 3-90˚ has negative correlation with storage of 4th layer tank in the model.

To identify the most important factors controlling LAMTT, a multi-regression analysis was carried out using the following parameters: areal percentage of slope between 3-90˚, storage of Layer 4, coverage of Ss, coverage of forest, and soil evaporation. Since the correlation between them is considerably high, independent parameter of the best model is only storage of Layer 4 (Table 5.7, Table 5.8 and Table 5.9). This result suggests groundwater storage is the most important factor controlling LAMTT. In the mountainous areas, forest is the dominant land use, soil evaporation is low and slope is high. Therefore, it can be inferred that groundwater storage is small in the mountainous and thus LAMTT is also small. On the other hand, in the plain area, groundwater storage and LAMTT is large.

Additional parameter in the second best multi-regression model was coverage of Ss. This may be because sand-shale-conglomerate of Mesozoic is deposited as alluvial fans in the study area and forms good groundwater aquifer. This result also support that groundwater storage associated with topography is the most important factor controlling LAMTT.

In the previous study, the importance of groundwater storage or its topographic control has not been clarified. This is probably because mountainous small catchments have been mainly focused in the previous studies and few meso-scale catchments that include plains with large groundwater storage have been studied.

Table 5.1 Summary of topographic indices for each SC.

| ID | Elevation (m) | Area (km$^2$) | Weighted Slope (°) | MaxL_river* (km) |
|---|---|---|---|---|
| SC1 | 1211.10 | 268.00 | 28.60 | 28.10 |
| SC2 | 615.60 | 518.50 | 25.78 | 36.24 |
| SC3 | 448.00 | 905.70 | 23.01 | 52.02 |
| SC4 | 2455.40 | 480.30 | 23.63 | 43.23 |
| SC5 | 376.20 | 2172.70 | 22.57 | 84.59 |

* MaxL_river: Maximum length of river

Table 5.2 Percentage of slope ranks in each SC.

| Slope (°) | SC1 | SC2 | SC3 | SC4 | SC5 |
|---|---|---|---|---|---|
| 0~3 | 2.03 | 9.49 | 16.21 | 6.8 | 1.06 |
| 3~5 | 1.58 | 2.65 | 3.35 | 10.28 | 14.65 |
| 5~8 | 2.93 | 3.83 | 3.99 | 10.25 | 6.39 |
| 8~15 | 9.38 | 9.48 | 9.86 | 10.93 | 17.62 |
| 15~25 | 21.32 | 19.02 | 18.62 | 13.73 | 16.46 |
| 25~30 | 14.94 | 12.86 | 11.7 | 8.88 | 10.04 |
| 30~45 | 41.67 | 37.06 | 31.69 | 30.57 | 28.49 |
| 45~60 | 6.08 | 5.56 | 4.53 | 8.22 | 5.16 |
| 60~75 | 0.07 | 0.05 | 0.05 | 0.33 | 0.12 |
| 75~ | 0 | 0 | 0 | 0.01 | 0 |

Table 5.3 Coverage (%) of surface soil types in each SC.

|  | SC1 | SC2 | SC3 | SC4 | SC5 |
|---|---|---|---|---|---|
| Brown forest soil | 57.06 | 73.00 | 67.98 | 75.20 | 49.55 |
| Podsol | 5.51 | 6.49 | 5.65 | 12.39 | 10.47 |
| Andosol | 17.70 | 7.89 | 8.66 | 3.57 | 28.48 |
| Lithosol | 2.41 | 1.47 | 1.12 | 2.78 | 5.40 |
| Rocky land | 1.11 | 0.57 | 0.46 | 1.09 | 1.50 |
| Red yellow soil | 4.38 | 5.21 | 5.58 | 4.37 | |
| Gley soil | 2.08 | | 1.99 | | |
| Others | 0.69 | | 0.09 | | 1.03 |

Table 5.4 Coverage (%) of land use types in each SC.

|  | SC1 | SC2 | SC3 | SC4 | SC5 |
|---|---|---|---|---|---|
| Forest | 86.71 | 76.46 | 67.55 | 93.84 | 67.11 |
| Agriculture | 8.29 | 15.53 | 16.14 | 0.44 | 13.31 |
| Residence | 1.78 | 1.24 | 1.78 | 1.03 | 2.87 |
| Range grass | 1.93 | 4.47 | 7.44 | 2.84 | 6.02 |
| Transportation | 0.03 | 0.22 | 0.48 | 1.74 | 0.46 |
| Water | 0.50 | 1.22 | 1.99 | 0.11 | 2.21 |
| Institution | 0.06 | 0.16 | 0.74 | - | 0.93 |
| Rice | 0.49 | 0.59 | 3.21 | - | 6.52 |
| Pasture | - | 0.12 | 0.66 | - | 0.57 |

Table 5.5 Coverage (%) of surface geology types in each SC.

|      | SC1   | SC2   | SC3   | SC4   | SC5   |
|------|-------|-------|-------|-------|-------|
| Ba   | 77.67 | 61.17 | 45.13 | 2.99  | 22.17 |
| Wf   | 17.85 | 13.91 | 19.72 | 7.11  | 16.04 |
| Ss   | 1.95  | 22.01 | 15.37 | 6.04  | 10.64 |
| Gr   | 2.54  | 1.31  | 2.33  | 20.43 | 5.54  |
| Gc   |       | 1.61  | 9.85  | 6.19  | 12.32 |
| Smc  |       |       | 3.96  | 23.71 | 16.9  |
| Dg   |       |       | 3.43  | 23.62 | 12.43 |
| An   |       |       | 0.21  | 3.52  | 2.56  |
| Sscs |       |       |       | 3.98  | 0.88  |
| Li   |       |       |       | 2.26  | 0.5   |
| Cs   |       |       |       | 0.15  | 0.03  |

Table 5.6 Correlation matrix among LAMTT and related factors.

|  | Slope | Storage | Ss | Forest | E | LAMTT |
|---|---|---|---|---|---|---|
| Slope | 1.00 | | | | | |
| Storage | -0.85 | 1.00 | | | | |
| Ss | -0.74 | 0.54 | 1.00 | | | |
| Forest | 0.81 | -0.86 | -0.58 | 1.00 | | |
| E | -0.67 | 0.48 | 0.89 | -0.74 | 1.00 | |
| LAMTT | -0.90 | 0.93 | 0.80 | -0.89 | 0.74 | 1.00 |

Table 5.7 Multi-regression Coefficients

|  | Model | Unstandardized Coefficients | | Standardized coefficients | | |
|---|---|---|---|---|---|---|
|  |  | B | Std. Error | Beta | t | Sig. |
| 1 | (Constant) | 4.87 | 1.85 |  | 2.63 | 0.08 |
|  | StorageL4 | 0.01 | 0.00 | 0.93 | 4.51 | 0.02 |
| 2 | (Constant) | 4.61 | 0.49 |  | 9.35 | 0.01 |
|  | StorageL4 | 0.00 | 0.00 | 0.71 | 10.85 | 0.01 |
|  | Ss | 0.19 | 0.03 | 0.42 | 6.35 | 0.02 |

a. Dependent Variable: LAMTT

Table 5.8 Multi-regression analysis for chose characters.

| Model | R | R Square | Adjusted R Square | Std. Error of the Estimate |
|-------|------|----------|-------------------|----------------------------|
| 1 | 0.93[a] | 0.87 | 0.83 | 1.48 |
| 2 | 1.00[b] | 0.99 | 0.99 | 0.39 |

a. Predictors: (Constant), StorageL4

b. Predictors: (Constant), StorageL4, Ss

Table 5.9 Results of ANOVA[c].

| | Model | Sum of Squares | df | Mean Square | F | Sig. |
|---|---|---|---|---|---|---|
| 1 | Regression | 44.47 | 1 | 44.47 | 20.32 | 0.02[a] |
| | Residual | 6.56 | 3 | 2.19 | | |
| | Total | 51.03 | 4 | | | |
| 2 | Regression | 50.72 | 2 | 25.36 | 163.43 | 0.01[b] |
| | Residual | 0.31 | 2 | 0.16 | | |
| | Total | 51.03 | 4 | | | |

a. Predictors: (Constant), StorageL4

b. Predictors: (Constant), StorageL4, Ss
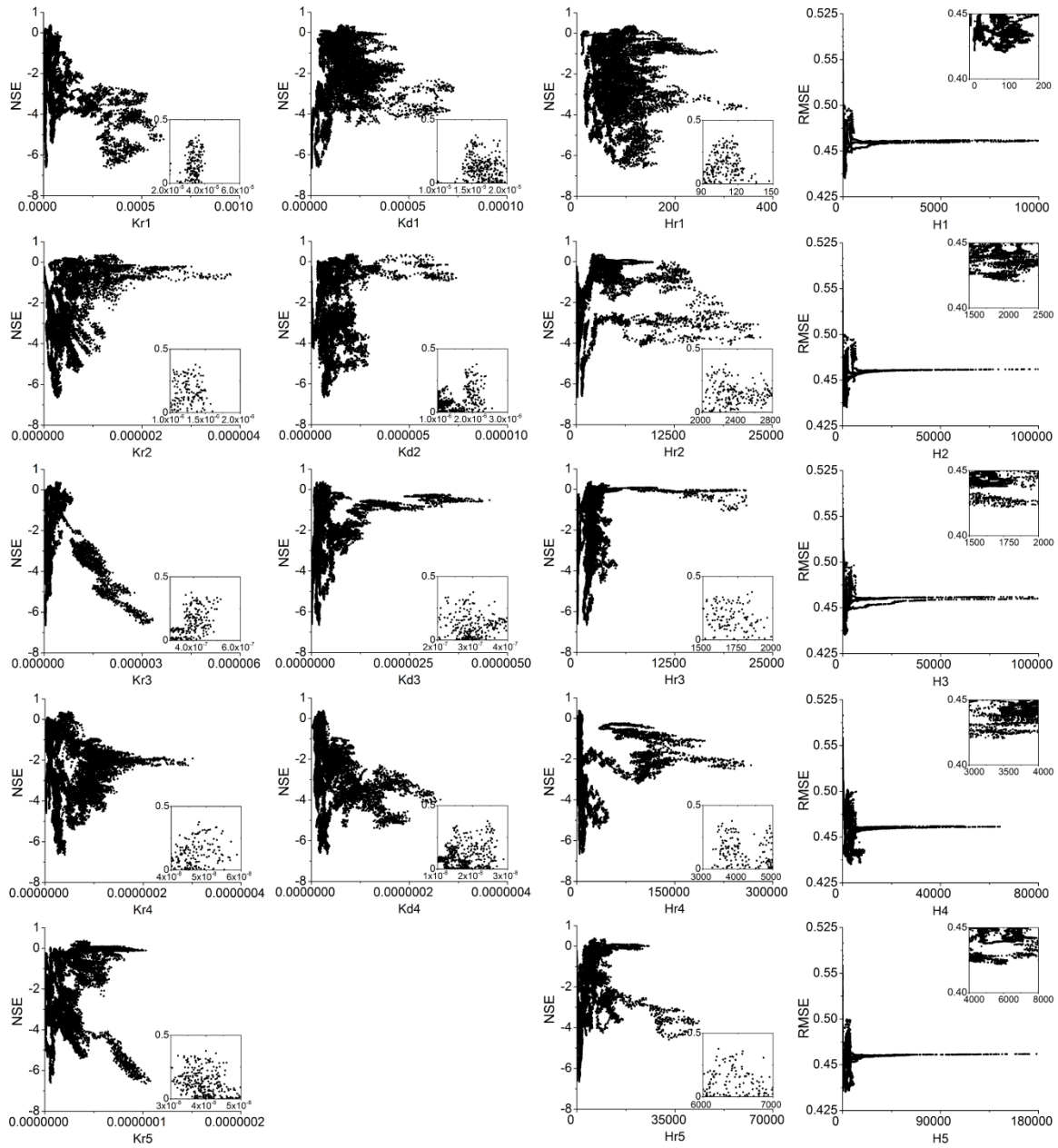
c. Dependent Variable: LAMTT

Figure 5.1 Scatter diagrams of Monte Carlo simulations for examining sensitivity of water flow simulation to model parameters for SC3.
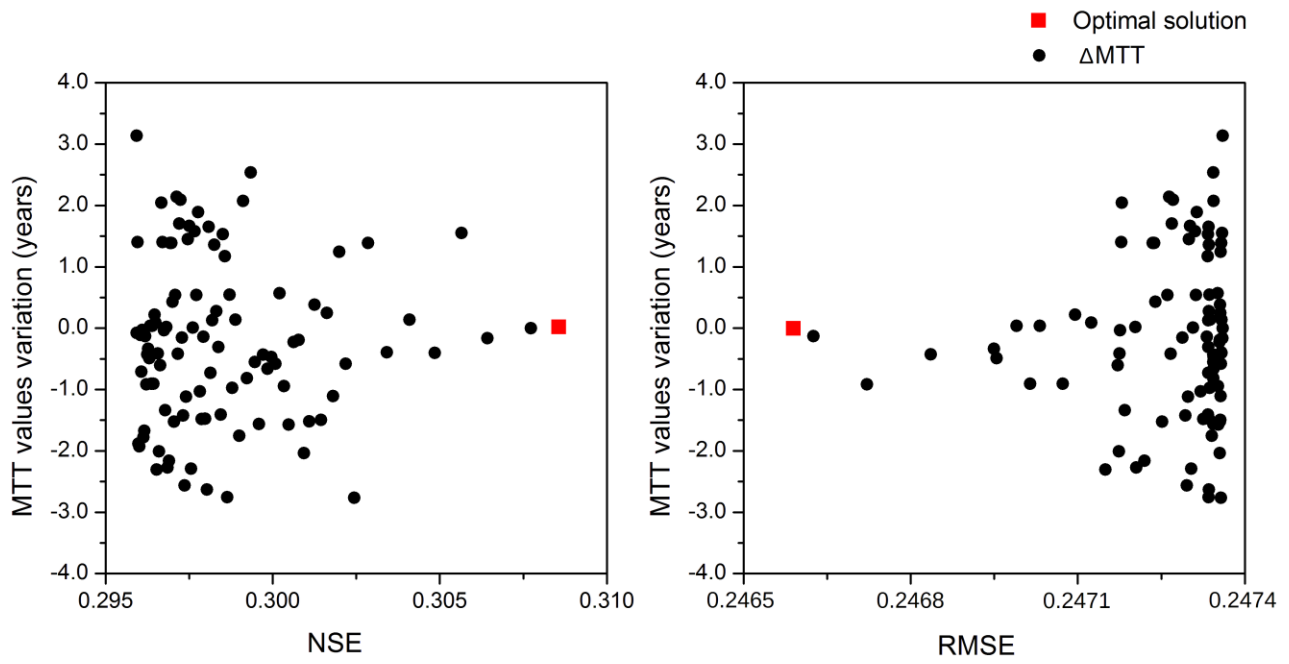
Figure 5.2 Results of 100 Monte Carlo simulations for sensitivity analysis: relationship of long-term mean MTT deviation (ΔMTT) with (left) Nash-Sutcliffe efficiency (NSE) for water flow simulation, and (right) combined root mean square error (combined-RMSE; see text for definition) for isotope transport simulation for SC3.
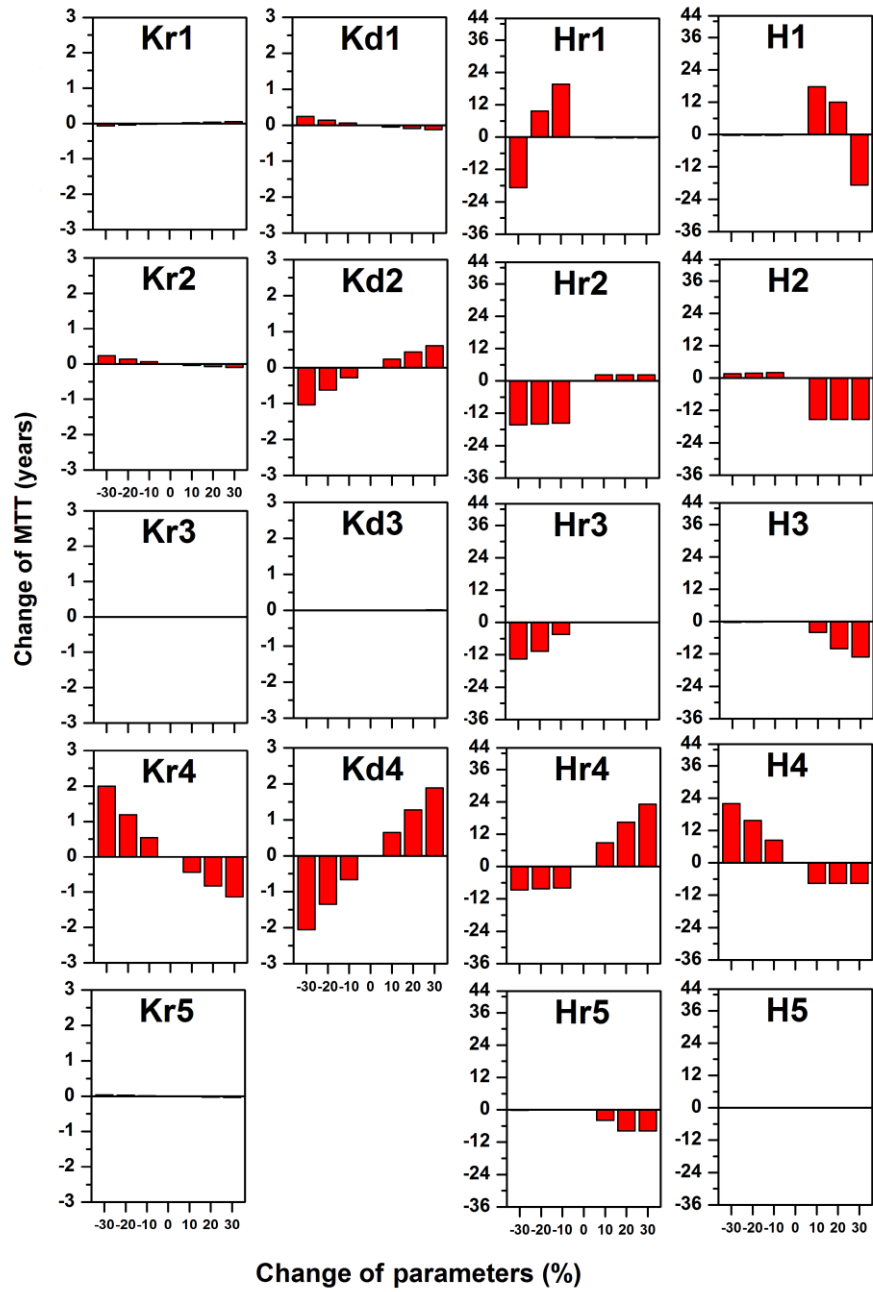
Figure 5.3 Sensitivity of water flow simulation to model parameters for SC3.

a)

$$y_1 = -0.11 \cdot x + 8.47$$

$$R_1^2 = 0.223$$

$$y_2 = 6.70 \cdot \exp\big((15.57 - x)/43.60\big) - 0.88$$

$$R_2^2 = 0.265$$

b)

$$y_1 = -0.0105 + 9.48$$

$$R_1^2 = 0.351$$

$$y_2 = 10.40 \cdot \exp(-0.0020 \cdot x)$$
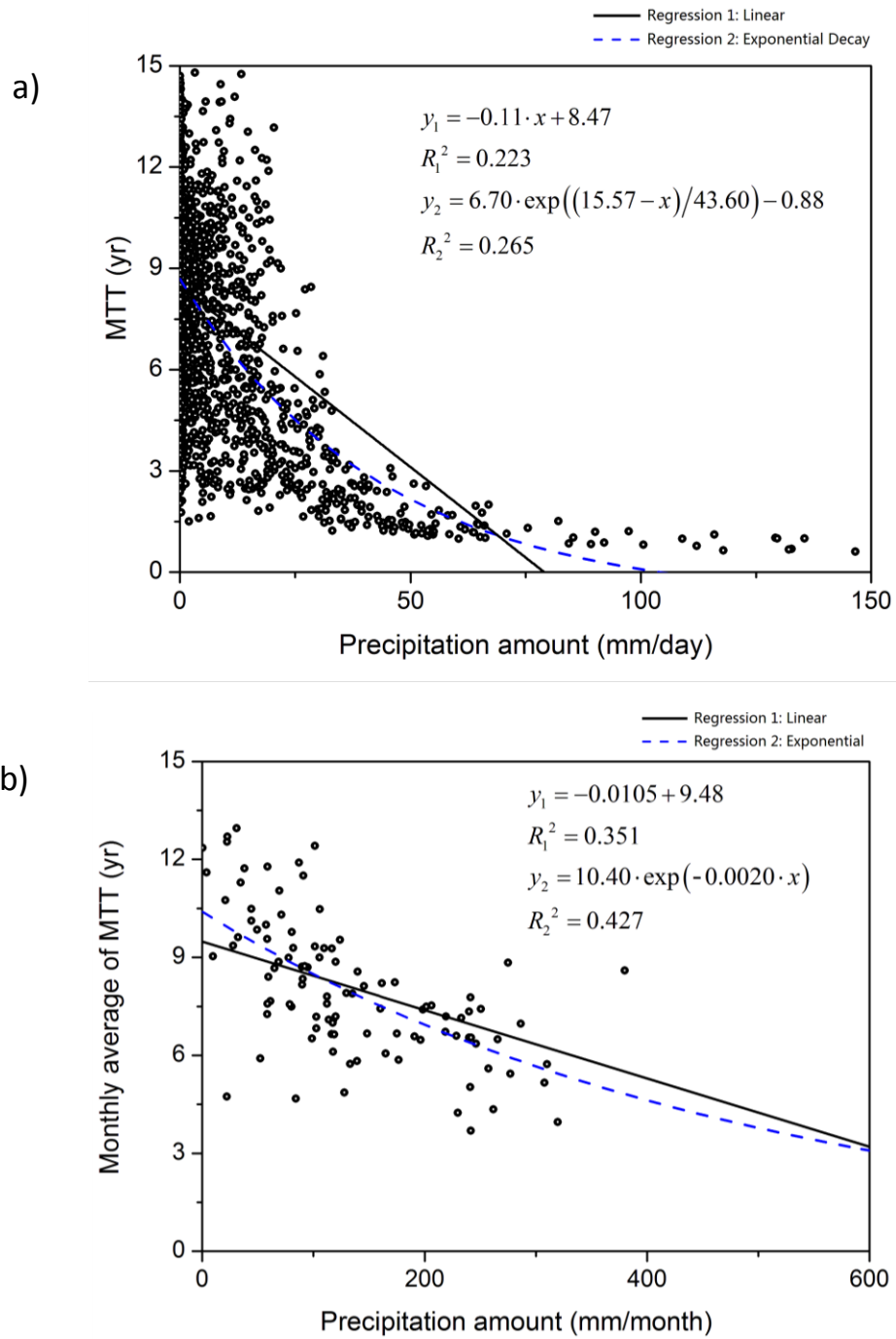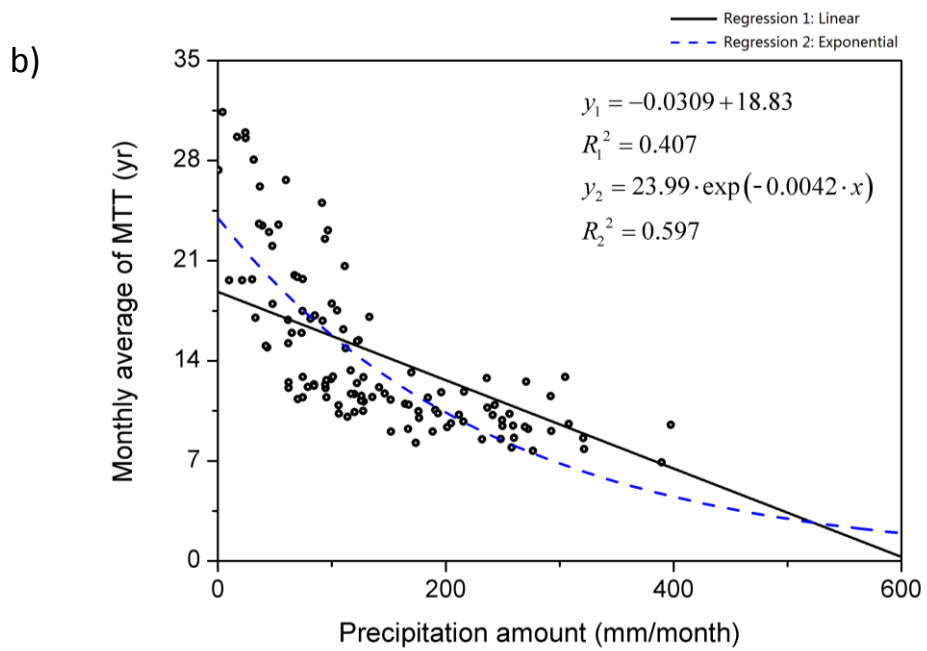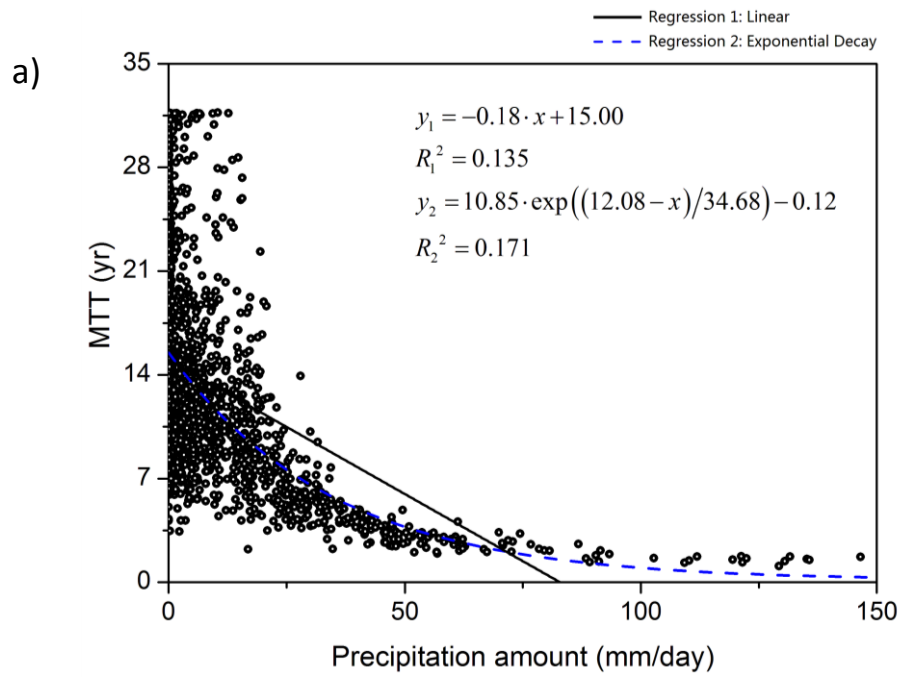
$$R_2^2 = 0.427$$

Figure 5.4 Relationship between MTT and precipitation amount in SC1; (a) daily average and (b) monthly average.

Figure 5.5 Relationship between MTT and precipitation amount in SC2; (a) daily average and (b) monthly average.

a)



$$y_1 = -0.23 \cdot x + 17.22$$
$$R_1^2 = 0.181$$
$$y_2 = 23.01 \cdot \exp\left(-(x+6.92)/48.32\right) - 2.45$$
$$R_2^2 = 0.203$$

b)



$$y_1 = -0.0356 + 20.14$$
$$R_1^2 = 0.578$$
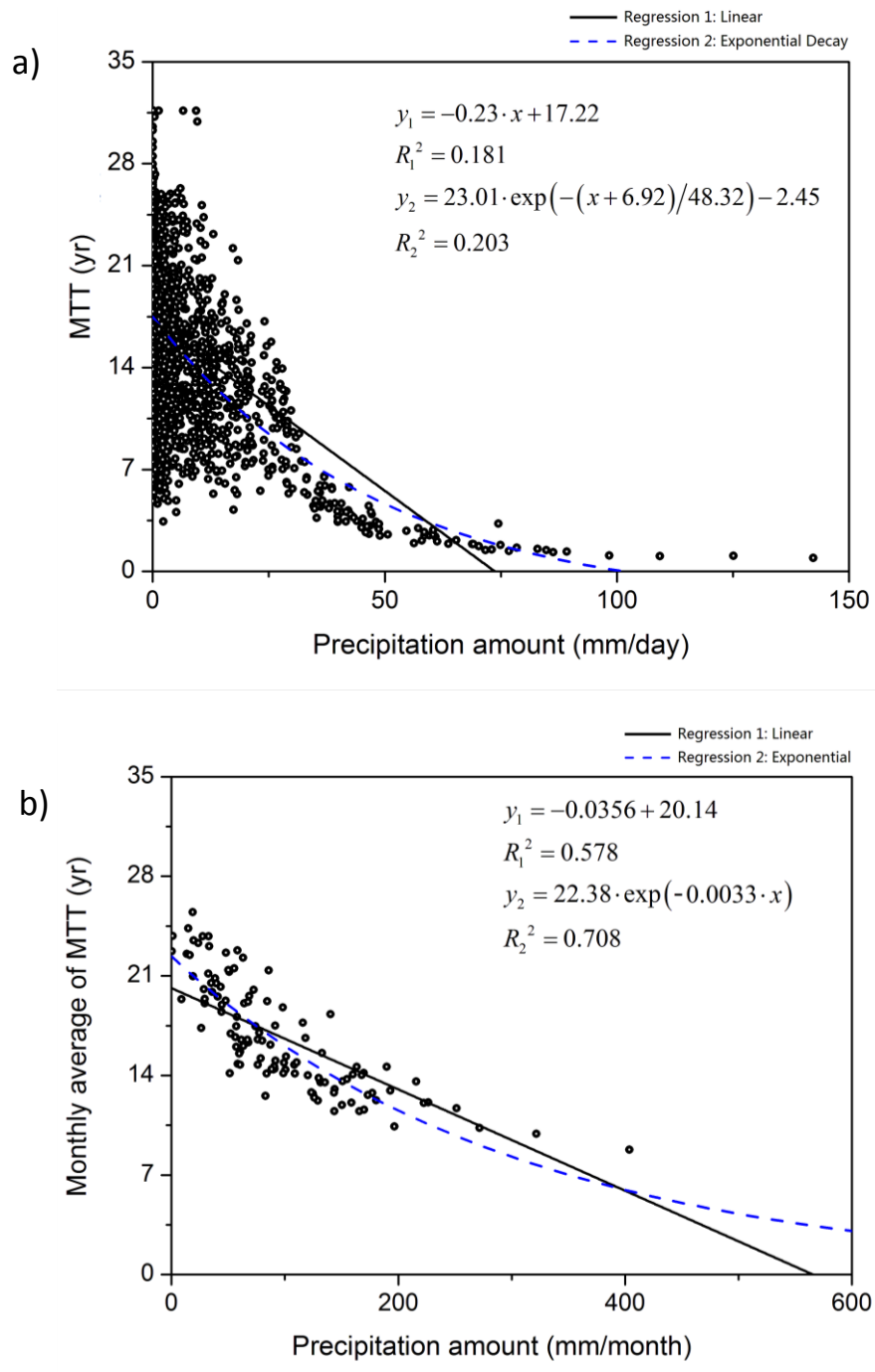$$y_2 = 22.38 \cdot \exp(-0.0033 \cdot x)$$
$$R_2^2 = 0.708$$

Figure 5.6 Relationship between MTT and precipitation amount in SC3; (a) daily average and (b) monthly average.
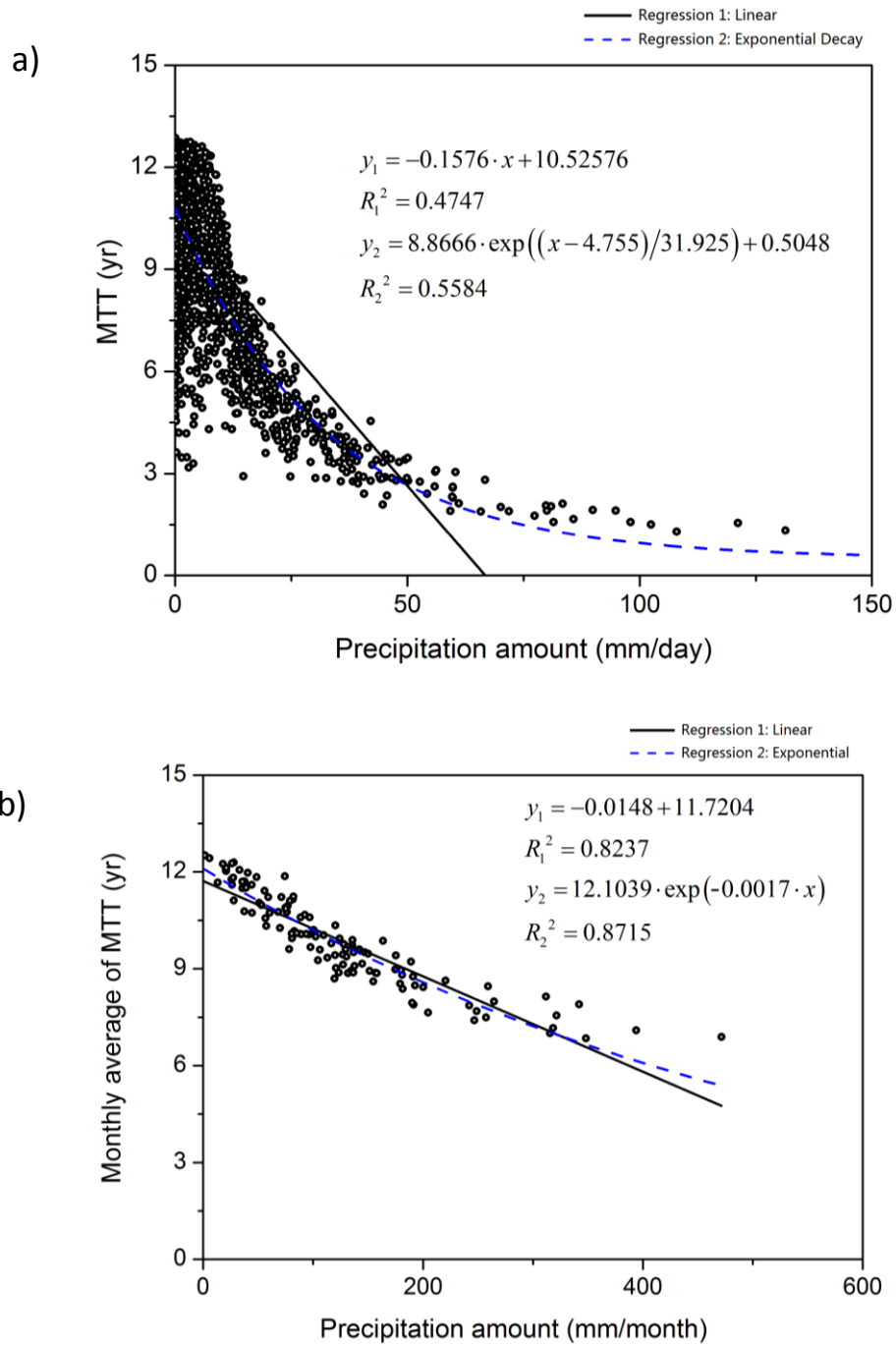
Figure 5.7 Relationship between MTT and precipitation amount in SC4; (a) daily average and (b) monthly average.
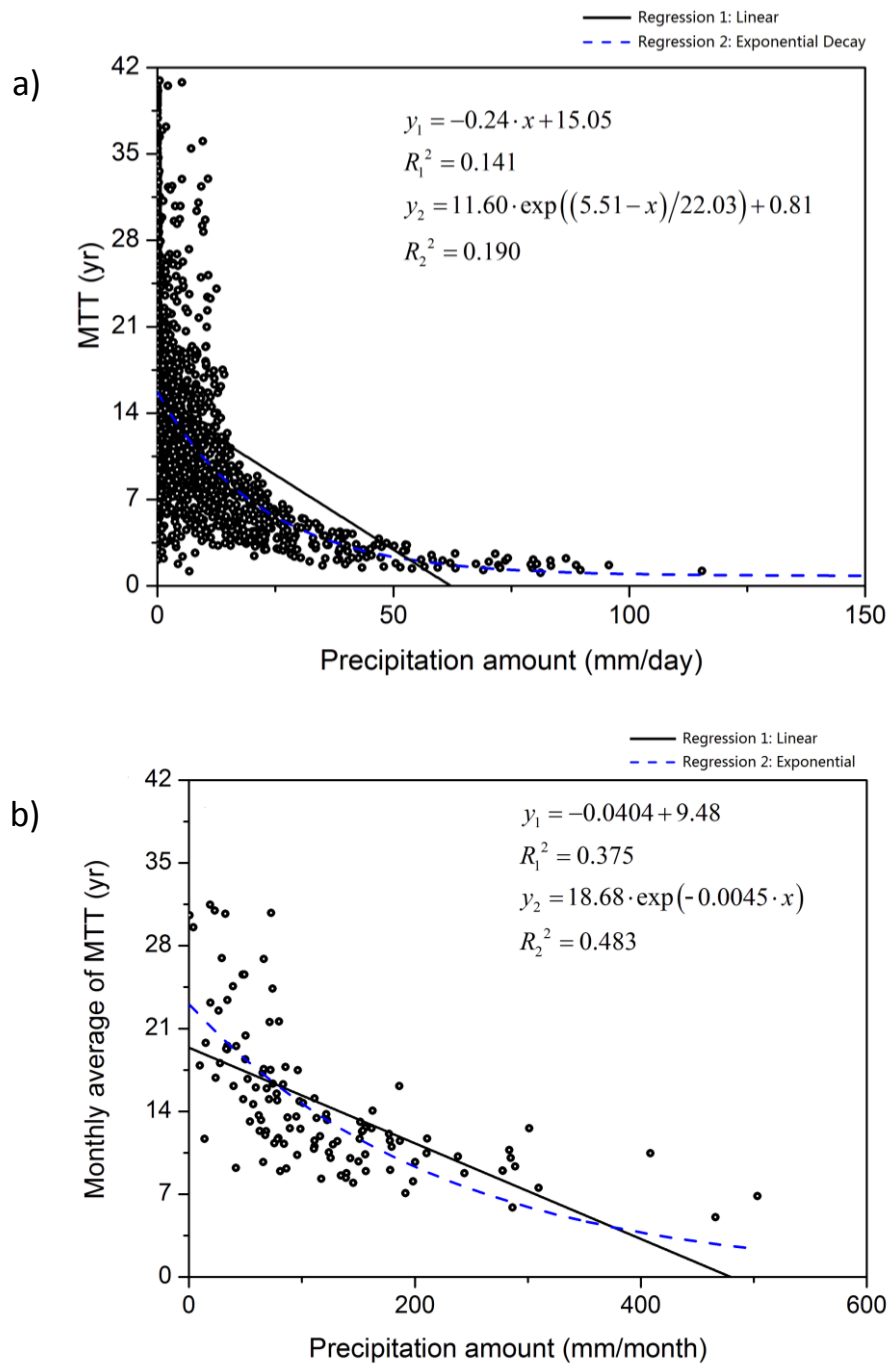
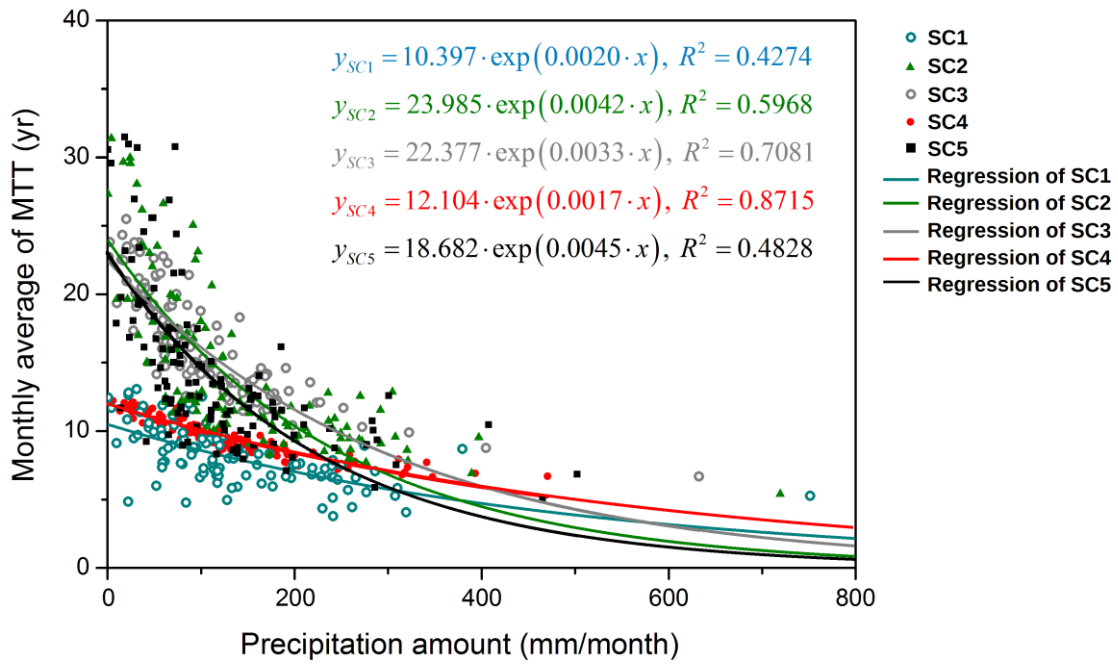Figure 5.8 Relationship between MTT and precipitation amount in SC5; (a) daily average and (b) monthly average.

Figure 5.9 Inter-catchment comparison of relationships between monthly average MTT and precipitation amount.
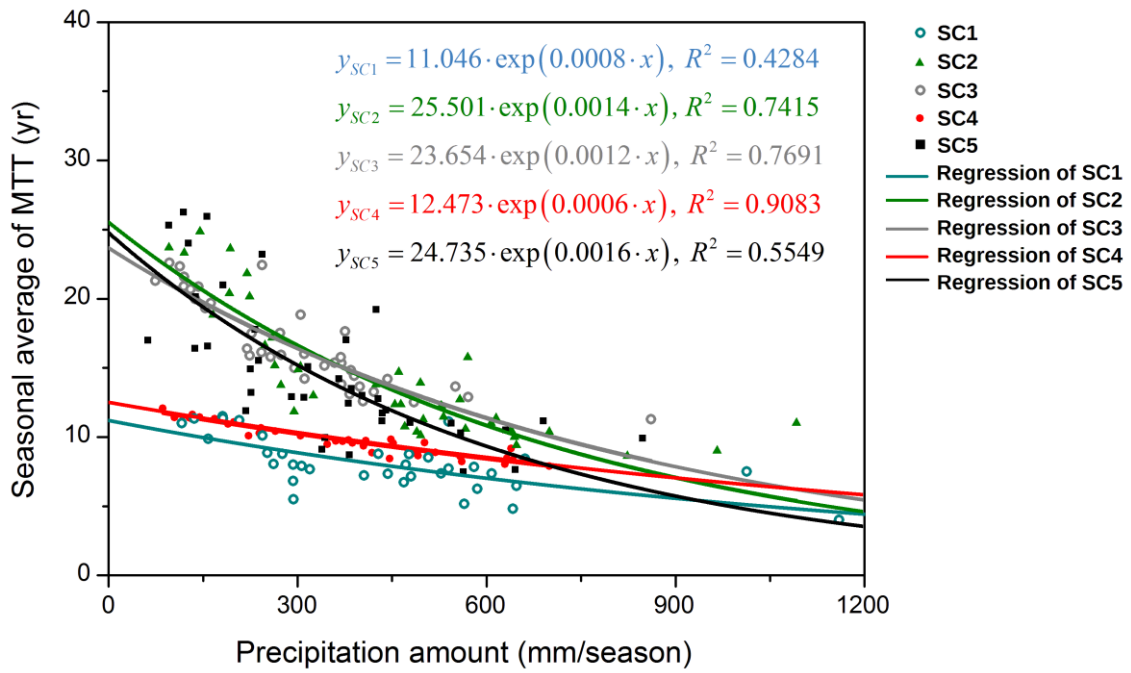
Figure 5.10 Inter-catchment comparison of relationships between 3-month average MTT and precipitation amount.
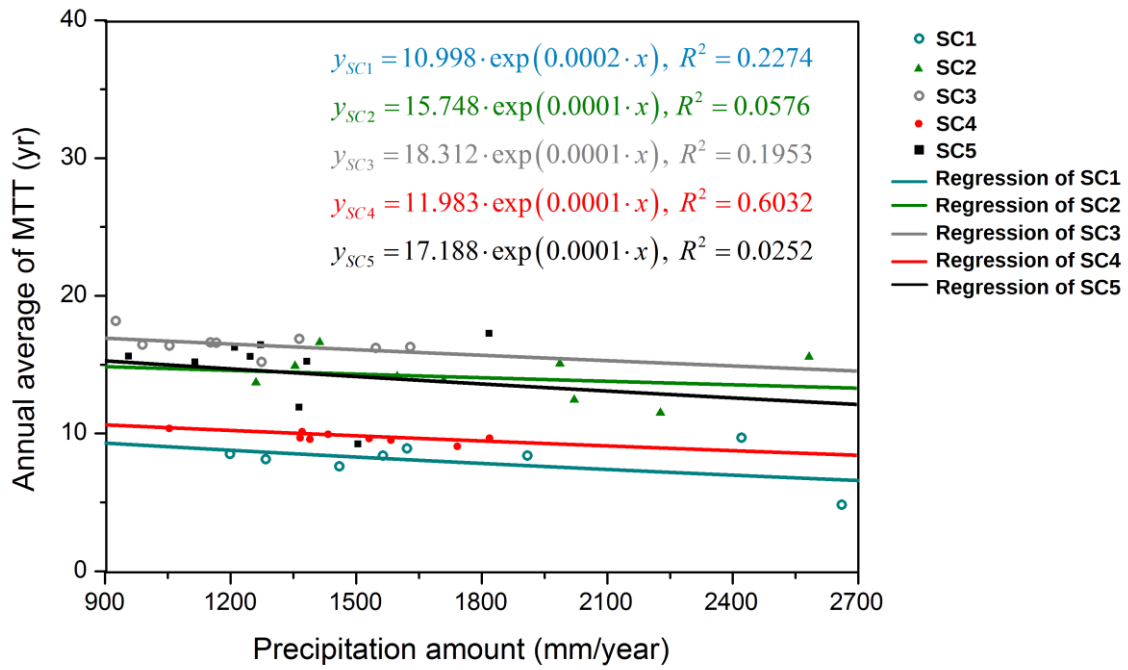
Figure 5.11 Inter-catchment comparison of relationships between annual average MTT and precipitation amount.

Figure 5.12 Spatial distribution of surface soil types and their coverage in each SC.
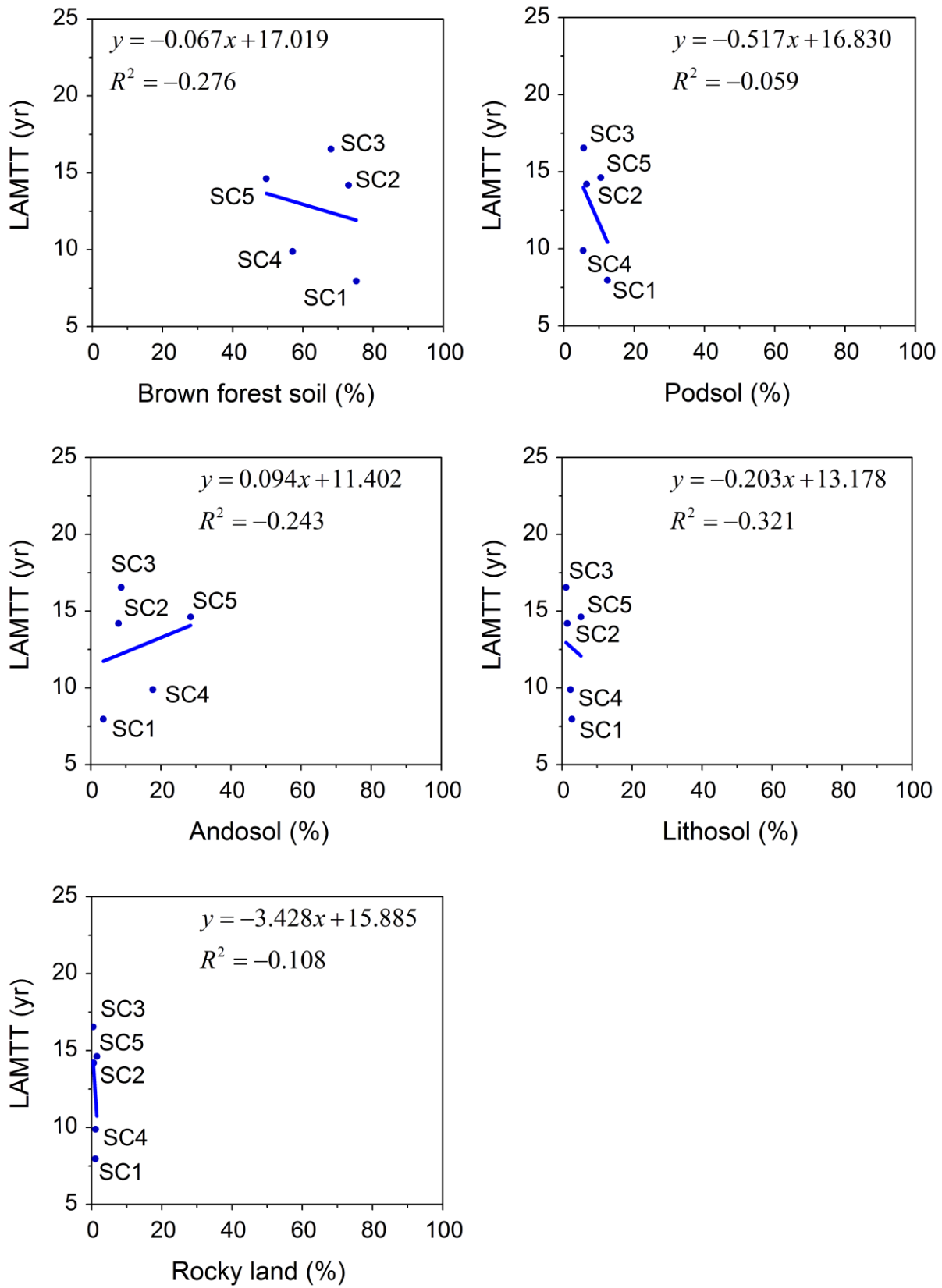
Figure 5.13 Releationship of LAMTT and coverage of surface soil types in each SC.
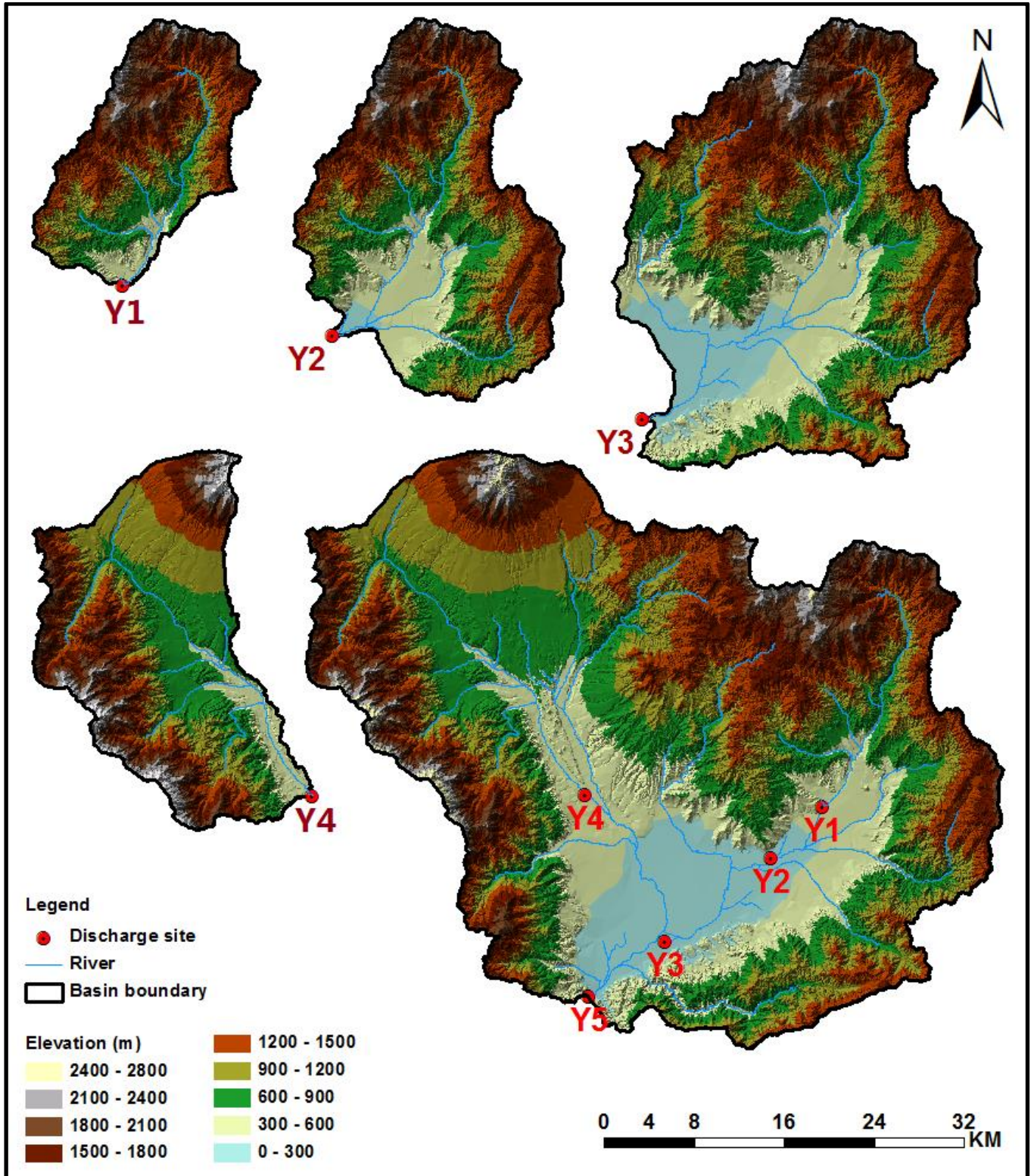
Figure 5.14 Topographical condition of each SC.
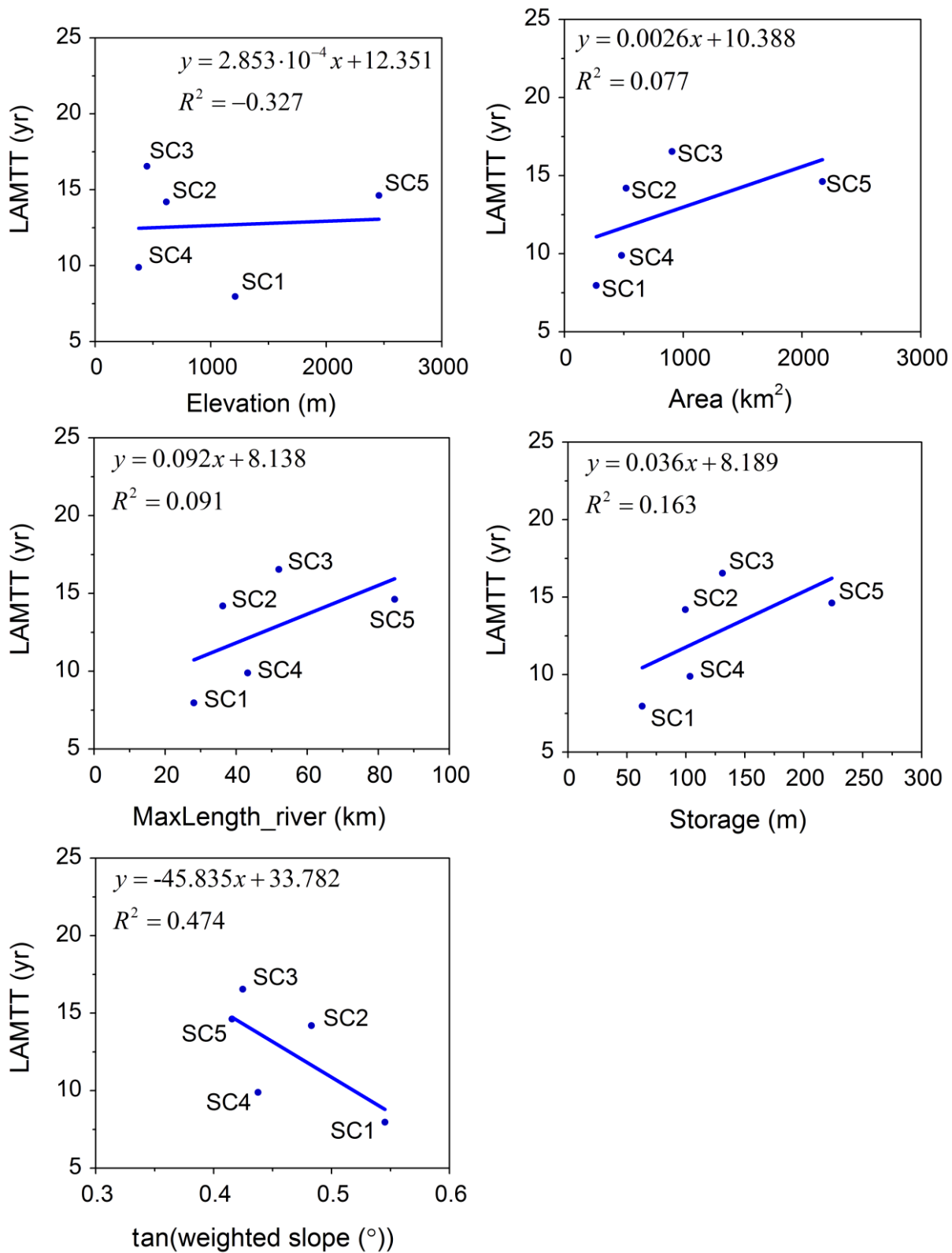
Figure 5.15 Relationship of LAMTT and topographical index of for SC.
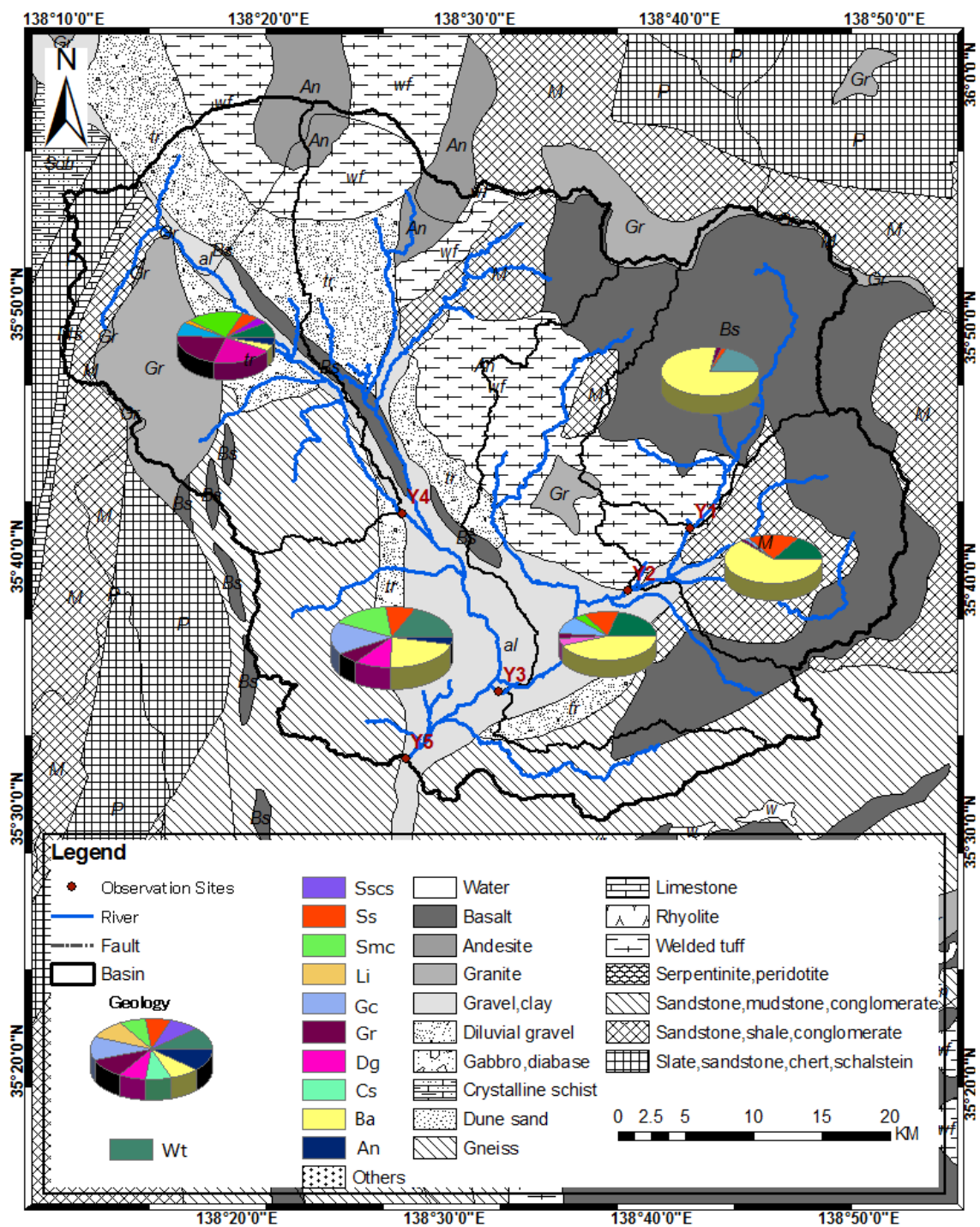
Figure 5.16 Spatial distribution of surface geology types and their coverage in each SC.
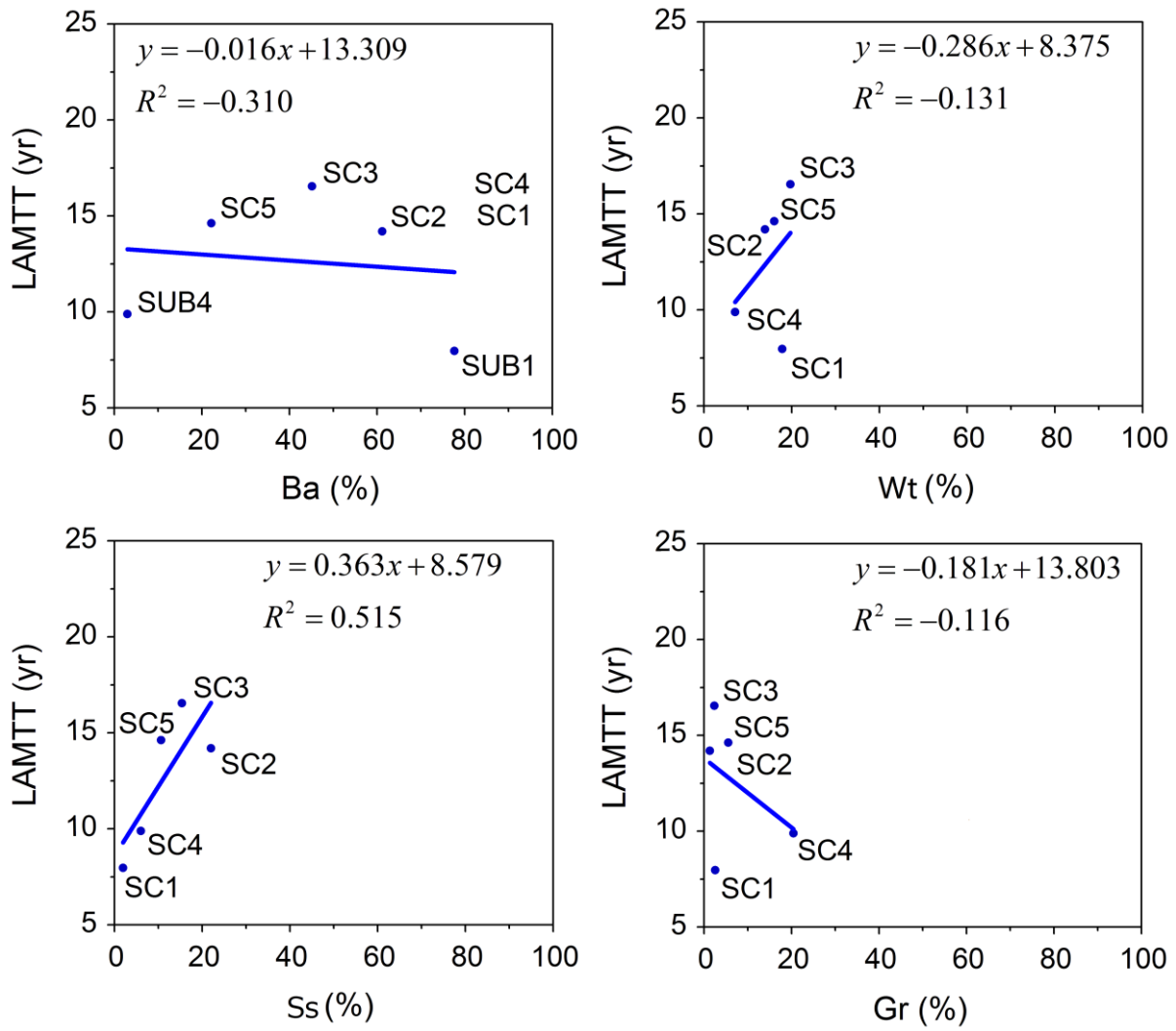
Figure 5.17 Relationship of LAMTT and coverage of surface geology types in each SC.

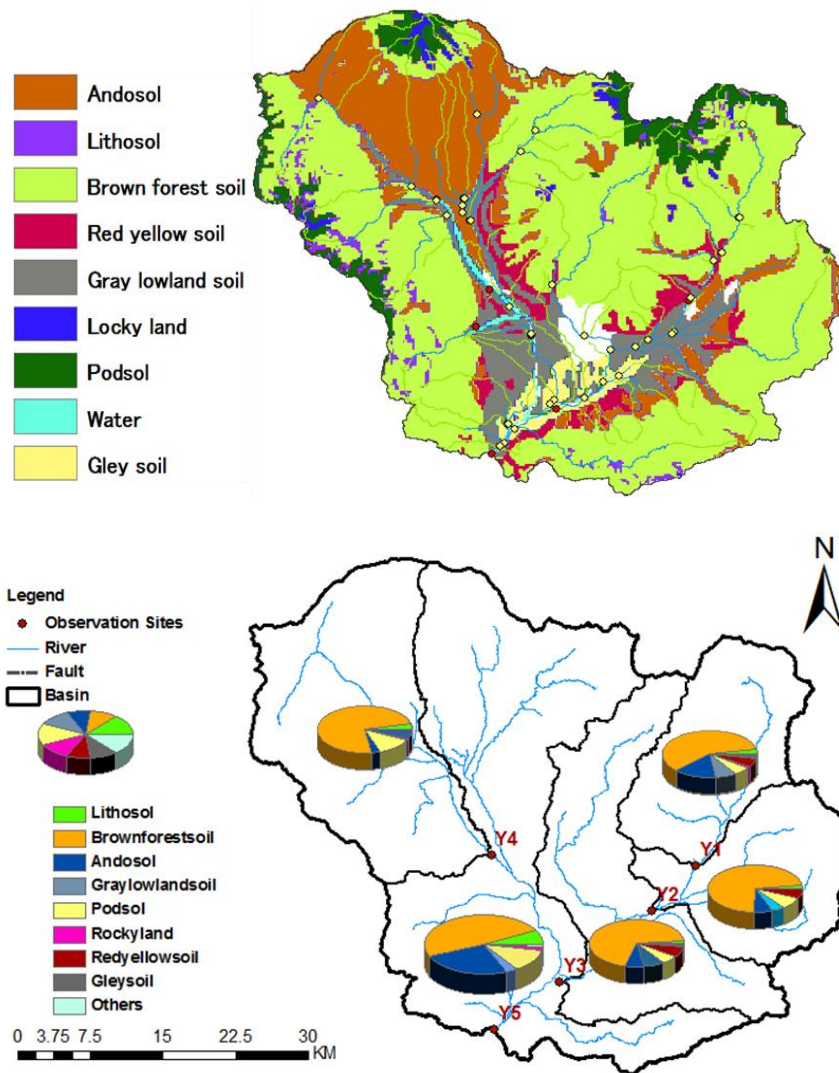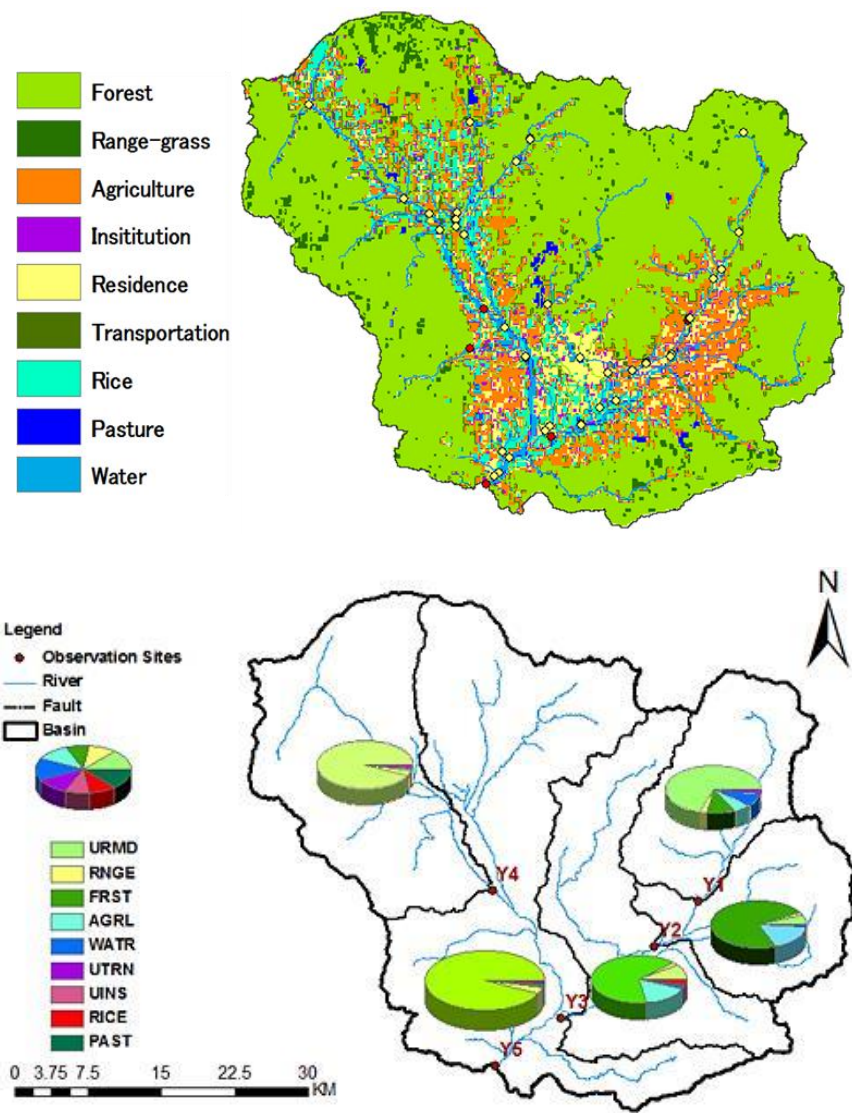Figure 5.18 Spatial distribution of land use types and their coverage in each SC.
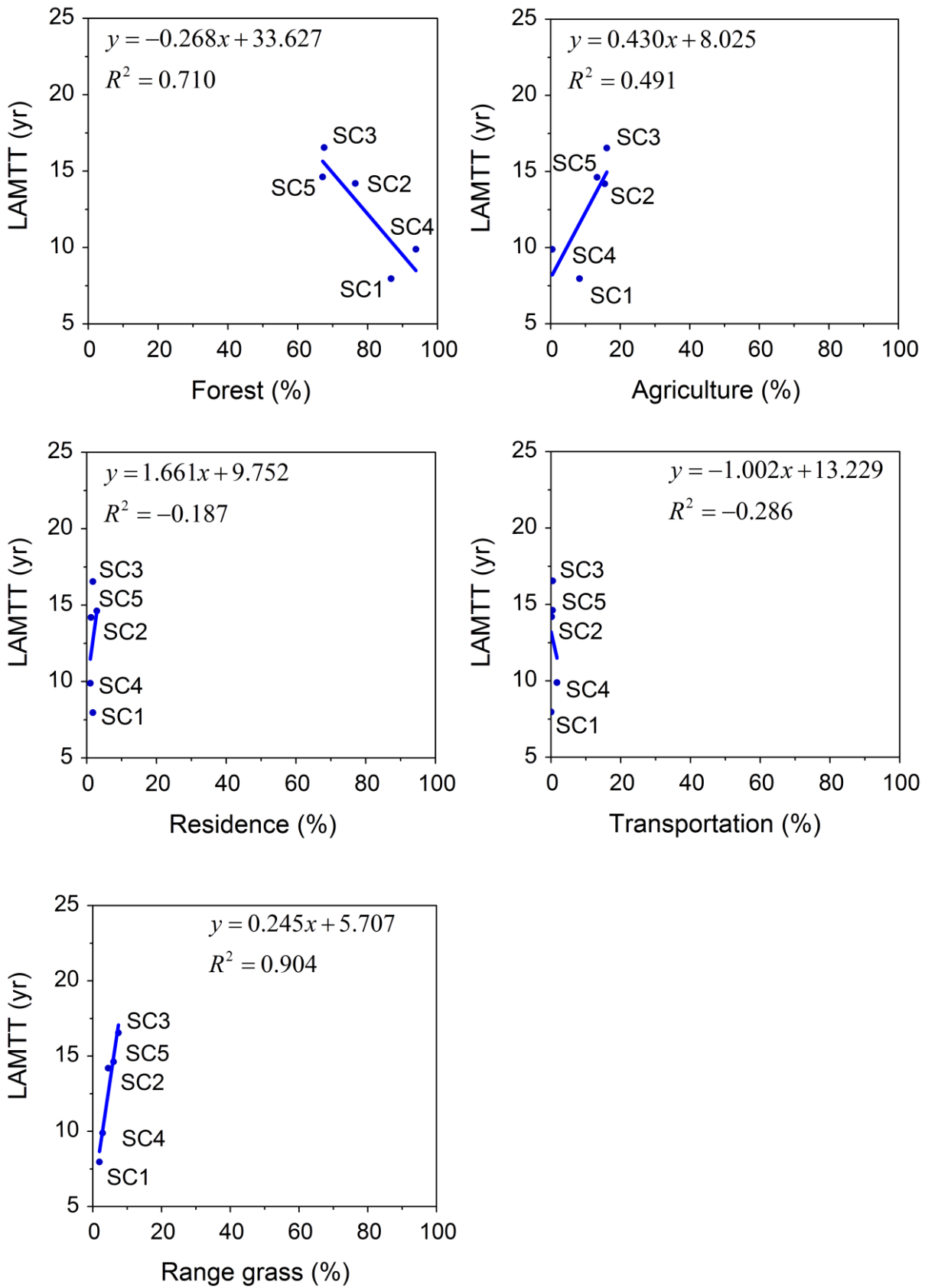
Figure 5.19 Relationship of LAMTT and coverage of land use types in each SC.
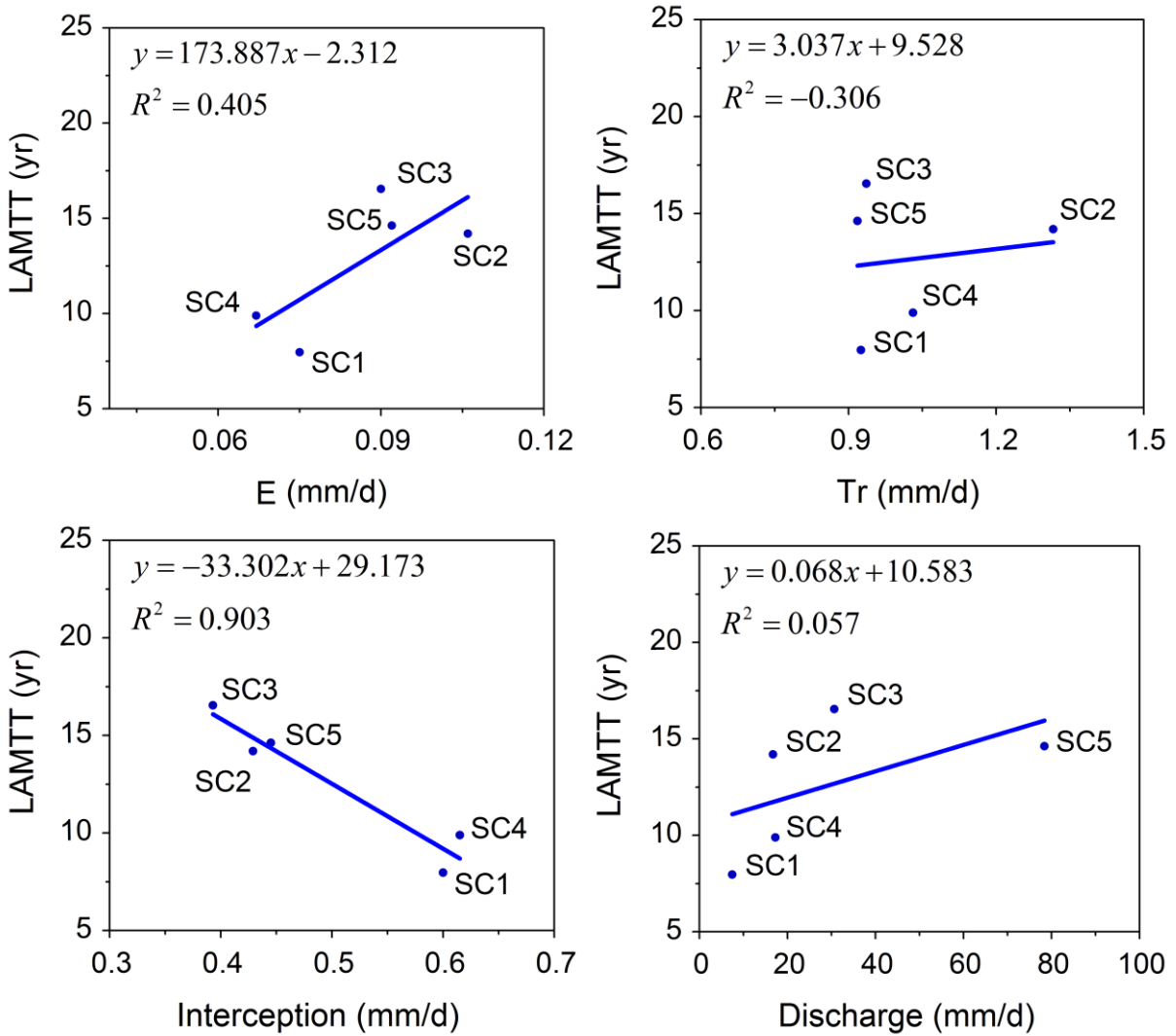
Figure 5.20 Relationship of LAMTT and water fluxes in each SC.

$$y_{layer1} = 0.31 \cdot x + 11.63, \quad R^2 = -0.12$$

$$y_{layer2} = -0.08 \cdot x + 14.16, \; R^2 = -0.32$$

$$y_{layer3} = 0.17 \cdot x + 10.19, \quad R^2 = -0.17$$

$$y_{layer4} = 0.47 \cdot x + 4.87, \quad R^2 = 0.83$$

$$y_{layer5} = 0.04 \cdot x + 10.03, \quad R^2 = 0.02$$

Figure 5.21 Relationship between LAMTT of each SC and storage in each layer.
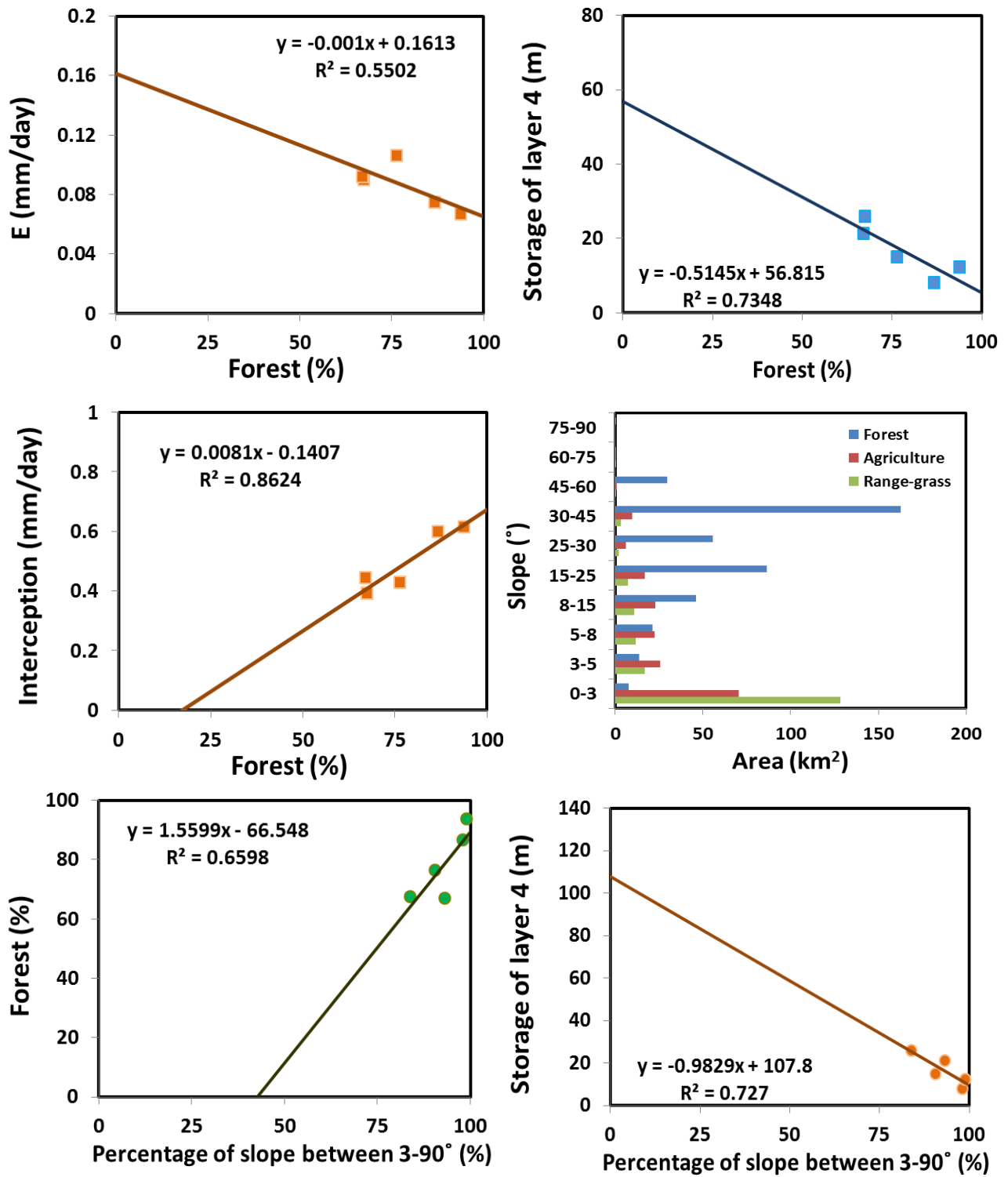
Figure 5.22 Correlation among potential factors controlling LAMTT.

# Chapter 6
# Conclusions

In this study, an approach to estimate the time-variant MTT and TTD using a five-layer tank model with isotopic tracers was proposed and tested for the five sub-catchments (SC1 to SC5) within Fuji River catchment, central Japan. The main conclusions are summarized as follows.

The long-term average MTT for each SC was estimated to be from 8.0 to 16.5 years. These values of MTT are almost comparable with previously reported values using the independent methods for the same region. In addition, the tank model used for the transit time estimation was calibrated and then validated by comparing observed and simulated results of not only water balance but also isotope balance. Although optimized model-parameters have some uncertainties, potential errors in estimating the MTT are relatively small (e.g., $< \pm 3.0$ years). Therefore, it is concluded that the use of the tracer-aided tank model for estimating catchment transit time is valid.

Daily/monthly/seasonal MTT was highly variable in time. Instantaneous TTD also varied markedly; the peak transit time is longer in drier periods than in wetter periods and form of the TTDs could not be approximated by any fun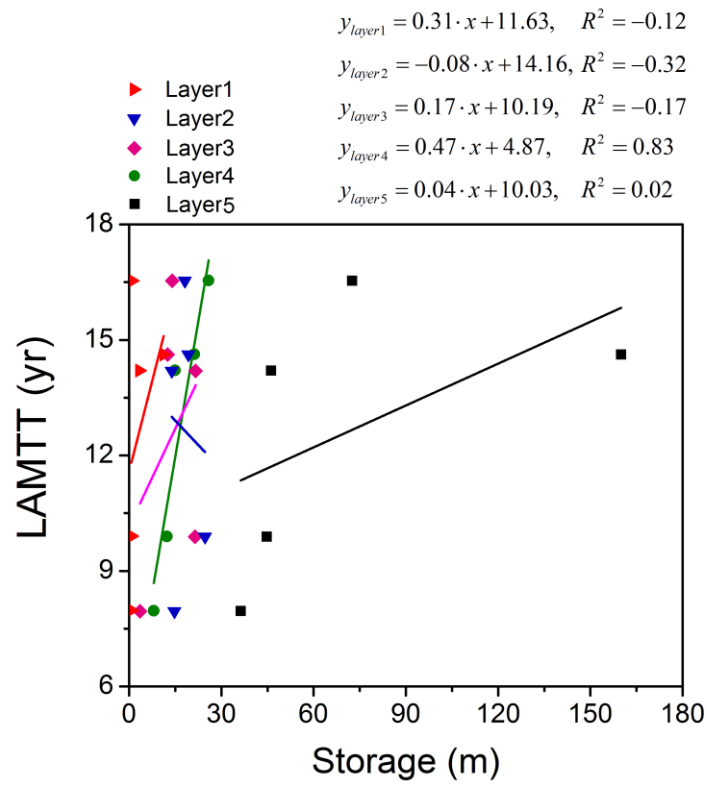ctions previously proposed. The predominant factor controlling temporal variability of MTT is precipitation amount. Occurrence of precipitation alters TTD, with increases in younger components, and shortens the MTT. In other words, river water is repeatedly refreshed by precipitation and ages during rainless periods. Thus, the steady-state assumption for MTT and TTD estimation is not appropriate.

Long-term MTT values correlated with mean slope, coverage of Mesozoic sand stone/shale, coverage of forest (or conversely the other land use types), evaporation, interception and storage

(especially, of the 4-th tank) for each catchment. All of these are related to the amount of groundwater storage, which is smaller in mountainous areas and greater in plain areas. Such a topographic control of LAMTT for meso-scale catchments is a new finding, since the most previous studies have focused on mountainous small catchments.

# Acknowledgements

First and foremost I offer my sincerest gratitude to my supervisor and mentor, Dr Tsutomu Yamanaka, for his wide knowledge, guidance, patience, encouragement, and continuous help during my Ph.D study at University of Tsukuba.

I would like to express my deep respect to Professor Michiaki Sugita, Professor Maki Tsujimura, Professor Jun Asanuma, and other Hydrological group advisors, for their constructive advice and encouragement during the period of achievement of this work.

Many thanks to my colleagues of the Graduate School of Life and Environmental Sciences, University of Tsukuba, especially Dr. Henda Jelassi, Dr. Pei Wang, Dr. Yaping Liu, Dr. Shakti P.C., Dr. Byambakhuu Ishgaldan, Dr. Kumar Pankaj, Dr. Yoshifumi Wakiyama, who have gave me lots of valuable suggestions and a lot of help for my life. As well as Mr. Yoshihiko Oshiro, Mr. Masaya Kano, Mr. Yuki Makino, and all the members of Yamanaka Laboratory for their support and discussion.

Last but not least, I would like to thank my parents for their unconditionally encouragement and mental support throughout my degree. In particular, the patience and understanding shown by my mum, dad during this period is greatly appreciated.

# References

Allen, R.G., Pereira, L.S., Raes, D., and Smith, M., Crop evapotranspiration: Guidelines for computing crop water requirements. *FAO Irrigation and Drainage Paper No 56, FAO, Rome.* 1998.

Amin, I.E., Campana, M.E., A general lumped parameter model for the interpretation of tracer data and transit time calculation in hydrologic systems. *Journal of Hydrology*.179: 1-21. 1996.

Anderson, M.G., Burt, T.P., Process Studies in Hillslope Hydrology, *Wiley, Chichester*. 1990.

Blöschl, G., Sivapalan, M., Scale issues in hydrological modelling: a review. *Hydrological Processes*, 9:251-290. 1995.

Bolin, B. and Rodhe, H., A note on the concepts of age distribution and transit time in natural reservoirs. *Tellus* 25:58-62. 1973.

Boots, B. N., Concepts and techniques in modern geography. *Voronoi (Thiessen) Polygons*, 45:4-5. 1986.

Botter, G., Bertuzzo, E., and Rinaldo, A., Transport in the hydrologic response: Travel time distributions, soil moisture dynamics, and the old water paradox, *Water Resources Research*, 46(03514), doi:10.1029/2009WR008371, 2010.

Brutsaert W. 2005.Hydrology-An Introduction. *Cambridge University Press*, 454-455. 2005.

Cappa, C.D., Hendricks, H.B., Depaolo, D.J., and Cohen, R.C., Isotopic fractionation of water during evaporation. *Journal of Geophysical Research*, 108:D16-4525, doi:10.1029/2003JD003597, 2003.

Craig, H., and Gordon, L.I., Deuterium and oxygen 18 variations in the ocean and marine atmosphere. *In proc. Stable Isotopes in Oceanographic Studies and Paleotemperatures*, Spoleto, Italy. edited by E. Tongiogi, 9-130, V. Lishi e F., Pisa.1965.

DeWalle, D.R., Edwards, P.J., Swistock, B.R., Aravena, R., Drimmie, R.J., Seasonal isotope hydrology of three Appalachian forest catchments. *Hydrological Processes*, 11 (15):1895-1906. 1997.

Duffy, C. J., Dynamical modeling of concentration–age–discharge in watersheds, *Hydrological Processes*, 24:1711-1718, 2010.

Dunn, S. M., Birkel, C., Tetzlaff, D., and Soulsby, C., Transit time distributions of a conceptual model: their characteristics and sensitivities. *Hydrological Processes*, 24:1719-1729. 2010.

Dunne, T., and Black, R. D., Partial area contributions to storm runoff in a small New England watershed, *Water Resources Research*, 6:1296-1311. 1970.

Fischer, H.B., List, E.J., Koh, R.C.Y., Imberger, J., and Brooks, N.H., Mixing in inland and coastal waters. *Academic Press*. 1979.

Gat, J.R., Shemesh, A., Tziperman, E., Hecht, A., Georgopoulos, D., Basturk, O., The stable isotope composition of waters of the eastern Mediterranean Sea. *Journal of Geophysical Research*, 101(C3):6441-6452. Doi:10.1029/95JC02829. 1996.

Geyer, W.R., Morris, J.T., Pahl, F.G., and Jay, D.A., Interaction between physical processes and ecosystem structure: A comparative approach, *Estuarine science: A synthetic approach to research and practice*. 177-206. 2000.

Goode, D.J., Direct simulation of groundwater age. *Water Resources Research*, 32 (2):289-296. 1996.

Heidbuchel, I., Troch, P.A., Lyon, S.W. and Weiler, M., The master transit time distribution of variable flow systems. *Water Resources Research*, 48:6, doi:10.1029/2011WR011293, 2012.

Hrachowitz, M., Soulsby, C., Tetzlaff, D., Dawson, J.J.C., and Malcolm., I.A., Regionalization of transit time estimates in montane catchments by integrating landscape controls, *Water Resources Research*, 45(05421), doi:10.1029/2008WR007496. 2009.

Hrachowitz, M., Soulsby, C., Tetzlaff, D., Dawson, J.J.C., Dunn, S.M. and Malcolm, I.A., Using long-term data sets to understand transit times in contrasting headwater catchments, *Journal of Hydrology*, 367:237-248. 2009.

Hrachowitz, M., Soulsby, C., Tetzlaff, D., and Speed, M., Catchment transit times and landscape controls-does scale matter? *Hydrological Processes*, 24(1): 117-125, 2010.

Ikawa R, Yamamoto T, Shimada J, Shimizu T. Temporal variations of isotopic compositions in gross rainfall, throughfall, and stemflow under a Japanese cedar forest during a typhoon event. *Hydrological Research Letters* 5: 32-36. doi: 10.3178/hrl.5.32. 2011.

Kato, T., Development of a water quality tank model classified by land use for nitrogen load reduction scenarios. *Paddy and Water Environment*, 3(1):21-27, DOI: 10.1007/s10333-005-0069-4. 2005.

Khatiwala, S., Visbeck, M., and Schlosser, P., Age tracers in an ocean GCM, *Deep-Sea Res.Pt*. 48:1423-1441, 2001.

Kirchner, V., Kelly, C.A. and Harvey, R.J., Thioridazine for dementia. *Cochrane Library*, issue 4. Oxford: Update Software. 2000.

Kirchner, S., Kieu, T., Chow, C., Casey, S., Blumberg, B., Prenatal exposure to the environmental obesogen tributyltin predisposes multipotent stem cells to become adipocytes. *MolEndocrinol*.

Kubota, T., Tsuboyama, Y, Estimation of evaporation rate from the forest floor using oxygen-18 and deuterium compositions of throughfall and stream water during a non-storm runoff period, *Journal of Forest Research*, 9:51‑59. 2004.

Li, H., Concepts and applications of water transport time scales for coastal inlet systems, *US Army Corps of Engineers, ERDC/CHL CHETN-IV-77*, 2010.

Lindström, G. and Rodhe, A. Transit times of water in soil lysimeters from modelling of oxygen-18. *Water, air and soil pollution*, 65:83-100. 1992.

Love, D., Uhlenbrook, S., zaag, P., Regionalising a meso-catchment scale conceptual model for river basin management in the semi-arid environment, *Physics and Chemistry of the Earth*, 36:747-760. doi:10.1016/j.pce.2011.07.005. 2011.

Lv M.X., Hao Z.C., Liu Z., Yu Z.B., Conditions for lateral downslope unsaturated flow and effects of slope angle on soil moisture movement. *Journal of Hydrology*. 486:321-333. doi:10.1016/j.jhydrol.2013.02.013.  2013.

Maloszewski, P.,  and Zuber, A., Determining the turnover time of groundwater systems with the aid of environmental tracers, I-Models and their applicability. *Journal of Hydrology.* 57:3-4. 207-231.1982.

Maloszewski, P., Rauert, W., Stichler, W., and Herrmann, A., Application of flow models in an alpine catchment area using tritium and deuterium data. *Journal of Hydrology*, 66:319-330. 1983.

Makihara, Y., A method for improving radar estimates of precipitation by comparing data from radars and raingauges. *J. Meteor. Soc. Japan,* 74, 459-480. 1996.

Majoube, M. Fractionnement en oxygene-18 entre la glace et la vapeur d'eau. *J. Chim. Phys.*, 68:625-636. 1971.

McDonnell, J.J., A rationale for old water discharge through macropores in a steep, humid catchment. *Water Resources Research*, 26:2821-2832. 1990.

McDonnell, J. J., McGuire, K., Aggarwal, P., Beven, K. J. , Biondi, D., Destouni, G., Dunn, S., James, A., Kirchner, J., Kraft, P., Lyon, S., Maloszewski, P., Newman, B., Pfister, L., Rinaldo, A., Rodhe, A., Sayama, T., Seibert, J., Solomon, K., Soulsby, C., Stewart, M., Tetzlaff, D., Tobin, C., Troch, P., Weiler, M., Western, A., W¨orman, A., and Wrede, S., How old is stream water? Open questions in catchment transit time conceptualization, modeling and analysis. *Hydrological Processes*, 24:1745-1754. 2010.

McGlynn, B., McDonnell, J., Stewart, M., and Seibert, J., On the relationships between catchment scale and streamwater mean residence time. *Hydrological Processes*, 17(1):175-181. 2003.

McGuire, K.J., DeWalle, D.R., and Gburek, W.J., Evaluation of mean residence time in subsurface waters using oxygen-18 fluctuations during drought conditions in the mid-Appalachians. *Journal of Hydrology*, 261(1-4):132-149. 2002.

McGuire, K.J., McDonnell, J.J., Weiler, M., Kendall, C., Welker, J.M., McGlynn, B.L., and Seibert, J., The role of topography on catchment-scale water residence time. *Water Resources Research*, 41(5):W05002. doi:10.1029/2004WR00365. 2005.

McGuire, K.J., McDonnell, J.J., Weiler, M., Kendall, C., McGlynn, B.L., Welker, M. and Seibert, J., The role of topography on catchment-scale water residence time. *Water Resources Research*, 41(5), doi:10.1029/2004WR003657. 2005.

McGuire, K.J., and McDonnell, J.J., A review and evaluation of catchment transit time modeling. *Journal of Hydrology*, 330(3-4):543-563. 2006.

McGuire, K. J., Weiler, M. and McDonnell, J.J., Integrating tracer experiments with modeling to assess runoff processes and water transit times, *Advances in Water Resources*, 30:824-837, doi:10.1016/j.advwatres.2006. 07.004. 2007.

Miyazaki T., Water flow in unsaturated soil in layered slopes. *Journal of Hydrology*, 102:201-214. 1988.

Moel, H., Asselman, N.E.M., Aerts, J.C.J.H., Uncertainty and sensitivity analysis of coastal flood damage estimates in the west of the Netherlands. *Natural Hazards and Earth System Science*, 12(4):1045-1058. DOI: 10.5194/nhess-12-1045-2012. 2012. Nakamura, R., Runoff analysis by electrical conductance of water. *Journal of Hydrology*, 14:197-212. 1971.

Montgomery, D.R., Dietrich, W.E., Torres, R., Anderson, S.P., Heffner, J.T., Loague, K., Hydrologic response of a steep, unchanneled valley to natural and applied rainfall. *Water Resources Research*, 33(1):91-109. 1997.

Nash, J.E. and Sutcliffe, J.V., River flow forecasting through conceptual models part I -A discussion of principles, *Journal of Hydrology*, 10(3):282-290. 1970.

Niehoff, D., Fritsch, U., Bronstert, A., Land-use impacts on storm-runoff generation: scenarios of land-use change and simulation of hydrological response in a meso-scale catchment in SW-Germany, *Journal of Hydrology*, 267:80-93. 2002.

Ozyurt, N.N., Bayari, C.S., LUMPED: a Visual Basic code of lumped-parameter models for mean residence time analyses of groundwater systems, *Computers & Geosciences*, 29:79-90, doi:10.1016/S0098-3004(02)00075-4. 2003.

Ozyurt, N.N., Bayari, C.S., Unsteady state lumped parameter modeling of 3H and CFCs transport: analyses of mean residence time in a mountainous karstic aquifer. *Hydrologic Processes* 19, in press. 2005.

Richer, P., Savage, B.D., Wakker, B.P., The FUSE spectrum of PG 0804+761: A study of atomic and molecular gas in the lower galactic halo and beyond. *The Astrophysical Journal*, 549:281-292, 2001.

Rank, D., Adler, A., Araguás Araguás, L., Froehlich, K., Rozanski, K., Stichler, W., Hydrological parameters and climatic signals derived from long-term tritium and stable isotope time series of the River Danube. In: *IAEA, Isotope Techniques in the Study of Environmental Change, IAEA-SM-349*, 191-205. 1998.

Reed, W. G., and J. B. Kincer, The preparation of precipitation charts. *Monthly Weather Review*, 45:233-235. 1917.

Rodhe, A., Nyberg, L., and Bishop, K., Transit Times for Water in a Small Till Catchment from a Step Shift in the Oxygen 18 Content of the Water Input. *Water Resources Research*, 32(12):3497, doi:10.1029/95WR01806. 1996.

Sayama, T. and McDonnell, J.J., A new time-space accounting scheme to predict stream water residence time and hydrograph source components at the watershed scale, *Water Resources Research*, 45, W07401, doi:10.1029/2008WR007549. 2009.

Scherrer, S., Naef, F., A decision scheme to indicate dominant hydrological flow processes on temperate grassland. *Hydrological Processes*, 17(2):39-401. 2003.

Shaman, J., Stieglitz, M., Burns, D., Are big basins just the sum of small catchments? *Hydrological Processes*, 18: 3195-3206. 2004.

Shapiro, A.M., and Cvetkovic, V., Stochastic analysis of solute travel time in heterogeneous porous media. *Water Resources Research*, 24:1711-1718. 1988.

Soulsby, C., Tetzlaff, D., Dunn, S.M., and Waldron, S., Scaling up and out in runoff process understanding—Insights from nested experimental catchment studies, *Hydrological Processes*, 20:2461-2465, doi:10.1002/hyp.6338. 2006.

Soulsby, C., Tetzlaff, D., Towards simple approaches for mean residence time estimation in ungauged basins using tracers and soil distributions. *Journal of Hydrology*, 363:60-74. 2008.

Speed, M., Tetzlaff, D., Soulsby, C., Hrachowitz, M., Waldron, S., Isotopic and geochemical tracers reveal similarities in transit times in contrasting mesoscale catchments. *Hydrological Processes*, 24 (9):1211-1224. 2010.

Stewart, M.K., McDonnell, J.J., Modeling base flow soil water residence times from deuterium concentrations, *Water Resources Research*, 27:2681-2693. 1991.

Sugawara, M., Tank model. In: *Singh, V.P. (Ed.). Computer Models of Watershed Hydrology, Water Resources Publications, Colorado*, 165-214. 1995.

Sugawara, M., and Maruyama, F., A method of prevision of the river discharge by means of a rainfall models, Symposia Darcy. *International Association Science Hydrological Publication*, 42, 3:71-76. 1956.

Sugita, M., Tanaka, T., Hydrologic Science. *Kyoritsu Shuppan Co*, 275pp. 2009.

Tetzlaff, D., Seibert, J., and Soulsby, C., Inter-catchment comparison to assess the influence of topography and soils on catchment transit times in a geomorphic province. *Hydrological Processes*, 23(13):1847-1886. 2009.

Tetzlaff, D., Malcolm, I.A., and Soulsby, C., Influence of forestry, environmental change and climatic variability on the hydrology, hydrochemistry and residence times of upland catchments, *Journal of Hydrology*, 346:93-111, doi:10.1016/j.jhydrol.2007.08.016. 2007.

Tetzlaff, D., Soulsby, C., Hrachowitz, M., Speed, M., Relative influence of upland and lowland headwaters on the isotope hydrology and transit times of larger catchments. *Journal of Hydrology*, 400:438-447. doi:10.1016/j.jhydrol.2011.01.053. 2011.

Thom, R.M., Borde, A. B., Richter, K. O. and Hibler, L.F., Influence of urbanization on ecological processes in wetlands. Land Use and Watersheds: Human Influence on Hydrology and Geomorphology in Urban and Forest Areas, *Water Science and application*, 2:5-16. 2001.

Uhlenbrook, S., Roser, S., and Tilch, N., Hydrological process representation at the meso-scale: the potential of a distributed, conceptual catchment model. *Journal of Hydrology*, 291, 278–296. 2004.

Van der Velde, R., Su, Z. and Van Oevelen, P.J. Soil moisture remote sensing using active microwaves and land surface modeling. Enschede, *University of Twente Faculty of Geo-Information and Earth Observation (ITC)*, ITC Dissertation 176, ISBN: 978-90-6164-296-1. 2010.

Weiler, M., McGlynn, B., McGuire, K., and McDonnell, J.J., How does rainfall become runoff? A combined tracer and runoff transfer function approach. *Water Resources Research 39: doi: 10.1029/2003WR002331. issn: 0043-1397.* 2003.

Wigmosta, M. S., and Perkins, W. A., Simulation the effects of forest roads on watershed Hydrology. Land Use and Watersheds: Human Influence on Hydrology and Geomorphology in Urban and Forest Areas, *Water Science and application*, 2:127-143. 2001.

Wolock, D.M., Hornberger, G.M., Musgrove, T.J., Topographic effects on flow path and surface water chemistry of the Llyn Brianne catchments in Wales, *Journal of Hydrology*, 115(1-4):243-25. 1990.

Woods, R., Chapter 3: Hydrologic Concepts of Variability and Scale. *Encyclopedia of Hydrological Sciences*, 23-40. 2005.

Yamanaka, T., Study on the atomspheric boundary layer using water vapor isotopes. K. Yoshimura, K. Ichiyanagi and A. Sugimoto (Eds): "Use of Isotope Ratios of Water in Meteorology", *Meteorological Society of Japan*, Tokyo, 61-76. 2009. (in Japanese)

Yamanaka T, Onda Y. On measurement accuracy of liquid water isotope analyzer based on wavelength-scanned cavity ring-down spectroscopy (WSCRDS). *Bulletin of Terrestrial Environment Research Center, University of Tsukuba* **12**, 31–40 .02011. (in Japanese).

Yamanaka, T., Tsujimura, M., Oyunbaatar, D., and Davaa, G., Isotopic variation of precipitation over eastern Mongolia and its implication for the atmospheric water cycle. *Journal of Hydrology*, 333:21-34. 2006.

Yurtsever, Y., and Payne, B., Mathematical models based on compartmental simulation approach for quantitative interpretation of tracer data in hydrological systems. In: *Morfis, A., Paraskevopoulou, P. (Eds.), 5th International Symposium on Underground Water Tracers. A.A. Balkema*, 341-353. 1986.

Zuber, A., Mathematical models for the interpretation of environmental radioisotopes in groundwater systems. *Handbook of Environmental Isotope Geochemistry, Vol. 2, Part B (Eds. P. Fritz and J.Ch. Fontes), Elsevier, Amsterdam:* 1-59. 1986.

Zuber, A., Environmental Isotopes in the Hydrological Cycle: Principles and Application, Volume VI: Lumped parameter models, *UNESCO/IAEA, Vienna, Austria and Paris France*, 5. 2001.